GROWTH AND CATHODOLUMINESCENCE OF ZnS:Mn THIN FILMS

GROWTH AND CATHODOLUMINESCENCE OF ZnS:Mn THIN FILMS

by

MILIND DATTATRAYA BHISE, B.Tech.(Hons)

A Thesis

Submitted to the School of Graduate Studies

in Partial Fulfilment of the Requirements

for the Degree

Master of Engineering

McMaster University

MASTER OF ENGINEERING (1989) MCMASTER UNIVERSITY
Hamilton, Ontario

TITLE: Growth and Cathodoluminescence of ZnS:Mn thin films

AUTHOR: Milind D. Bhise, B.Tech.(Hons)
(Banaras Hindu University)

SUPERVISOR: Dr.A.H.Kitai

NUMBER OF PAGES: xv, 145

ABSTRACT

A novel technique of incorporating dopants in a thin film was designed. It was successfully used to dope ZnS thin films with Mn. Cathodoluminescent (CL) properties of these Mn activated ZnS films were studied. For a constant accelerating potential and beam current density, the CL emission intensity was found to increase with Mn content up to ~2 wt% Mn. A further increase in the Mn content lead to a decrease in the CL intensity. The optimum Mn content is different than that for electroluminescence (~0.7 wt%) and photoluminescence (~1.6 wt%). Emission spectra of ZnS:Mn with a higher Mn content (> 1.64 wt%) show an additional red band besides the usual 580 nm yellow band. The relative intensity of the red band to the yellow band increases with the Mn content. The phenomenon of concentration quenching and the red emission seem to be interrelated; an attempt has been made to explain the physical basis behind these phenomena. Coverage of rough ceramic substrates by ZnS thin films deposited by vacuum evaporation and atomic layer epitaxy (ALE) has been investigated. The results suggest a uniform coverage in the case of ALE deposited films, while those deposited by vacuum evaporation show a shadowing effect.

ACKNOWLEDGEMENTS

I would like to express my appreciation and gratitude to Dr. Adrian H. Kitai for his invaluable guidance throughout this project. His suggestions were helpful not only in developing the engineer in me but also the individual.

I wish to thank Doris Stevanovic for the RBS spectra, Monica Katiyar for proof reading and Keith Ellison for helping me in printing the thesis. Skillful help of the machine shop personnel is also acknowledged.

Constant encouragement from my parents has been instrumental for the completion of this work. Without their love and support, I would have never seen this day.

TABLE OF CONTENTS

LIST OF ILLUSTRATIONS

LIST OF TABLES

This thesis is dedicated to my parents,

Dattatraya and Vinda Bhise.

Man must cut doubt with the sword of knowledge.

The Bhagavad Gita, iv.41,42.

CHAPTER 1

INTRODUCTION AND LITERATURE REVIEW

1.1 Introduction

Luminescence is a general term which includes the many phenomena involving absorption of energy by a substance and its emission as a visible or near visible radiation. It is, then, obvious that excitation is necessary for luminescence. Depending on the nature of the excitation, the luminescent process is called : photoluminescence (excited by photons), cathodoluminescence (electrons or cathode rays), electroluminescence (electric field across the material), chemiluminescence (utilization of reaction energy) etc.

Although crystalline solids are the most important of the luminescent materials, all phases of matter exhibit this property. It should be noted that the luminescence of most phosphors involves impurities (activators) and/or structural defects.

The possibility of a cheap, flat cathode ray tube (CRT) and a flat panel television has motivated a systematic study of the basic physics of and the effect of cathode rays on the zinc sulphide type phosphors. In the commercial flat panel market, the phenomenon of cathodoluminescence was

successfully used, in vacuum fluorescent displays, by ISE of Japan [1]. Subsequently, science has advanced much further; but still a thorough understanding of the phenomenon of cathodoluminescence and its dependence on the various parameters has not been possible.

It should be pointed out that a large number of applications of the thin film phosphors necessitates a wise choice of the phosphor material as well as that of the deposition technique. As will be discussed later, zinc sulphide doped with manganese (ZnS:Mn), which has a broad band emission centered at 580 nm, is the most widely used semiconductor thin film phosphor [2].

To be a competitive material for the applications stated above, different conditions have to be satisfied viz. high peak luminescence ($\gtrsim$ 30 fL), relatively high luminescence efficiency ($\gtrsim$ 1-5 lm/w), a fast response to pulsed excitation ($<$ 10 μs), high resolution, substantial life time, low cost etc. ZnS:Mn is one wide band gap semiconductor, that comes close in satisfying at least some of these conditions.

It has been experimentally observed that the luminescent characteristics of ZnS:Mn are strongly dependent on the concentration of Mn. A number of research groups [3,4] have reported a maximum intensity of photoluminescence at $\sim$ 2 mol% Mn. The corresponding figure for electrolumine-

luminescent (ACTFEL) [5] device is, ~ 1 mol% Mn, after which there is a drastic drop in the intensity [6,7]. No real effort has been made to study the effect of Mn concentration on the cathodoluminescent properties of this material, to our knowledge.

A novel method of incorporating a known amount of manganese has been successfully developed and used during the current investigation. This method allows doping of the parent film (200nm thick) anywhere beyond .05 wt %. The lower limit is determined mainly by the accuracy of thickness monitoring equipment. The present study is aimed at understanding the growth of ZnS:Mn thin films as well as investigating the influence of manganese concentration on the cathodoluminescent characteristics of the films.

1.2 Literature Review

In this section we shall review some of the important techniques for the preparation of thin films, with a specific reference to the growth of zinc sulphide. An emphasis is placed on vacuum evaporation, it being used to grow the films for the present study. Luminescent properties of ZnS doped with Mn and the effect of the amount of the dopant is also discussed.

1.2.1 Methods of Thin Film Deposition :

Thin film deposition techniques have, in the past

decade or two, become extremely sophisticated. The word 'thin' usually implies that one of the geometrical parameters of the three dimensional structure is much less than the other two. Deposition techniques are conveniently classified as physical methods which depend on evaporation or sputtering and chemical methods which depend on a specific chemical reaction. In practice there is often an overlap of the two. Although the oldest method, vacuum evaporation is still one of the most widely used techniques, the newer techniques viz. sputtering, molecular beam epitaxy (MBE), atomic layer epitaxy (ALE), metal-organic chemical vapour deposition (MOCVD) are now in widespread use.

1.2.1.1 Vacuum evaporation :

In spite of being referred to as a single process, the deposition of thin films by vacuum evaporation consists of several distinguishable steps:

1. Transition of a condensed phase into a gaseous state
2. vapour traversing the space between the evaporation source and the substrate at reduced gas pressure.
3. condensation of the vapour upon the arrival on the substrate

The last step is perhaps the most critical [8].

Vacuum deposition of the thin films of the II-VI

compounds (ZnS, ZnSe, CdS, CdSe etc) follows the Volmer-Weber growth mehcanism [9]. The essential steps in this growth mode can be identified as -

i) nucleation and formation of islands

ii) coalescence of the islands and

iii) formation of a continuous film.

Evaporation may result by resistance heating or by electron beam induced heating of the source. It has been proved, both qualitatively as well as quantitatively, that vapourization of a compound is usually accompanied by dissociation and/or association [8]. Of interest to us is the former, as it is known to occur in most chalcogenides. The II-VI compound like ZnS will hence vapourize as

$$ZnS_{(s)} = Zn_{(g)} + \tfrac{1}{2} S_{2(g)}$$

It is clear that, both the constituents of the compound should be equally volatile to get a stoichiometric film. It should be emphasized that, this is a necessary, but by no means a sufficient, condition to get a stoichiometric film. When arriving at the substrate, the individual particles should get adsorbed in the proper ratio and then recombine to form the desired compound. The sticking coefficient along with the rate of impingement of the individual species plays a major role in determining the stoichiometry of the film.

The major factors affecting the quality of the thin film are :- nature and quality of the substrate, temperature

of the substrate, geometry of the deposition system, chamber pressure, nature and quality of the source etc [9]. Of these, the substrate temperature is undoubtedly the most influencial. Studies of [10] show that the crystallinity of zinc sulphide thin film is best when the substrate is maintained at ~ 200 °C during the vacuum deposition of the semiconductor. Zn and S will not stick to the substrate at this temperature unless a compound is formed. Keeping this in mind all the films grown for the present investigation were grown at T_{sub} = 200 °C. A post deposition anneal is sometimes carried out, but is not expected to significantly improve the quality of ZnS films deposited at ~200°C.

Films so obtained are known to be predominantly cubic (zinc blende) [7,10,11], with a highly preferred orientation in the (111) direction. The presence of moisture in the deposition chamber is detrimental to the quality of the film.

1.2.1.2 MOCVD of ZnS thin films :

The less demanding vacuum conditions for the technique of metal-organic chemical vapour deposition (0.1torr or more) [12..15] make this method inherently simpler than MBE or ALE. Normally, the thin film is obtained on a heated substrate as a result of a chemical reaction of the organometallic compound (usually dimethylzinc for ZnS deposition) and a cation containing gaseous species (usually

H_2S for ZnS deposition) [12,13]. The main difficulty with this technique is the problem of the effect of gas flow control on the ultimate film quality [16]. A premature reaction between DMZ and H_2S can occur, which adds to the already existing problems of the method [12,13].

ZnS thin films have been successfully grown on a variety of substrates by different investigators . Shibata et al [17] studied the microstructure of the films deposited by MOCVD. It revealed the presence of pronounced, columnar grains throughout the thickness dimension. The crystal structure was found to be predominantly hexagonal, unlike vacuum deposited films which are predominantly cubic. Comparing the half width of the most intense X-Ray diffraction peak ($2\theta = 28.5°$) of the ZnS thin films grown by MOCVD and electron beam evaporation, they found that the previous had better crystallinity.

1.2.1.3 Atomic Layer Epitaxy :

Suntola et al [18] first proposed this technique for the deposition of epitaxial thin films. Currently, a variety of the II-VI and III-V semiconductors are being grown by this method on different substrates [19]. Unlike the traditional methods which control the thin film deposition through the source, ALE exhibits a surface controlled growth. Growth of the thin film takes place one monolayer at time and full coverage of the surface occurs. Details of

this deposition method may be found in [20]. Theis [21] did TEM studies on the thin films of ZnS:Mn prepared by various methods. His results indicate a better crystallinity of ALE grown films when compared to the electron beam deposited films, grown at the same substrate temperature. Bhise et al [22] (see also chapter 2 of this thesis) found that ALE was a superior growth technique when compared to vacuum evaporation, for the growth of ZnS on rough substrates.

1.2.2 Incorporation of Mn :

Manganese may be incorporated in the zinc sulphide host by various methods viz. ion implantation [23,24], coevaporation [6], MOCVD [17,25] and thermal diffusion [26..28]. Some researchers have reported a dependence of the luminescent properties of the semiconductor on the method of Mn incorporation [3]. The reason for this is probably the change in the spatial distribution of the dopant species in ZnS. Ion implantation is known to give a gaussian profile for the distribution [29] while thermal diffusion tends to give a Mn rich surface. Of course, annealing these films will help redistribute the dopant species uniformly and randomly, throughout the host.

Knowing the diffusivity of Mn in zinc sulphide and the time of diffusion, one can calculate (approximately) the average distance a Mn atom diffuses through ZnS (based on $\sqrt{Dt}$). From [80],

$$D = 6.8 \times 10^{-15} \ cm^2 \ sec^{-1}$$

where D the diffusivity of substitutional Mn. Hence after 4 hours at 400°C, the approximate distance a Mn atom traverses is ~990Å. These conditions are an approximation to those used for the present study.

1.2.3 What makes a good phosphor :

1.2.3.1 The Suitable Host:

It is known that a large variety of inorganic materials can be used as a host for luminescent materials [30]. A suitable host for a luminescent phosphor should have a large enough band gap, so as to emit visible light without significant absorption, and should do so at practical efficiency. This immediately narrows the choice to semi-conductors with E_g >2eV and insulators. Wide band gap II-VI semiconductors have been the most popular choice. Of these, zinc sulphide, is perhaps the most widely used semiconductor host. Incidently, Mn doped ZnS was one of the first materials studied for electroluminescence (EL) [31]. The band gap of 3.67 eV is wide enough to pass the complete visible spectrum of light. Shown in fig. 1.1 is a part of the ZnS (cubic) lattice, with a substitutional impurity.

ZnSe, CdS, CdSe and their solid solutions [32,33] have also been studied as possible hosts. Indeed, some of these materials might prove to be a better choice for

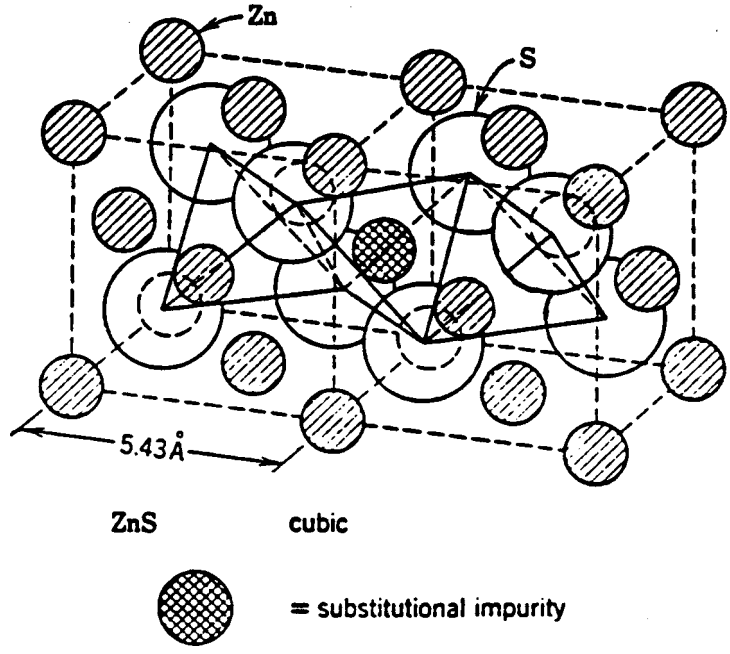

Fig 1.1 Part of the ZnS (cubic) lattice with substitutional impurity.

specific applications. Along with the II-VI semiconductors, alkaline earth sulphides and selenides [30,34] have also been investigated.

Compounds of the II-VI type crystallize in either the zinc blende or wurtzite structure [35]. For zinc sulphide, the transition temperature of the reaction zinc blende (cubic) - wurtzite (hexagonal) is 1020 ^{o}C. However, both the structures are present in the poly-crystalline thin films of ZnS. The technique of thin film deposition often influences the crystalline structure of the end product. Films prepared by vacuum evaporation are known to be predominantly cubic [10,11] while those prepared by atomic layer epitaxy (ALE) are predominantly hexagonal [18]. Suntola et al [18] have reported their ALE films to be predominantly cubic.

As this study is on ZnS:Mn, a brief mention should be made about its relevant physical properties (See table 1.1).

table 1.1

type	m.p.	Refl. colour	Refr. index	density
cubic	1020°C ↓ tr	colourless	2.368	4.04 g/cc
hex.	1850°C		anisotropic	

1.2.3.2 The Suitable Activator :

It was said before that luminescence in most of the

inorganic crystals is due to singularities, either impurities (activators) or lattice defects, in the host lattice. Let us examine the nature of an activator in the 'suitable' host ZnS. The most important condition [36] is that the activator should have a large absorption cross section for the exciting particle. Theoretical calculations [37] estimate the cross section for manganese to be 2×10^{-16} per cm^2. An extensive study of the role of different activators in ZnS has been done by a number of researchers. Their investigations have substantially proved that Mn is the most efficient activator in ZnS [36]. A simple explanation, based on the band theory, tells us that the activator provides additional energy levels in the host crystal. A more detailed picture can be found in section 3.2 of this thesis.

1.2.3.3 Luminescence due to the activator :

Mn^{2+}, like all other transition metal ions, exhibits a broad band, near-gaussian emission spectrum. The band is centered at 580 nm [2], thus giving an orange -yellow emission with a FWHM of approximately 0.23 eV for optimum concentration (see fig. 1.2). McClure [38] studied the absorption spectra of ZnS:MnS mixed crystals and discovered that the absorption bands possess a fine structure that becomes distinct at low temperatures. He also showed that there exists a weak absorption peak at a longer wavelength,

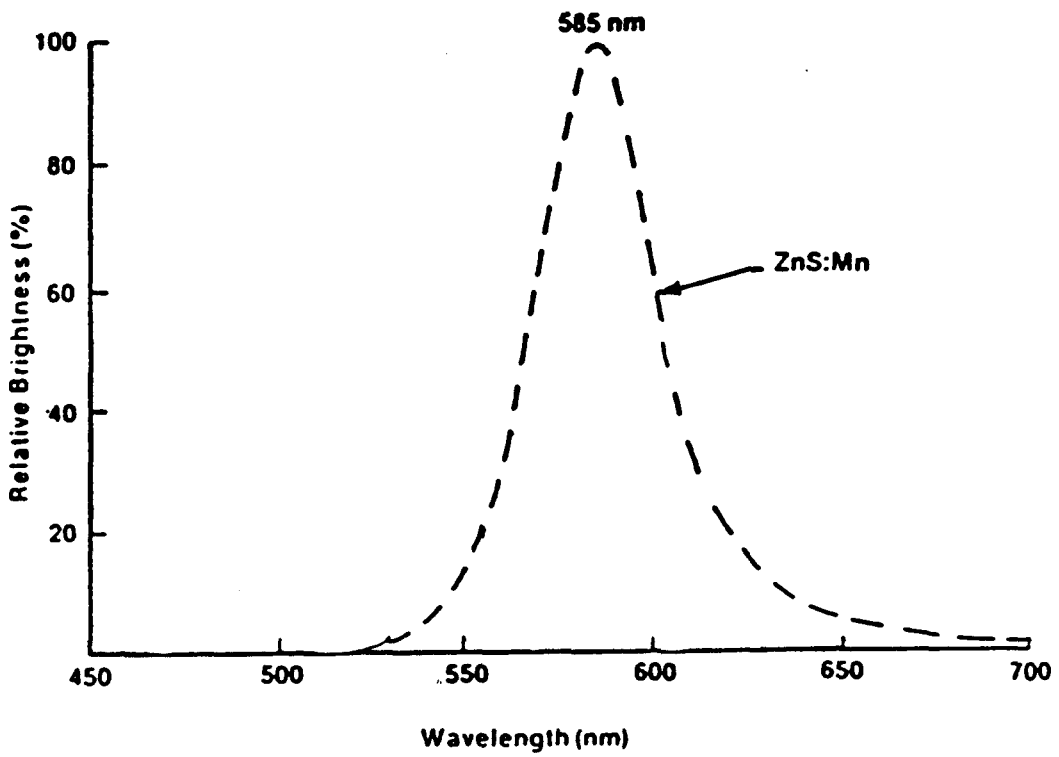

Fig 1.2 Typical emission band of Mn activated ZnS attributed to deexcitation of 3dlevels and essentially independent of the exciting method, [33].

making a total of five absorption bands due to Mn^{2+}. All of them are due to the d-d transitions, normally forbidden in the free ion state (fig 1.3)

Koda et al [2] measured the effect of pressure on the Mn^{2+} emission in zinc sulphide, and found that pressure induces a red shift of the emission peak to an order of ~0 .049 eV per 1 % change in the nearest neighbour distance.

Fe^{2+} shows a red luminescence with the band centered at 660 nm. As shown by Jaffe and Banks [39], Fe^{2+} red emission in ZnS if often accompanied by Zn^{2+} blue emission.

Garlick and Dumbleton [40], in 1954, found that Co^{2+} ion in ZnS shows an IR emission with a peak at 3.2μm, which they attribute to the d-d transitions in the cobalt ion. The optimum cobalt concentration was found to be 0.1 %. Strangely, Ni^{2+} doesn't show any detectable emission in zinc sulphide until 5μm (at 77 K), as pointed out by Garlick [41]. Iron, nickel and cobalt are thought to be 'killer' centres in ZnS as they quench the luminescence. Vanadium in zinc sulphide [42] emits at 2μm, again in the infra-red region of the spectrum.

Like the d-d transitions in case of the transition metal activators, the f-f transitions in the rare earths are the cause for luminescence. The emission comprises of many narrow lines characteristic of the f-f transition.

Tm^{3+} in ZnS [43] gives the most intense line in the blue region (478 nm) while Tb^{3+} [44,45] luminesces in the

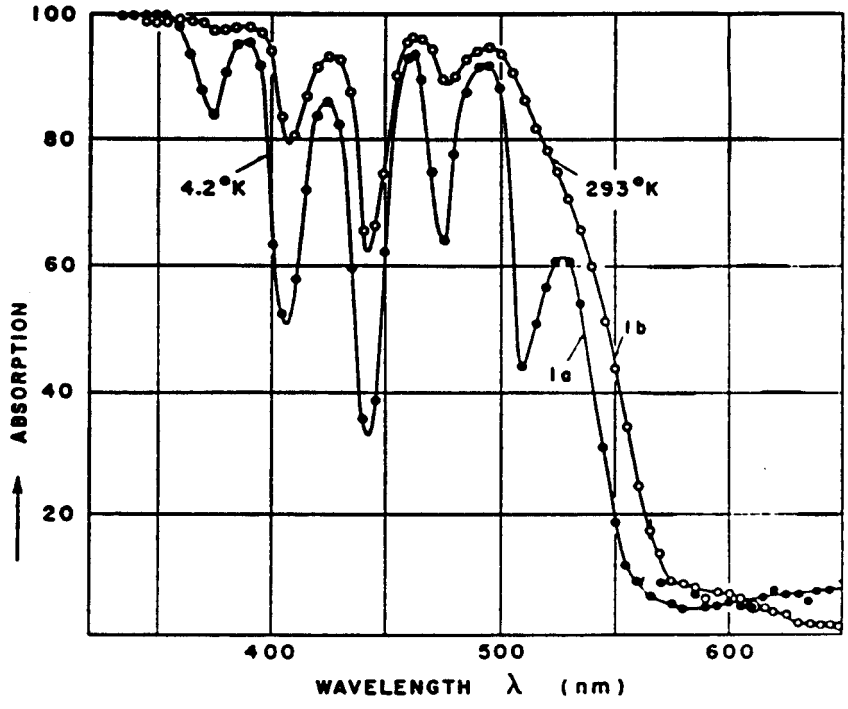

Fig 1.3 Absorption spectra of a ZnS:Mn crystal at different temperatures. (taken from [76]).

blue region (478 nm) while Tb^{3+} [44,45] luminesces in the green.

In table 1.2 are given the emission wavelengths of various activators in ZnS.

table 1.2

Phosphor	Peak emiss. wavelength
ZnS:Cu,Al	516 nm
ZnS:Cu,In	436 nm
ZnS:Cu	480 nm
ZnS:Mn	585 nm
ZnS:Tb	540 nm (most intense)
ZnS:Tm	478 nm (most intense)
ZnS:Pb,Cu	490 nm

1.2.4 Role of Mn in ZnS:Mn :

Mn^{2+} being isovalent with Zn^{2+} and of comparable ionic radii [46] - 0.80Å and 0.83Å respectively, can be expected to substitute the zinc ion in the ZnS lattice (fig 1.1). Schneider et al [47] have proved this using electron paramagnetic resonance. It is known that Mn can be incorporated in the ZnS lattice up to very high concentrations - in fact up to complete miscibility according to Nitsche [48].

As the luminescence in this material is due, solely, to the excitation and decay of the Mn ion, one would expect the intensity of luminescence to increase with Mn concentration. Such is not the case in practice. It has been observed that the intensity of luminescence of ZnS:Mn increases initially, till a certain optimum concentration of

the activator [3,4,6,7,27,55..58], after which there is a drastic reduction in the intensity. This phenomenon is termed as 'quenching'. A similar behaviour is observed in case of the efficiency of the phosphor. This typical behaviour is a characteristic of luminescent ZnS:Mn, irrespective of the exciting mechanism. The physical basis of concentration quenching is, as yet, poorly understood.

Let us examine the role Mn plays in the electro- photo- and cathodoluminescence of ZnS:Mn.

1.2.5 Electroluminescence in ZnS:Mn :

The following section deals with the role of manganese in electroluminescence (EL) of ZnS:Mn. Most of the research in this field has been carried out on ac driven thin film EL devices (ACTFEL). Let us first understand the essentials of such a device. Although luminescence under the action of an electric field i.e. electroluminescence, was discovered as early as 1936 [31], it was only in the past two decades that the TFEL devices have been attracting a lot of attention.

The most popular device design, due to its superior efficiency and brightness, constitutes an active layer (often ZnS:Mn) sandwiched between two insulating layers (Y_2O_3, $BaTiO_3$ etc) and two electrodes. Fig.1.4 shows a schematic of an ACTFEL device. The accepted physical model

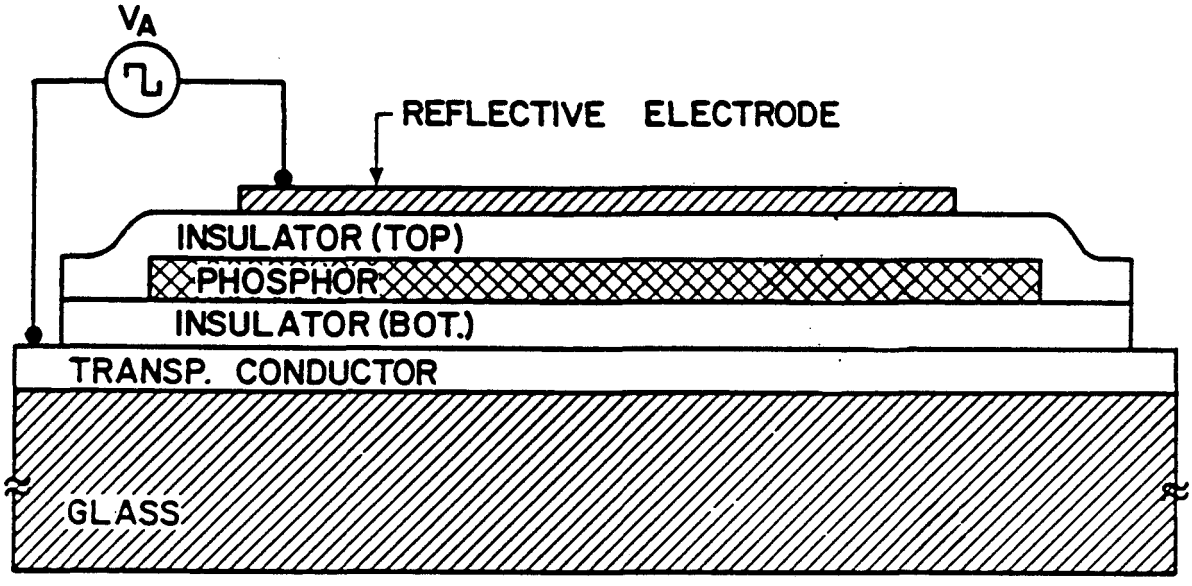

Fig 1.4 Schematic of an ACTFEL device.

of the light generating process in these devices, first proposed by Chen and Krupka [51], suggests:

... trapping of carriers at the localized sites at or near the ZnS/dielectric interface

... tunneling of the carriers from the interface states to the conduction band with the application of the electric field

... impact excitation of localized centres by hot electrons

... radiative decay of the excited centres

Warren et al [3] carried out a detailed study on the phenomenon of concentration quenching in ZnS:Mn. Their study of ZnS:Mn TFEL devices (dc driven) indicated that, upto a Mn concentration (c_{Mn}) less than 0.5 atomic % (1 mol%), there is a steady increase in the EL output; at higher concentrations quenching occurs. Films in this case were prepared by radio-frequency sputtering technique. Similar results were reported by [50] when the films were grown by MOCVD, which rules out any dependence on the film fabrication method. Hurd and King [6] also studied the effect of Mn concentration on the electroluminescent intensity of ZnS:Mn ACTFEL devices. The thin films in this study were deposited by the electron beam evaporation method. Fig 1.5 shows their results. The brightnesss reaches a maximum at 1 ± 0.3 mol% Mn. It may be seen that the brightness for c_{Mn} =1.3 ± 0.3 mol% is about 30 times as

much as that at c_{Mn} = 5 ± 0.3 mol%.

Qualitatively similar results have been obtained by Sasakura et al [7], who reported a maximum brightness at ~ 1 mol% Mn (fig 1.5). The ratio of the brightness for the ACTFEL devices with c_{Mn} = 1 % to that with c_{Mn} = 5 %, in this case, was only ~ 12.5.

Efficiency of an ACTFEL device, defined as the ratio of luminescent power output to the power input, is influenced by the Mn concentration in qualitatively the same way as the brightness is. Marrello and Onton [51] reported that Mn EL efficiency is highly inhomogeneous in the ZnS thickness direction, with the dominant emission occurring near the cathodic semiconductor/ dielectric interface. They incorporated Mn, in the form of thin probing layers in ZnS and by time resolved spectroscopy found that excitation of Mn doped layer near the cathode was maximum. The crystallinity and orientation of the ZnS film is also known to affect the efficiency. Fig 1.6 shows the influence of Mn concentration on the EL efficiency of an ACTFEL, due to [7].

Mn concentration has a pronounced effect on the emission spectrum of the EL device, beyond c_{Mn} = 1 mol %. The emission spectra often shows an additional second peak towards the lower energy, besides the regular yellow one at 580 nm [52,53]. These emission bands have a peculiar temperature dependence as pointed out by Neumann [56]; with increasing Mn concentration different emission bands prevail

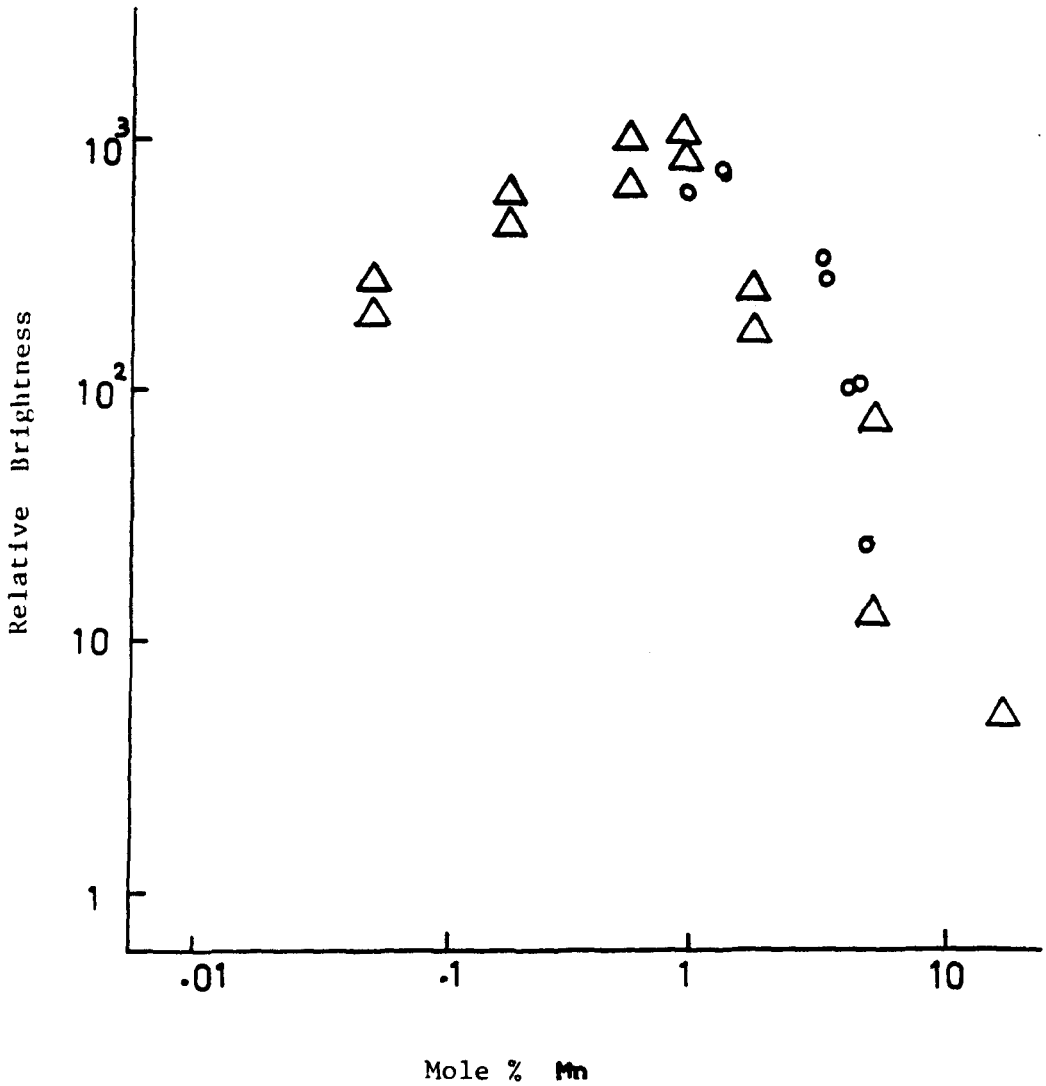

Fig 1.5 Brightness as a function of Mn concentration for EL of ZnS:Mn, after o[6] and Δ[7].

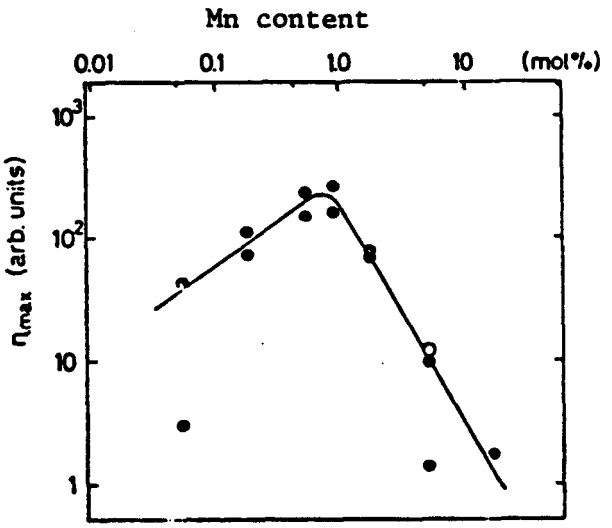

Fig 1.6 EL efficiency vs Mn concentration for ZnS:Mn ACTFEL, due to [7].

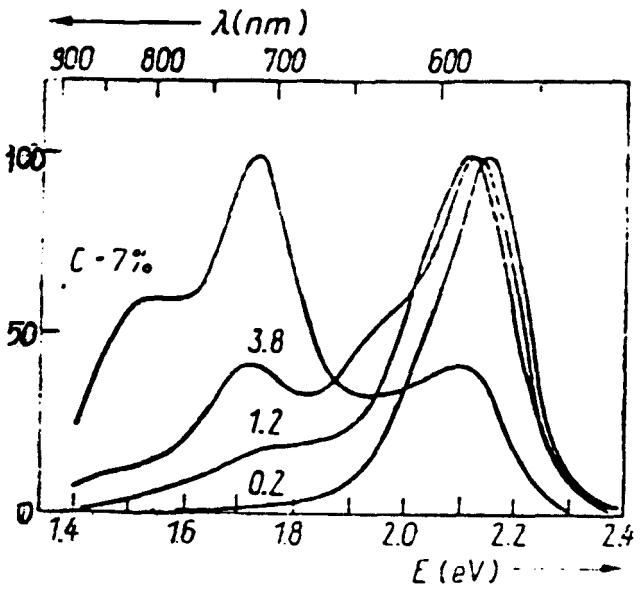

Fig 1.7 EL emission spectra of ZnS:Mn devices with different Mn content [53].

at different temperature. Fig.1.7 gives an excellent idea about the influence of c_{Mn} on the EL emission spectra of ZnS:Mn. The general trend may be noted :

i) at c_{Mn} > 1% an additional red band starts appearing at 720 nm. Marello and Onton [52] have also reported seeing this low energy band. We have reported here, for the first time, a similar effect in ZnS:Mn excited by an electrons [27].

ii) the intensity of the red emission band increases, in comparision with that of the yellow band, with c_{Mn}.

iii) for c_{Mn} > 4% a new band appears in the IR region (at 820 nm).

TRS (time resolved spectroscopy) [53] has shown that the red peak lags its yellow counterpart (fig.1.8). The authors report that the excitation spectra for the different emissions, is, in principle, similar to that of an isolated Mn^{2+} ion. They observed that at low temperatures, there is a decrease in the relative intensity of the lower energy bands, suggesting a possible energy transfer from excited Mn^{2+} to the red centres. Warren et al [3], in their study of dc pulsed EL of ZnS:Mn, did not find appreciable difference in the spectral content of the emission upto 0.9% Mn. Hence it is clear that the red bend appears after a particular 'threshold' Mn concentration.

To identify the nature of the luminescent centres, Benoit et al [53] carried out decay time studies.

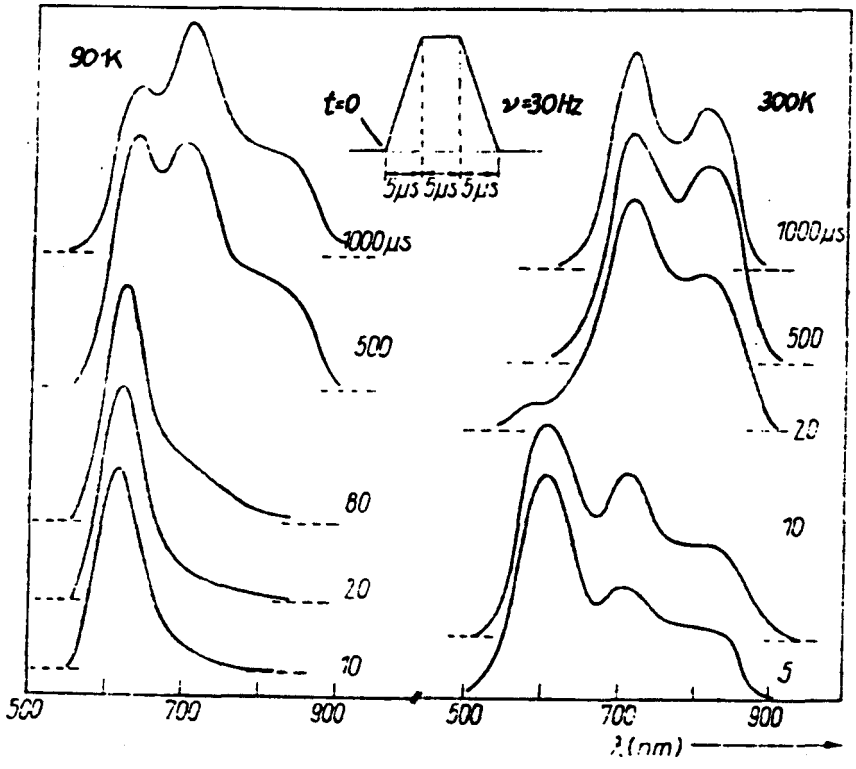

Fig 1.8 Time resolved EL emission spectra of ZnS:Mn, after Benoit et al [53] showing the time lag between yellow and red emission.

Accordingly, the decay characteristics of the red emission are different from the corresponding value of the yellow. In other words, different centres contribute to the red and yellow emissions (See fig 1.9). They found that the excitation spectra of the two centres to be almost identical which strengthens the claim of an energy transfer mechanism (see section 5.4.2).

τ, the radiative lifetime of the Mn^{2+} centre in ZnS is strongly dependent on the amount of Mn present. Sasakura et al [7] found (fig 1.10) that the value of τ decreases with increasing Mn concentration.

It is also reported in the literature [54] that higher concentration of manganese results in stronger saturation effects in the ZnS:Mn ACTFEL. The Mn concentration also affects the steepness of the luminescence vs. applied voltage curve at high luminance, implying that the electrical properties of the ZnS:Mn change simultaneously with the increase in decay rate .

1.2.6. Photoluminescence in ZnS:Mn :

The study of luminescence, when the material is excited by photons, is, in many cases, helpful to understand the basic process(es) of the luminescence mechanism. Systematic investigations have been reported on the photoluminescent (PL) studies of ZnS:Mn by various research groups [3,4,55].

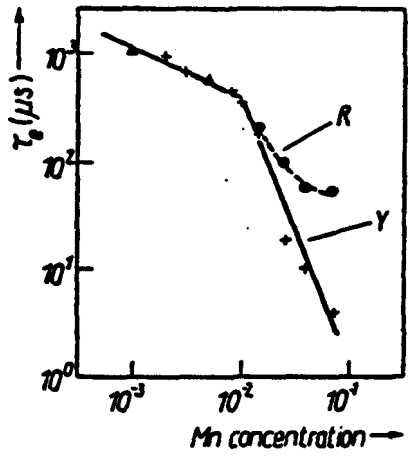

Fig 1.9 Effect of Mn concentration on the decays of red and yellow centres, after [53].

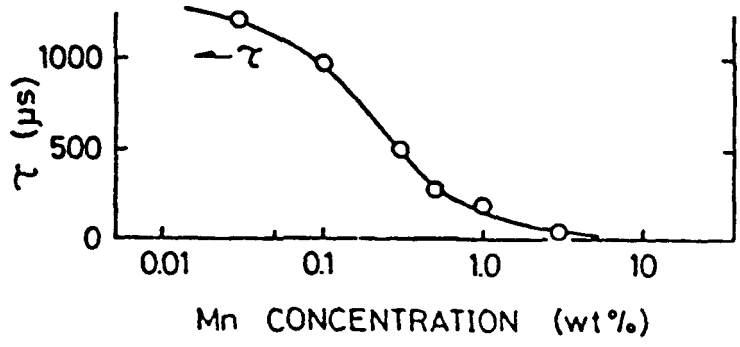

Fig 1.10 Effect of Mn concentration on the decay of EL in ACTFEL devices, taken from [7].

Intensity of PL is maximum at c_{Mn} ~2 mol%.[3,4]. Investigations by M. Katiyar [59] yielded a maximum at ~ 2.2%. Qualitatively similar to the one for EL, a quenching effect is observed in the PL of ZnS:Mn, at higher Mn concentration. Fig 1.11 shows the variation of photoluminescent intensity with c_{Mn}. Quenching is discussed further, in section 5.4.

For c_{Mn} upto 1% only the yellow emission peak (~2.1 eV) is observed which is due to the lowest energy transition $^4T_1(^4G)--^6A_1(^6S)$ in the $Mn^{2+}(3d^5)$ ions [36]. With a further increase in the concentration of Mn, a red (1.9 eV) and an infra red emission peak appears. Dang Dinh Thong and Goede [60] have found a temperature dependence of the intensities of the yellow and red peaks (fig. 1.12). The next plot (fig 1.13a) tells us that at higher levels of Mn doping, the red band dominates. Measurements at liquid nitrogen temperature, confirmed the presence of both the bands while those at 2K showed only the yellow band. Thong and Goede [57] argue that the lower energy emission is due to the decay of octahedrally coordinated Mn^{2+} (normally the Mn^{2+} ion is tetrahedrally coordinated in the cubic environment of ZnS). It may be recalled, from section 1.2.5, that similar observations have been made in case of the EL of ZnS:Mn.

The investigations of [56] were on ZnS:Mn single crystals. Dang Dinh Thong et al [57] obtained similar results for ZnS:Mn thin films. Dependence of the intensity

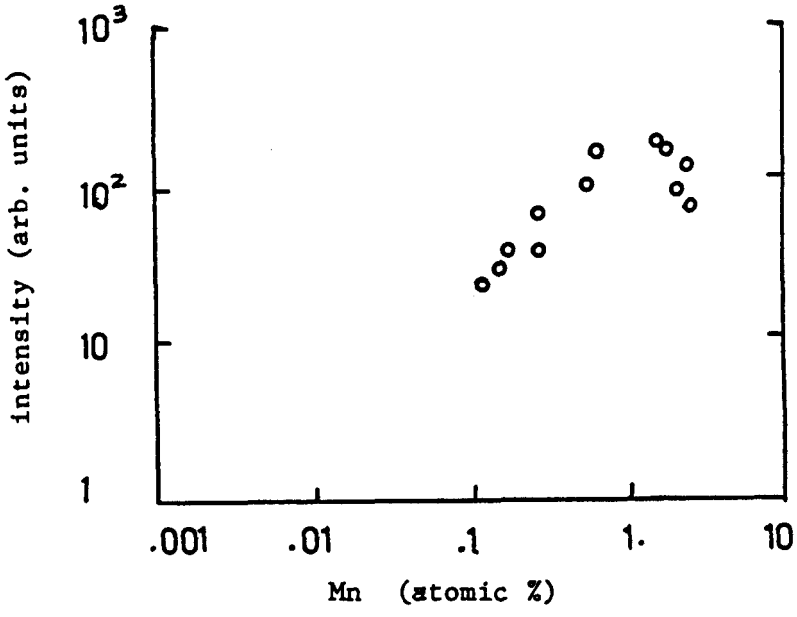

Fig 1.11 PL intensity vs c_{Mn}, after [3]

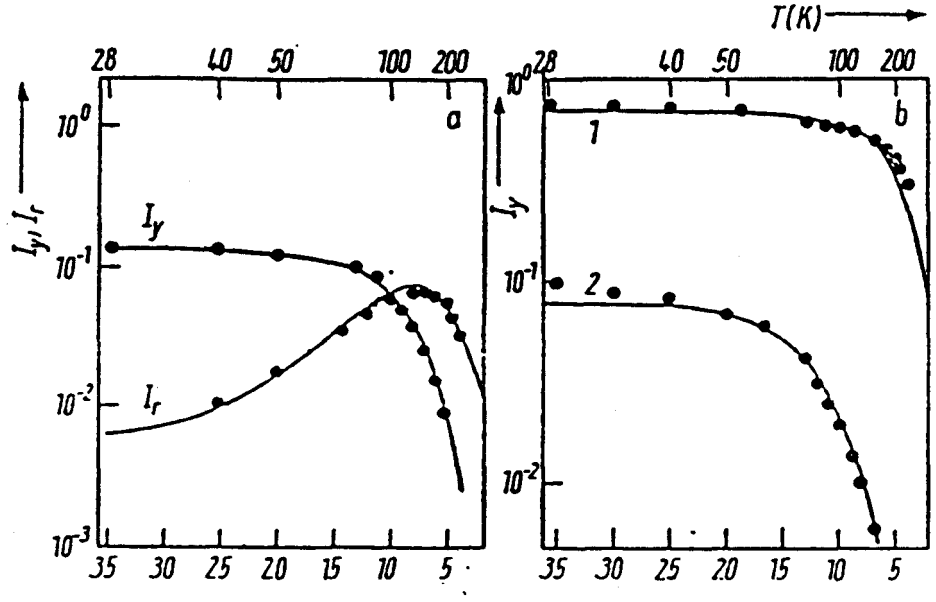

Fig 1.12 Temperature dependence of the intensities of the yellow and red emission bands for, a) c_{Mn} = 4.4% and b) 1:c_{Mn} = 1%, 2:c_{Mn} = 26.7% due to [57].

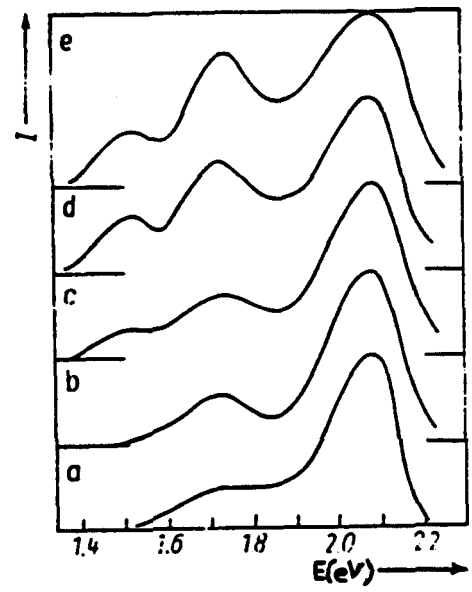

Fig 1.13 a PL emission spectra (100 K) of ZnS:Mn with varying Mn content, due to [56]; a: 2.4, b: 3.0, c: 3.6, d: 4.6 and e: 5.5 mol%.

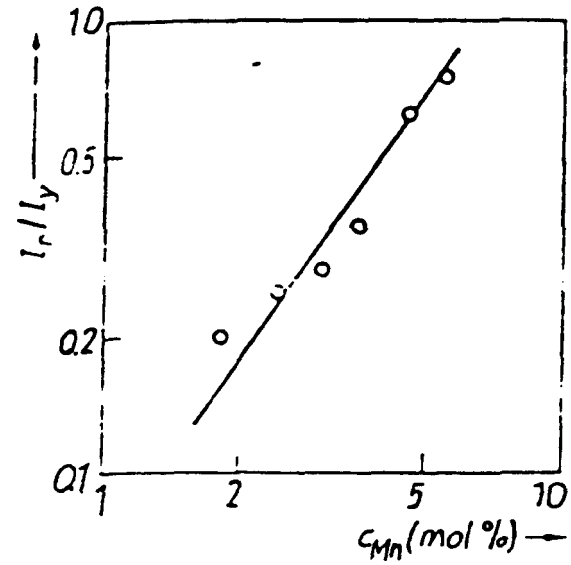

Fig 1.13 b I_r/I_y as a function of Mn concentration.

of the red band with respect to that of the yellow band with manganese concentration is depicted in fig.1.13b. The relationship can be approximately stated as:

$$B_r(c_{Mn}) = (c_{Mn})^{1.5}$$

Observed temperature and manganese concentration dependence can be satisfactorily explained by radiationless energy transfer from the optically excited Mn^{2+} caused by an exchange mechanism. In other words, the excitation becomes more or less 'mobile' at higher Mn doping levels and with a certain finite probability reaches either the centres for red emission or decays non-radiatively, by a final energy transfer. Migration of excitation energy in a solid and energy transfer from a sensitizer to an acceptor is a complex subject and requires a thorough investigation.

Benecke et al [59] reported that for c_{Mn} > 1 mole % two additional UV bands could be detected in the excitation spectrum besides the usual five bands associated with the internal transitions of the excited Mn.

1.2.7 Cathodoluminescence :

It was stated previously that luminescence due to the bombardment of energetic electrons is termed as cathodo-luminescence. The only relevant study, to the author's knowledge, was done by Leverenz [60] who found that adding an increasing amount of Mn in self activated ZnS, the original [Zn] emission band remains fixed in position but

decreases in efficiency as a new [Mn] band appears. The luminous efficiency of the Mn band increases upto about 1-2 wt% Mn.

CL studies have been done on a variety of materials [61]- single crystals, powder phosphors, thin foils as well as thin films. The first cathodoluminescent thin films of reasonable efficiency were produced by Studer and coworkers [62] in 1951.

Garlick and Sayer [63] investigated the change in the luminescence decay constant in powder layers, thin films, sintered layers and single crystals with the depth of penetration of the electrons; see fig. 1.14.

The luminance intensity at a constant accelerating potential of energetic electrons, varies with the beam current density as shown in fig. 1.15. A saturation [64] is observed with the current density. The results also point out an important characteristic of the Mn centre. A much slower decay of Mn activated phosphors causes saturation at lower values of current density.

The reported data on the dependence of the brightness of ZnS:Mn on the accelerating potential of the exciting electrons does not agree. The possible reasons will be discussed in a forthcoming chapter. Theis and Wengert [65] reported the validity of the Thomson-Whiddington law :

$$x = d(V_o - V_x)^2 \qquad .....(i.1)$$

where V_x is the potential at a depth x, V_o the initial

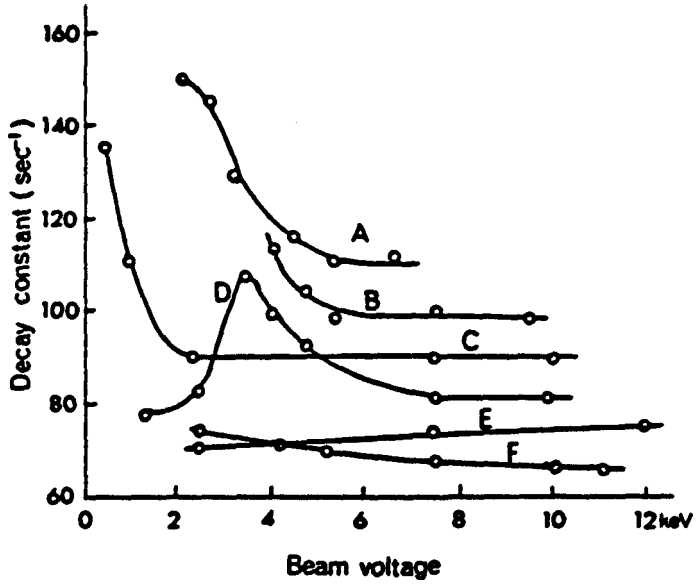

Fig 1.14 Decay constant versus beam voltage for Mn activated zinc silicate: A,B,C, evaporated layers; D, sintered disc; E,F, powderlayers.

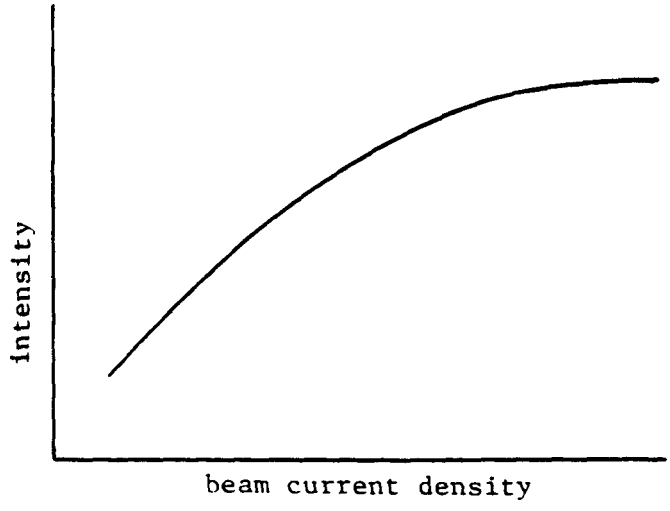

Fig 1.15 Schematic of the variation of luminescence intensity with the current density. The intensity of CL emission saturates beyond a certain value of current density.

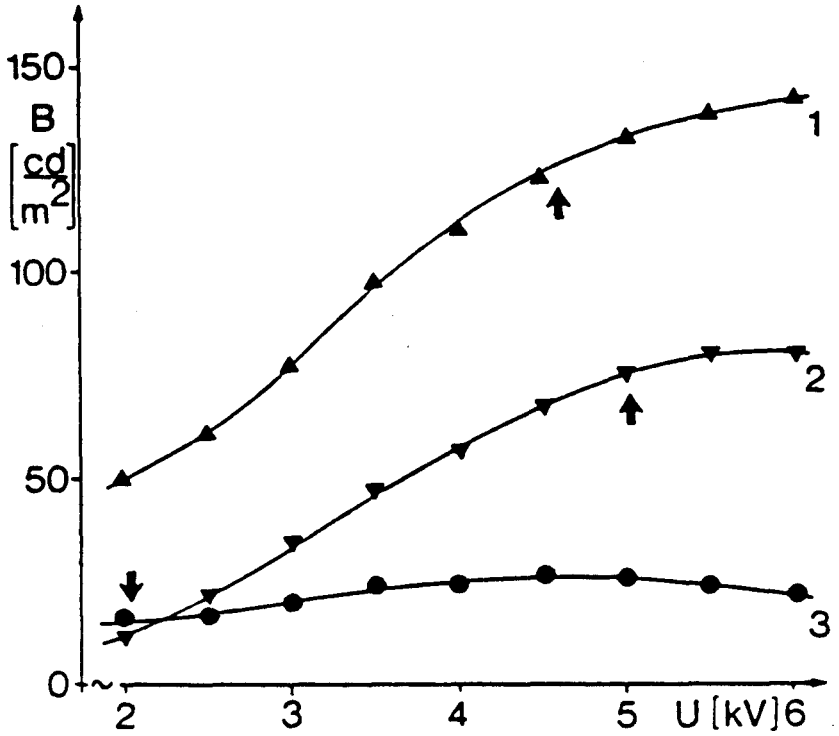

Fig 1.16 a CL intensity versus accelerating potential for three different ZnS:Mn films, 1: 630 nm, 2: 700 nm and 3: 120 nm. Arrows indicate full penetration according to equation (i.2), due to 65 .

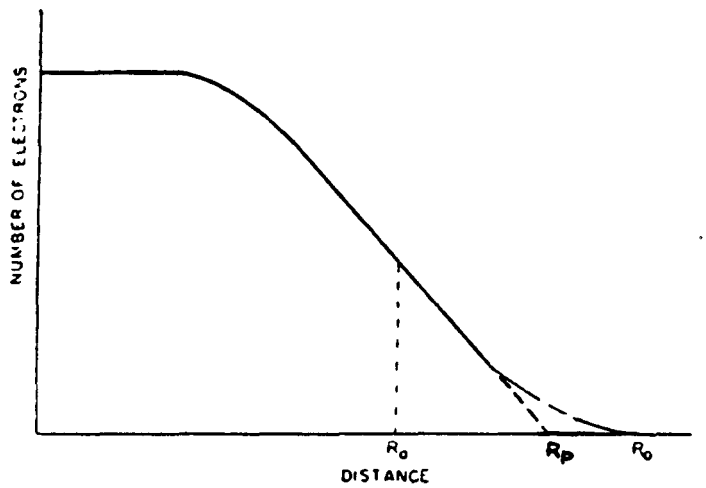

Fig 1.16 b Schematic electron absorption curve; R_a: average and R_p: extrapolated range.

accelerating potential and d a constant depending approximately on the density of the material. Espe [66] indicates that, for zinc sulphide, the formula can be written as

$$x = 2.83 \times 10^{-2} V_o^2 \qquad .....(i.2)$$

when x is in μm and V_o in kV. The results from [65] are reproduced in fig.1.16a. The arrows show the predicted voltage (based on equation i.2) at which full penetration of the bulk film is expected. Hence the luminance increases upto this point and stays more or less constant beyond it. The penetration depth as given by equation is the average penetration depth. The physical basis of the average penetration depth can be understood from the fig.1.16b. Feldman [67] investigated a series of materials and found that the penetration was given as

$$R = bV_o^n \qquad .....(i.3)$$

where b and n are constants, of which n is approximately independent of the material while b is a function of the atomic number Z and the bulk density ρ of the material. The value of b and n for ZnS [67] is 63Å and 2.4 respectively. At n = 2 the above expression translates to

$$R = bV_o^2 \qquad .....(i.4)$$

The similarity between equation (i.1) and (i.4) is obvious.

The main objective of the current work was to determine the effect of manganese concentration on the cathodoluminescent properties of ZnS:Mn thin films. So only

a narrow range of accelerating potential was selected viz. 3.5-5 kV. The results do not demostrate a dependence on the accelerating potential. The reasons for such a behaviour are discussed in chapter 3.

CHAPTER 2

STUDY OF THE COVERAGE OF ROUGH SUBSTRATES

2.1 Introduction :

The objective of the present study was to study the growth pattern of ZnS:Mn thin films. Although the films for luminescence study were grown on silicon substrates (the reasons are outlined in section 4.1.3), a detailed investigation was carried out to study the thin film growth on rough substrates. To see the effect of deposition technique, three different fabrication methods were employed.

2.2 Choice of the substrate :

Since the introduction of Inoguchi's [5] ZnS:Mn AC driven thin film electroluminescent device (ACTFEL, fig 1.4), numerous efforts have been made to improve its performance [7,28]. Recall that the device consists of a ZnS:Mn active layer sandwiched between two insulating layers and two electrodes. This unique structure avoids breakdown by preventing steady current flow through the device.

Recent investigations have focussed on the modification of this device in order to improve its appearance

and reliability using ceramic substrates. Traditionally, the insulating layers of an ACTFEL device have been sputter deposited or vacuum evaporated. It is also known that the dielectric constant and breakdown field is governed by preparation conditions of the dielectric films [36]. Sano et al [68], proposed and investigated, an ACTFEL device using a ZnS:Mn film grown on a multilayer ceramic substrate. As anticipated, their device had a better breakdown resistance and a lower driving voltage than that of the traditional one. The ceramic substrate in this device poses a unique problem for the growth of the ZnS:Mn film - namely that of surface roughness on the order of several microns.

The thin films, constituting the device, may be deposited by various techniques - vacuum deposition [7], sputtering [69], metal-organic chemical vapour deposition (MOCVD) [13,17], atomic layer epitaxy (ALE) [18,20,70], etc. It has been shown that the quality and crystallinity of the thin film is superior when it is grown by ALE [21]. Following sections deal with the novel study comparing the growth pattern of ZnS thin films deposited by three different methods - vacuum deposition (resistance heated), electron beam deposition and atomic layer epitaxy. In all the samples investigated, the ZnS thin films were grown on a multilayer ceramic substrate.

2.3 Deposition of thin films :

Thin films, of various thicknesses, of zinc sulphide were deposited on polycrystalline ceramic substrates. The substrates were made from a sintered, $BaTiO_3$ based complex perovskite. The average surface roughness was about 5 μm and the grain size less than 6 μm. Deposition was carried out by three different techniques, under identical conditions. In table 2.1 are shown the appropriate details about the deposition.

The vacuum deposition system, for the electron-beam assisted deposition is a diffusion pumped, conventional bell jar type one, capable of attaining high vacuum (10^{-6}-10^{-7}T). The electron gun has source-substrate distance of 250 mm and the normal to the plane of the substrate was at 30^{o} to the source. An accelerating potential of 2 kV was maintained during the deposition. The resistance heated source utilized a similar vacuum system. The source, in this case, was a Tantalum baffle boat and the angle between the substrate normal and vapour source was $\sim 10^{o}$. This system is described further in section 4.1.1.

The atomic layer epitaxy system, operating at atmospheric pressure, uses dimethyl zinc (DMZ) and hydrogen sulphide (H_2S) as reactants. A calculated volume of the

Table 2.1

Details of film deposition

sample No.	method	Press. Torr	T_{sub} °C	estimated thickness	Growth rate Å/s
Cer 1	vacuum dep.	$7x10^{-6}$	200	~ 450 nm	4.9
Cer 2	e-beam dep.	$2x10^{-6}$	200	~ 150 nm	10
Cer 3	"	$2x10^{-6}$	200	~ 1.5 μm	10
Cer 4	ALE	atmospheric	200	~ 138 nm	ref [20]
Cer 5	ALE	atmospheric	200	~ 69 nm	ref [20]

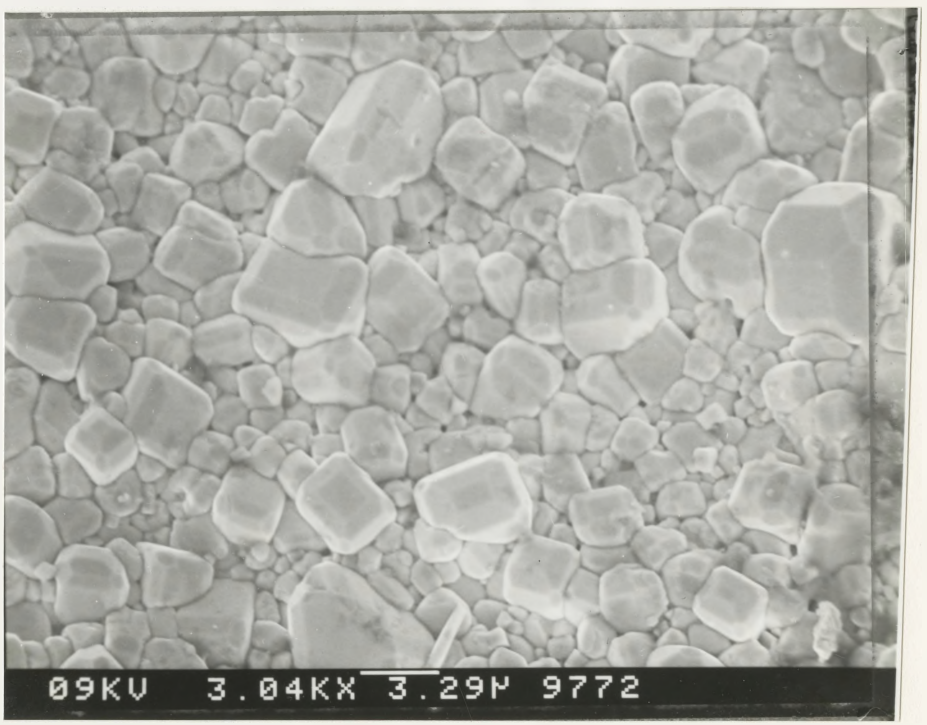

Fig 2.1 Typical SEM image of the ceramic substrate used.

reactants is admitted in the reaction chamber, whence they react on the previously heated substrate. After a given time (2 sec in this case) the reaction chamber is purged with an inert gas (N_2) to flush the excess unreacted material. This system has been described in detail [20].

It is known that the substrate temperature is extremely critical in thin film growth of ZnS [10]. For the sake of comparison, the substrate temperature was identical (200^{o}C) for all the samples investigated. A post deposition anneal was not carried out on any of the samples.

2.4 SEM Study :

It was mentioned earlier that the ceramic substrates used were somewhat rough. Fig.2.1 shows the virgin (no film deposited) substrate. The surface roughness and multi-grain structure is evident. The next figure (fig.2.2a) is a scanning electron micrograph of a ZnS thin film (sample Cer 1) deposited on the ceramic substrate. The film, which was grown by vacuum deposition, is about 450 nm thick. It can be clearly seen that the thin film is not very uniform on the substrate. Fig.2.2b shows the detail of the same film, revealing directionally favoured growth due to shadowing. To understand the physical basis behind this phenomenon,

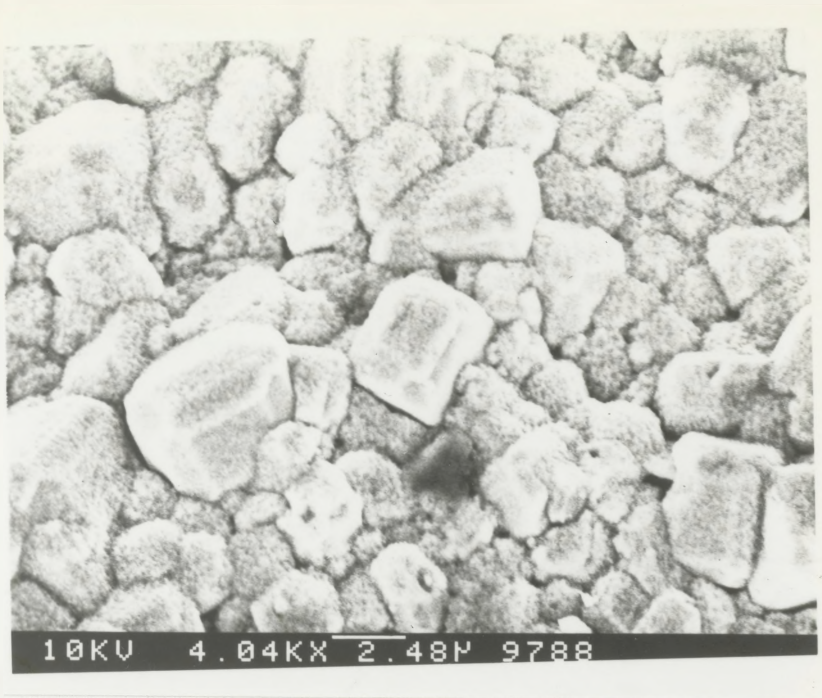

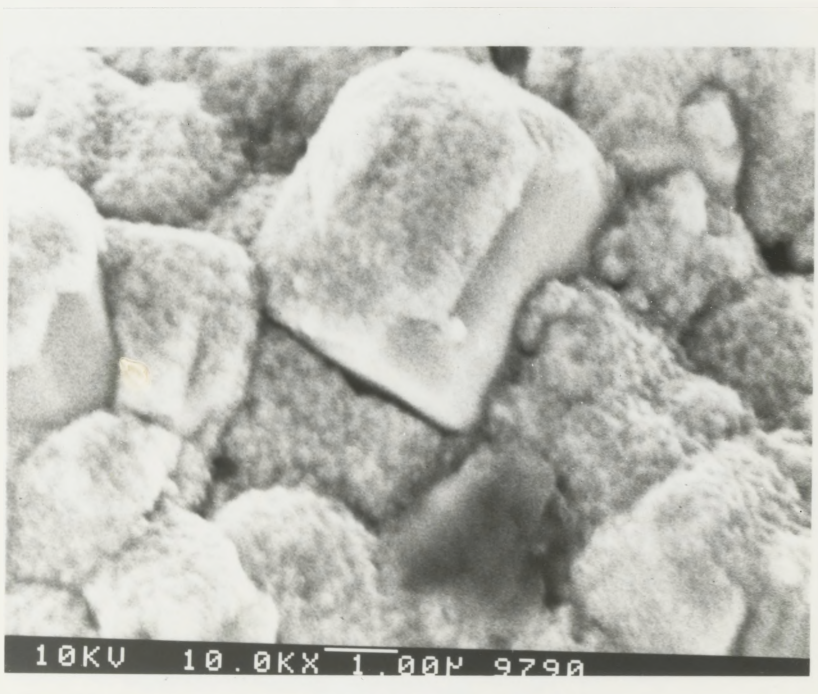

Fig 2.2 SEM image of a vacuum deposited ZnS thin film showing shadowing; a) 1 cm = 2.48 μm and b) 1 cm = 1.00 μm.

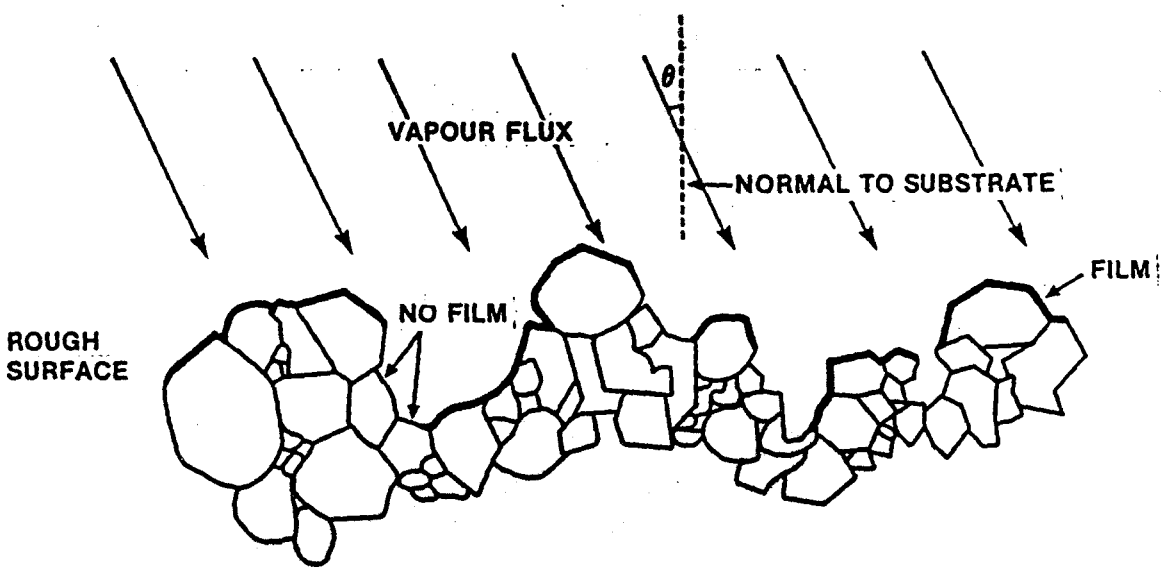

Figure 2.3

Schematic diagram showing the shadowing effect observed for thin ZnS films deposited on rough substrates. The shadowing is directional due to the angle of vapour flux θ.

consider fig. 2.3. Shown there, is an idealized view of the rough substrate. We know that, during thermal deposition (resistive and electron beam-heating), the source evaporates and these vapours condense on the substrate to form the thin film. Due to the surface roughness, some parts of the substrate do not 'see' the vapour stream. Consequently, film growth does not occur in these regions. Fig. 2.4a and 2.4b are the micrographs, taken at different magnification, of an electron-beam deposited ZnS film (sample Cer 2). Here again, the phenomenon of 'shadowing' is obvious. As seen from table 2.1, this film is approximately 150 nm thick. It may be pointed out that fig. 2.4a proves that this effect is not localized, but is observed throughout the substrate.

To see the effect of thickness on the growth pattern of the ZnS thin films, a thicker film (sample Cer 3), measuring approximately 1.5 μm was grown and then observed under the SEM. The results are now different. The film did not show any evidence of shadowing. Fig. 2.5a and 2.5b confirm the idea. This observation may be explained as follows. The films were grown with the substrate heated to 200^{o}C. Hence, surface diffusion might influence the thin film growth after a certain film thickness, leading to a more uniform coverage of the substrate. This agrees well

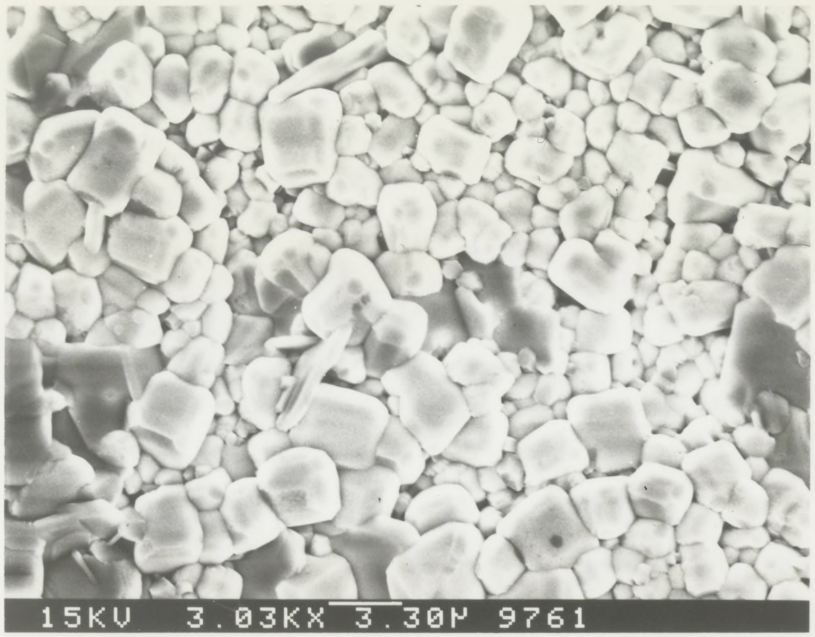

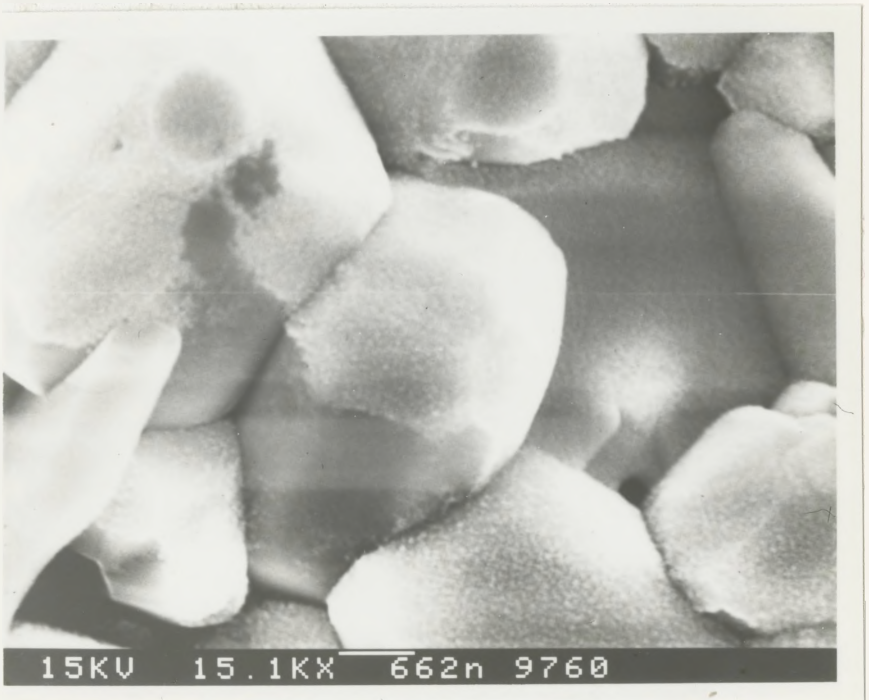

Fig 2.4 Scanning electron micrograph of a ZnS film (~150 nm) deposited by e-beam evaporation showing shadowing; a) 1 cm = 3.30 µm and b) 1 cm = 662 nm.

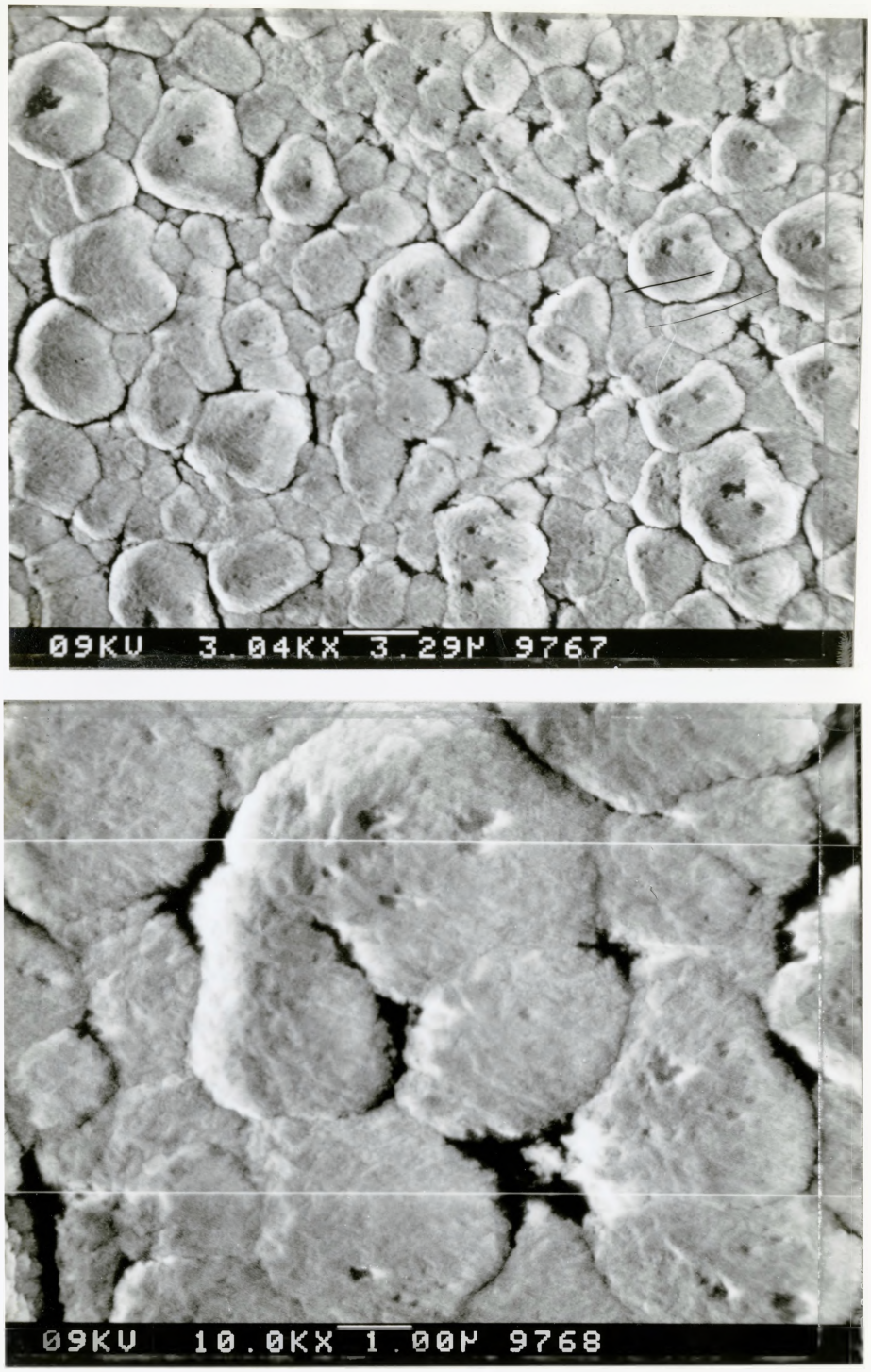

Fig 2.5 SEM images of a ZnS film (~1.5 μm) deposited by e-beam evaporation showing a more complete coverage of the substrate: a) 1 cm = 3.29 μm and b) 1 cm = 1.00 μm.

with the observations reported by Theis [21] wherein TEM analysis of electron beam deposited film showed that increasing film thickness leads to larger columnar grains and an increase in mean grain diameter. The small pit-like defects (fig. 2.5a and 2.5b) could be a result of outgassing of the sintered ceramic substrate. It is not seen in any other samples.

The third method of deposition used was atmospheric pressure atomic layer epitaxy. Use is made of the reaction between the two gaseous reactants [20], DMZ and H_2S, to give ZnS; the unreacted components are removed by flushing the reaction chamber with N_2. When the substrate is exposed to the DMZ vapour, these molecules are chemisorbed onto the substrate. A pulse of H_2S is then injected, following a N_2 purge which leads to the formation of ZnS on the substrate. It may, then, be seen that there is no possibility of any sort of shadowing to occur in case of the ALE and one would expect a uniform and complete coverage of the rough substrate. This is, indeed, the case in practice, as can be seen in fig. 2.6a and 2.6b. These micrographs are of a ~140 nm thick ZnS film grown by ALE (sample Cer 4). The film is very uniform and covers the entire substrate. A scan

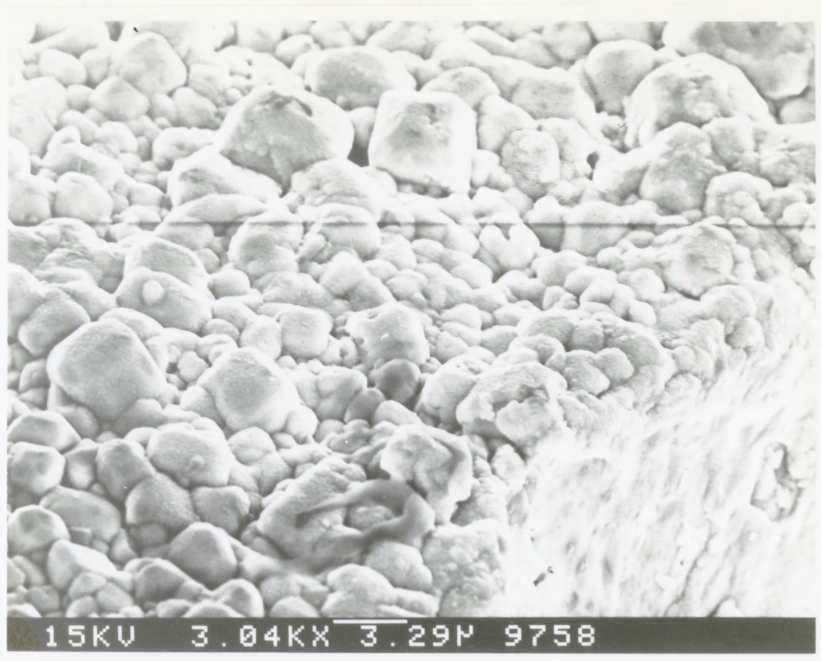

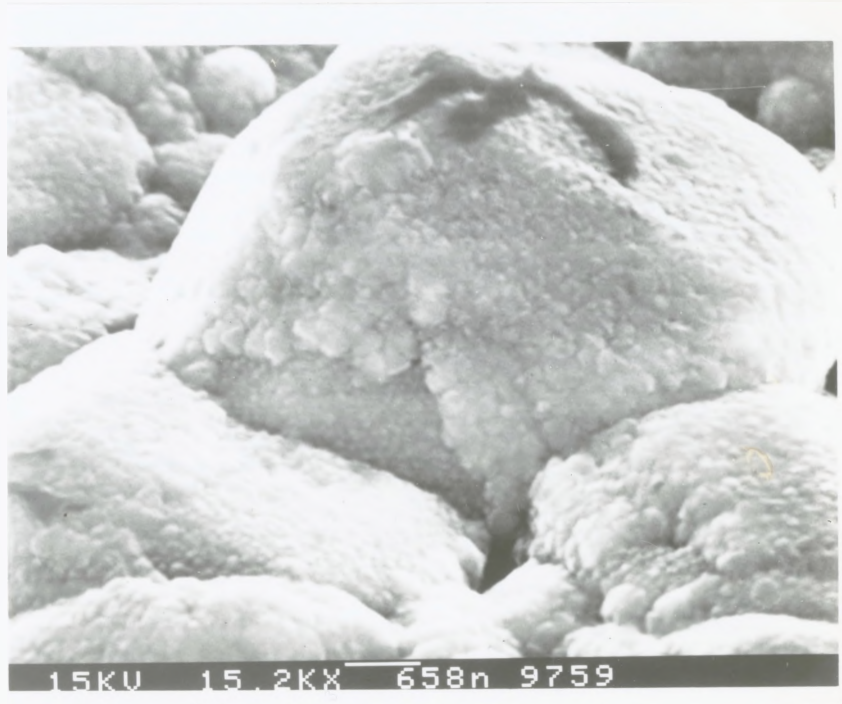

Fig 2.6 SEM images of ALE grown ZnS film (~138 nm): a) 1 cm = 3.29 μm and b) 1 cm = 658 nm. No shadowing is observed.

throughout the surface showed no discontinuities or even a slightest evidence of shadowing. It may be worthwhile to note that films of comparable thickness grown by the other two methods were non-uniform and discontinuous. Even a 450 nm thick film (sample Cer 1) exhibited shadowing. This makes the film undesirable for ACTFEL devices. Of course, an increase in the thickness tends to make the vacuum deposited and electron beam deposited film more continuous, but it should be remembered that, the optimum thickness of the ZnS:Mn layer in an ACTFEL device is often just 300 nm [5]. The above discussion clearly shows that the atomic layer epitaxy has distinct advantages for thin film fabrication on rough substrates, aimed at making thin film electroluminescent devices. As reported in [21], the crystallinity and homogeneity of these films is also very good.

The growth pattern of a thinner (~69 nm), ALE grown, (sample Cer 5) ZnS film was also investigated. The electron photo-micrographs of the same are reproduced below (fig. 2.7a, 2.7b). It can be seen that the film is not continuous, but rather a combination of minute 'droplets' or islands. It is interesting to note that these tiny 'droplets' are formed randomly on the substrate, i.e.

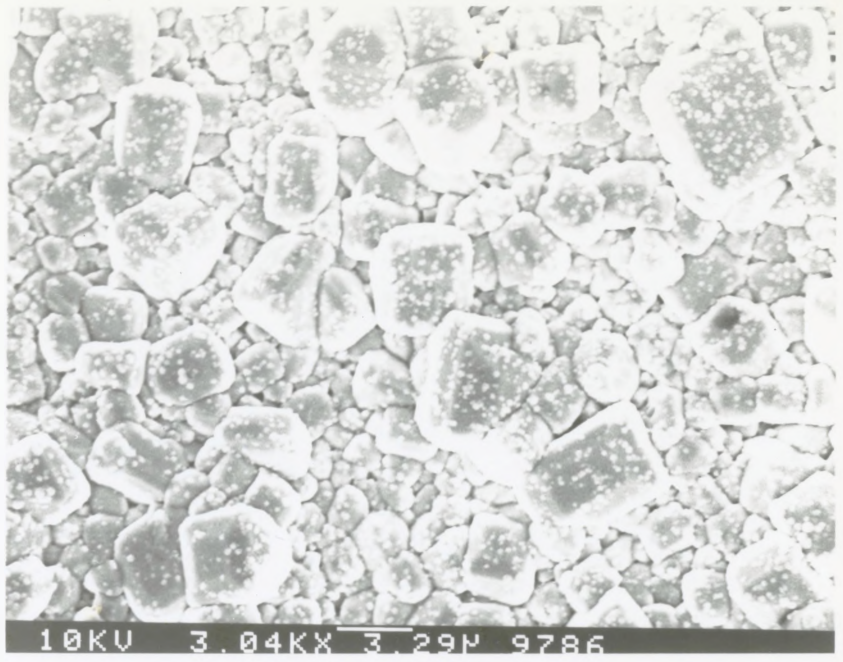

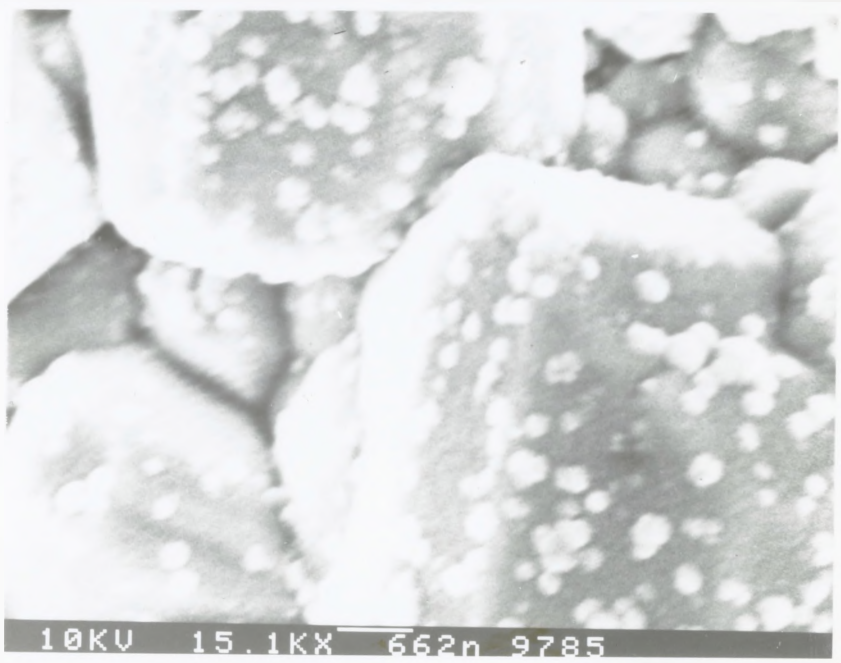

Fig 2.7 SEM images of a thinner (~69 nm) ZnS film deposited by ALE: a) 1 cm = 3.29 µm and b) 1 cm = 662 nm.

shadowing or preferential deposition is not observed. Thus, it may be concluded that, even at a lesser thickness, a spatially preferential thin film growth does not occur, when the film is deposited by the ALE.

2.5 Conclusion :

The results of this study are very encouraging. They point out the limitations of the traditional deposition techniques for the specific application quoted above. Use of ALE is recommended for ZnS thin film growth on rough substrates because discontinuities in and non-uniformity of the ZnS:Mn layer can lead to undesirable failures of the device. It should be stressed that these results are not valid when smooth substrates are used e.g. single crystal Si wafers, as in the present study of cathodoluminescence.

CHAPTER 3

THEORY OF CATHODOLUMINESCENCE

Fundamental aspects of cathodoluminescence and a detailed description of the light generating mechanism in ZnS:Mn will be discussed in this chapter. Albeit having a fairly long history of investigation (reports about luminescence in ZnS date back to the turn of the century), a thorough understanding of the process has, as yet, evaded analytic methods. Moreover, the excitation process is much more complex for cathode ray excitation than that for UV photon excitation. Scattering, energy loss during penetration,and charge cloud effects make the analysis of cathodoluminescence complex.

3.1 What happens to the incident energetic electron ?

3.1.1 Primary electron reflection :

A fraction of the incident electrons is likely to be backscattered (reflected) of the phosphor surface. Although often neglected, this process is certainly an important one. Everhart sees the process as a result of large angle Rutherford scattering [71]. The backscattering coefficient

is strongly affected by the atomic number of the phosphor rather than by the beam voltage. Tomlin [72] proposed an empirical formula for n, the backscattering coefficient of a material with atomic number Z :

$$n = (Z - 1.5)/6 \qquad \ldots(iii.1)$$

For a compound the value of Z is taken as the average atomic number of its elements. Theoretical estimates [73] lead to the values of 0.26 for zinc sulphide, which agree well with the solution of the above equation. We can then say that 26 % of the energy is lost to this phenomenon in case of ZnS.

3.1.2 Secondary electron emission:

It is important to realize that not all of the incident electrons can impart all their initial energy to the target electron. In fact an impinging energetic electron is capable of producing secondary electron(s) due to collisions. Ratio of the secondary electron current to the primary beam current behaves in a typical way with the accelerating potential, almost independent of the type of material (fig.3.1) [74]. Secondary electron emission increases initially with the beam voltage . Further increase in the accelerating potential drops the secondary electron emission.

3.1.3 Primary electron penetration:

The question about the penetration of the incident electrons is far from settled. Calculated ranges of incident

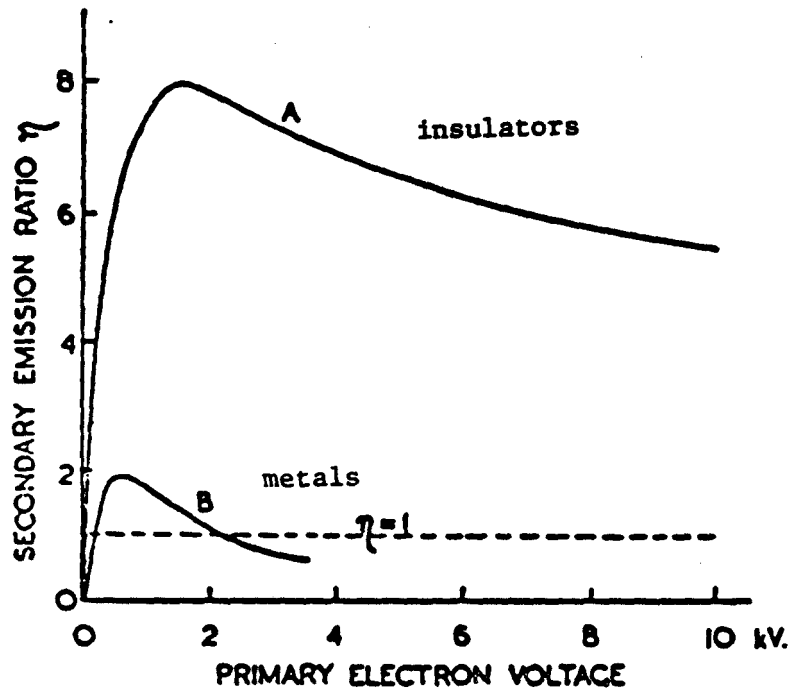

Fig 3.1 Curve showing the effect of beam voltage secondary electron emission.

(on ZnS) cathode rays based on equations i.1 and i.3 are given in table 3.1. It was discussed in section 1.2.7 that the Thomson -Whiddington law (equation i.1) gives the average range of the incident electron while equation i.3 gives the maximum range (see fig. 1.16b).

table 3.1

Calculated range of cathode rays in ZnS

Beam Voltage	Range from eq.(i.1)	Range from eq.(i.3)
1 kV	28.3 nm	6.3 nm
2 kV	113.2 nm	33.3 nm
3 kV	254.7 nm	87.9 nm
4 kV	452.8 nm	175.5 nm
5 kV	707.5 nm	299.8 nm

Experimental results of this study suggest that complete penetration of the film (˜200 nm) is achieved by 3.5 keV electrons. (see fig 5.9).

Depth of penetration of electrons in ZnS was discussed in section 1.2.7; accordingly equation (i.2) did predict a complete penetration of a ˜ 190 nm film of ZnS by 3.0 kV electrons.

3.2 Physics of Luminescence :

3.2.1 Discussion based on crystal field theory :

An impurity centre, due to its physical and chemical

properties that differ from those of the host atoms, can be thought to be a perturbed region of the otherwise regular lattice. Driven by the need of achieving a more stable configuration, the impurity atom will strive to rearrange its environment. Luminescence due to manganese which has an electronic configuration of [Ar] $4s^2$ $3d^5$ in the elemental state and [Ar] $3d^5$ in the Mn^{2+} state, is typical of an activator with an incomplete electronic shell.

The ground state of the free Mn ion is ^6S while the excited states are ^4G, ^4P, ^4D and so on. When the ion finds itself in a crystalline environment, some of the states split. The extent of splitting is determined by the type and strength of the crystal field. Mention should also be made about the influence of strain on the crystal field splitting. Parrot et al [75] have reported seeing shifts of 8.28 cm^{-1} in the splitting of Mn^{2+} level ^4E when ZnS:Mn single crystals were subjected to a uniaxial stress of 3.6×10^8 N/m^2.

For the case of our interest - ZnS:Mn - the field is cubic, in which the 4G state splits into $^4T_1$, $^4T_2$, $^4A_1$ and 4E (See fig 3.2). Shionoya argues [2] that only the first two levels i.e. $^4T_1$ and $^4T_2$, are dependent on the strength of the crystal field.

Let us now see the relative position of the Mn $3d^5$ levels with respect to the ZnS valence band edge. The diagram, due to Gumlich et al [76] is shown (fig 3.3). As

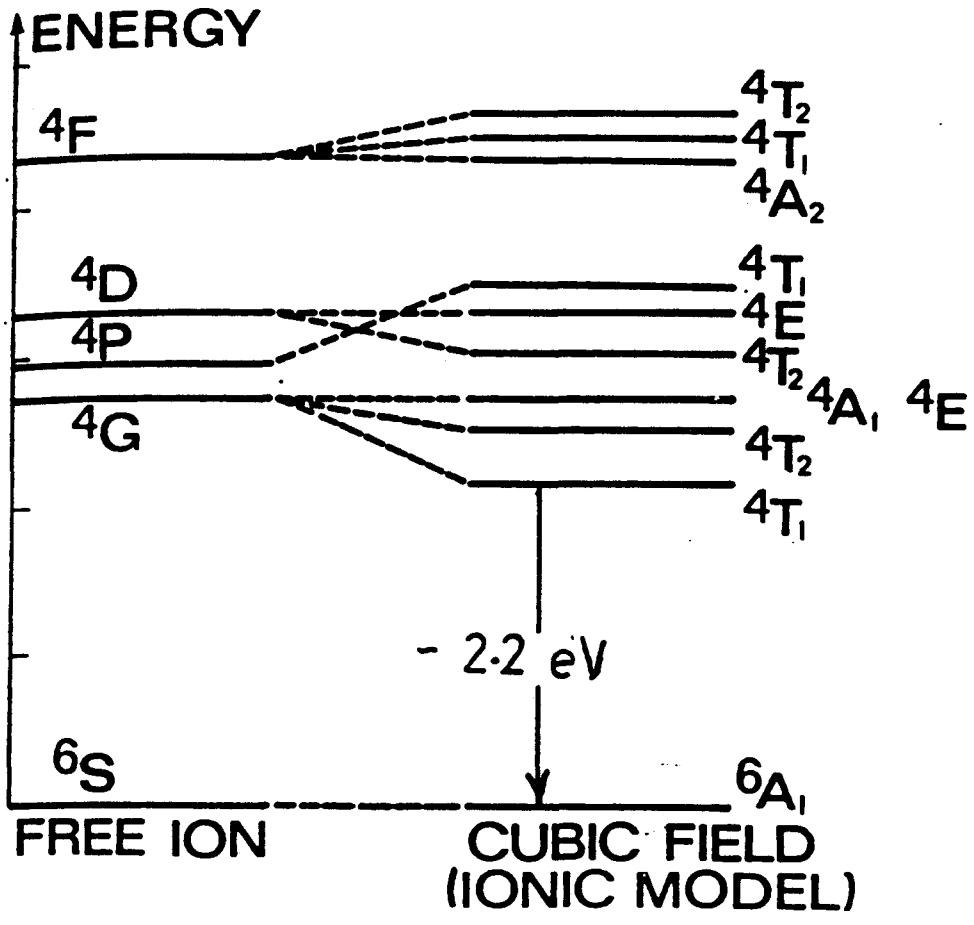

Fig 3.2. Energy levels of Mn^{2+} : a) free ion and b) in a cubic field of ZnS. Note the splitting of the various levels; yellow luminescence is a result of the transition shown.

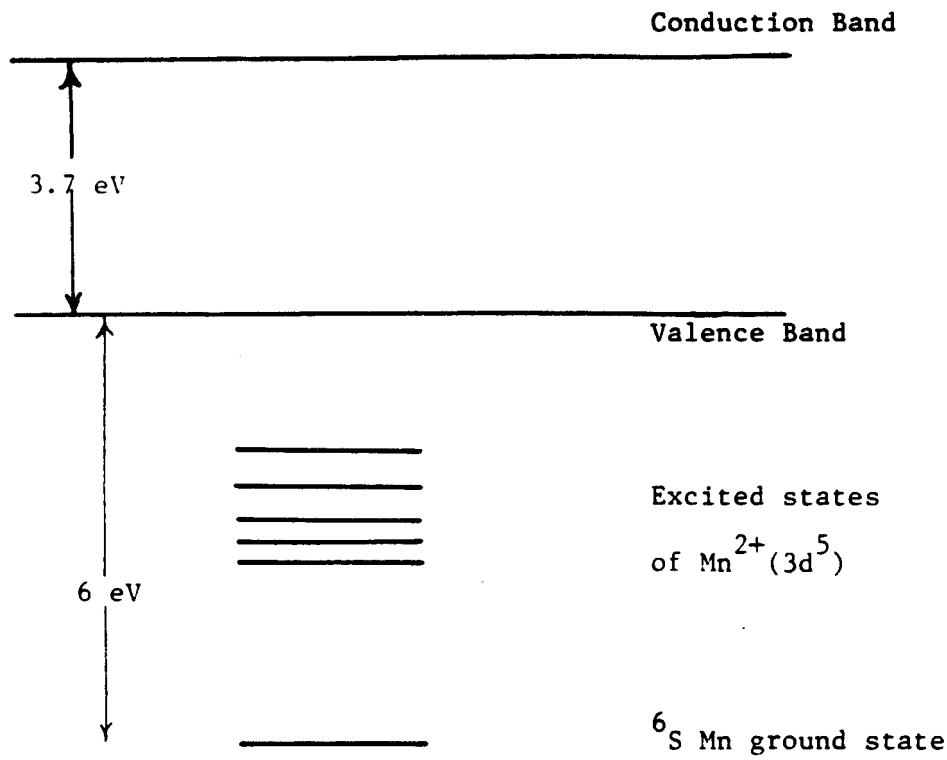

Fig 3.3 Band diagram of ZnS:Mn illustrating the energetic locations of the d levels of Mn^{2+} , after Gumlich et al [76].

seen, the ground state of Mn^{2+}, ^6S, lies about 6 eV below the valence band edge of the host - cubic zinc sulphide. It should also be noted that all the excited states of the Mn ion lie within the populated band of the wide band gap semiconductor. It is the transition $^6A_1(^6S)$ - $^4T_1(^4G)$, with an energy difference of ~2.1 eV, that gives rise to the characteristic yellow-orange emission of Mn. It must be remembered that the energy of the transition to $^4T_1$ and $^4T_2$ states decreases with increasing crystal field strength.

Study of the absorption spectra shows [38,76] the presence of five bands due to Mn^{2+}. Each of these can be associated to a particular d-d transition. See fig 1.3 for details. All transitions mentioned above are forbidden in the free ion state. In the crystal they are allowed, because of the crystal field perturbations, phonon-couplings and spin-orbit interactions.

We have seen that in the impurity activated phosphors, the intraband transitions of the activator is the dominant mechanism leading to luminescence. At the same time, if the energy absorbed by the host crystal is substantial, band-band transitions may occur in the host. In presence of traps, the excited electrons will decay, emitting characteristic radiation (depending on the value of E_g). For ZnS:Mn, the blue emission (corresponding to the band gap of ZnS) decays completely after 10^{-5} sec. It is the conventional yellow emission which dominates afterwards. A

similar observation was reported by Skolnick [78]. TRS of the emission of ZnS:Mn dc pulsed EL revealed the existence of two distinct bands. In addition to the yellow band at 2.1 eV, a very broad band extending from near the band gap of ZnS (~ 3.6 eV) to ~ 1.5 eV which vanishes after ~15 - 20 μsec (see fig 3.4) was detected. Skolnick attributes this band to the interband transition of the excited (hot) electron.

3.3 Scattering of the emitted light in the film :

Internal scattering of the light decreases the overall efficiency of the luminescent film. Light generated will either be reflected back into the film by the film surface or be transmitted, the choice being dependent on the critical angle as well as the angle the ray makes with the surface. It is evident from fig 3.5 that total internal reflection and scattering would account for a substantial loss of light generated. According to Leverenz [74], the portion ,f_e, of the total radiation f_t, which is emitted from both sides of the 'thin screen' of the phosphor is

$$f_e = (1-\cos\theta_c)\ f_t \qquad \ldots(iii.2)$$

where θ_c is the half angle of the cone of the light detected. For the present case, the emission was only from one side (top) of the ZnS thin film, hence the portion escaping from one side will be

$$f_e = (1-\cos\theta_c)\ f_t/2 \qquad \ldots(iii.3)$$

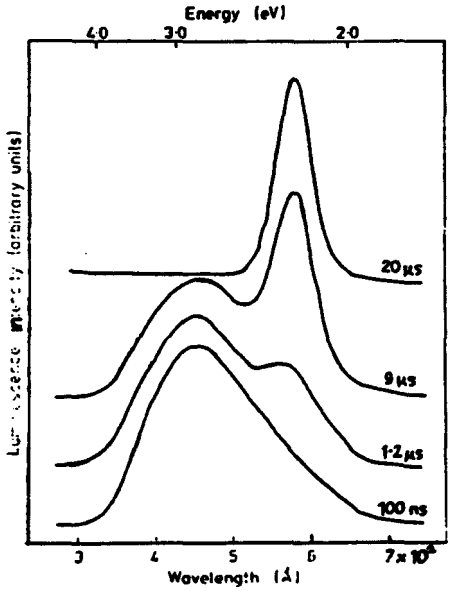

Fig 3.4 Time resolved EL spectra of ZnS:Mn; the blue broad band emission due to band-band excitation may be noted, after Skolnick [77].

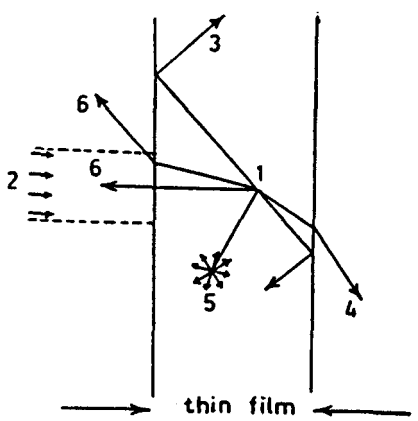

1: luminescent centre
2: electron beam
3: total internal reflection
4: light escaping from other side of the film
5: scattering
6: observed light

Fig 3.5 Schematic of the 'future'of an emitted light beam in a thin film excited by electrons.

If the refractive index of the material,in vacuo, is n, then $\sin\theta_c = 1/n$. Equation (iii.3) now can be written as

$$f_e = f^t[1 - (1 - n^{-2})^{1/2}]/2 \qquad \ldots(iii.4)$$

For the case of our interest (ZnS), n = 2.4; equation (iii.2) then gives,

$$f_e/f_t = [1 - (1 - 2.4^{-2})^{1/2}]/2 \qquad \ldots(iii.5)$$

$$= .046$$

Accordingly, to a first approximation, only 5% of the emitted light will be 'seen' from one side of the film.

3.4 Efficiency :

Non radiative energy transfer processes, internal scattering and backscattering of the primaries are some of the processes of energy loss competing with the cathodoluminescent process. Practical efficiencies for cathodoluminescence rarely exceed 25 %.

The absolute overall CL efficiency is given by [76]

$$t = \frac{(1-\eta)E_g}{E} \frac{\{\text{emission photon energy}\}}{E_g} \qquad \ldots(iii.6)$$

where E (also called minimum ionization energy) is the mean energy for the production of a free-electron and a free-hole pair, which for ZnS is estimated [77]to be $\sim 3E_g$ and η is the optical efficiency of the luminescent centres (η = 0.26 for ZnS according to [73]). Substituting the appropriate values for ZnS the overall maximum efficiency is calculated to be

14.1%. The experimental value of 4.5 % [83] is slightly different, probably due to numerous other factors not accounted for in equation (iii.6).

After a rather brief theoretical explanation of the phenomenon of cathodoluminescence (CL), the next chapter deals with the experimental set-up for the fabrication of thin films as well as CL measurements.

CHAPTER 4

EXPERIMENTAL : DESIGN AND TECHNIQUES

A detailed description of the experimental set-up will be given in this chapter. It would be appropriate to discuss the two fundamentally separate experiments viz. thin film growth and cathodoluminescence under different sections. What follows is the discussion of the experimental procedure and equipment used for the deposition of ZnS:Mn thin films. Section 4.2 deals with the latter.

4.1 Deposition of ZnS:Mn thin films :

4.1.1 The vacuum system :

The vacuum system used a diffusion pumped unit modified to adapt it to the specifications defined by the particular experiment.

A schematic of the system is shown in the accompanying figure 4.1. A pyrex cylinder (590 mm high, 470 mm diameter) sandwiched between two stainless steel (SS) plates constitutes the deposition chamber. The bottom plate is 18 mm thick and the corresponding dimension of the top plate is 12 mm. Both the plates have an identical diameter

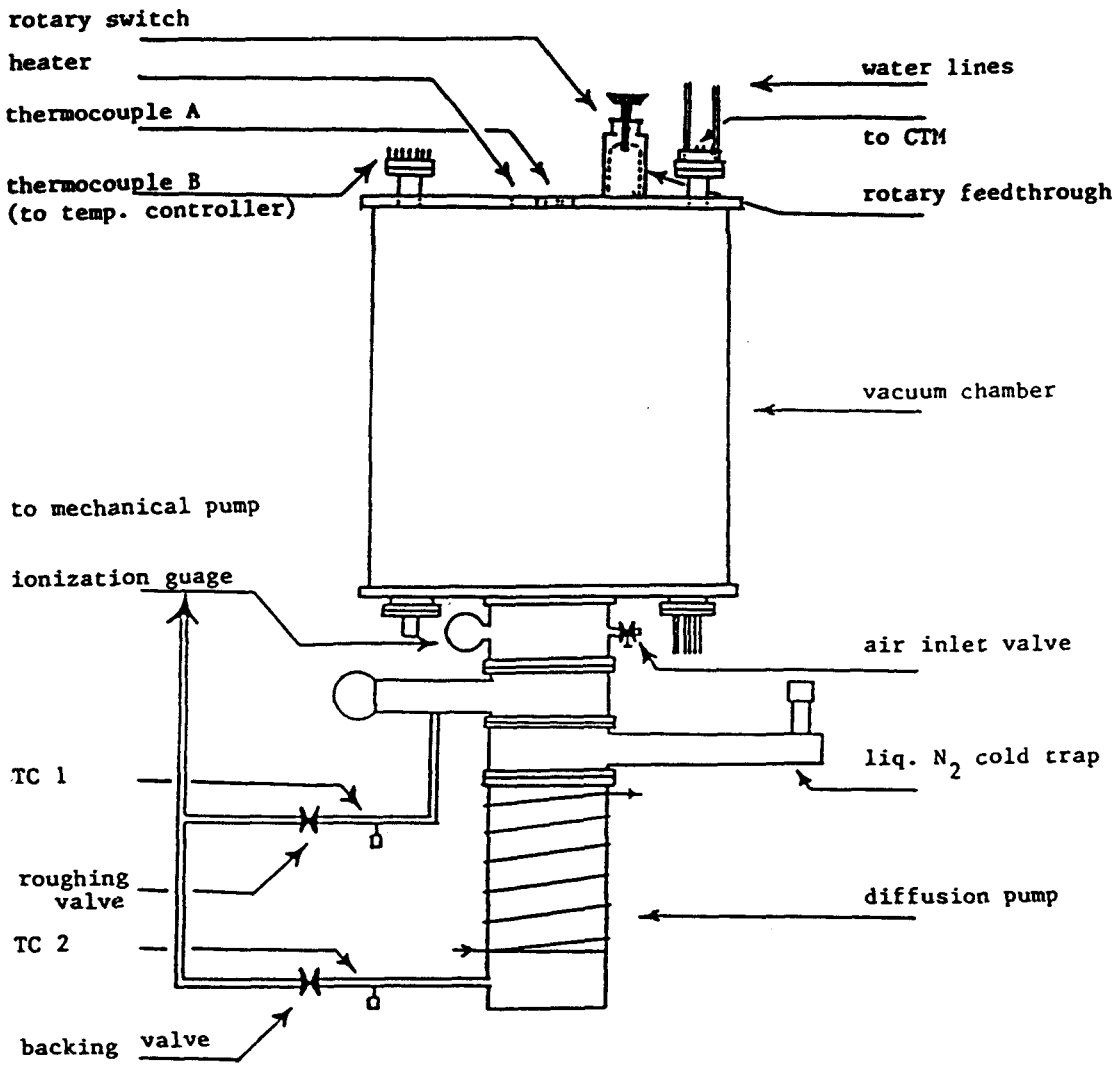

Fig 4.1 Schematic of the vacuum system

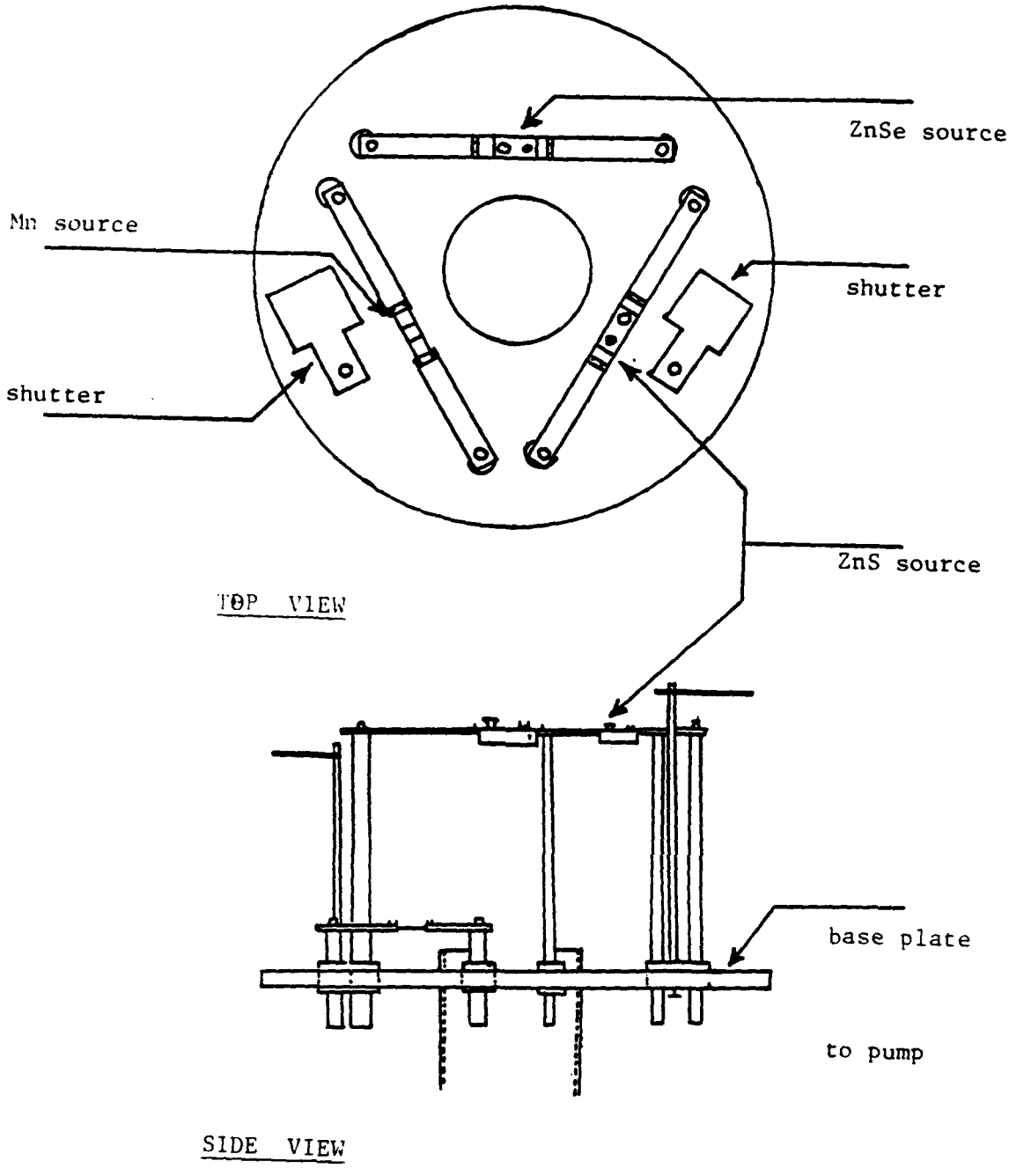

Fig 4.2 Details of the vacuum chamber.

of 500 mm. To ensure a leak proof vacuum seal, the plates were specially machined to yield a smooth surface. Key High Vacuum products, USA supplied the viton gaskets used for the seal.

A mechanical pump (Sargent Welch, model 1370) was used to attain the initial low vacuum. Further decrease in pressure was obtained using a NRC water cooled diffusion pump, equipped with a liquid nitrogen cold trap (speed 750 l sec^{-1}, model HS4 750). The operation of the two pumps was controlled by manually operated solenoid valves (labelled as 'roughing' and 'backing' in fig 4.1) and a pneumatic gate valve. Pressure at various positions in the system could be read on the CVC ionization gauge, GIC 110B, the sensing units being two thermocouple gauges TC1 and TC2 (GIC 004, capable of quite accurate readings until 10 μm) and an ionization tube of the type described in [82] manufactured by CVC, USA.

The chamber housed a substrate holder and three evaporation sources (fig. 4.2). The three different sources were designed to evaporate ZnS, ZnSe and Mn. For ZnS evaporation the source was a modified, commercially available Ta boat (R.D.Mathis, USA). A calibrated single phase transformer served to input a variable current, up to a maximum of 300 amp, to the evaporation sources through a high vacuum electrical feedthrough (Huntington, USA). To facilitate the recording of the boat temperature, a chromel-

alumel thermocouple was spot welded to the boat and connected to a Omega digital temperature controller. A SS shutter, to control the vapour flux, was placed over the evaporation source.

4.1.2 Design of the top plate :

Study of the effect of manganese concentration on the cathodoluminescent properties of ZnS thin films was of primary interest. The intention was to investigate ZnS:Mn samples with different levels of Mn doping (0.08 wt% - 25 wt%). A straightforward method would be to prepare the different samples, individually. It is obvious that this method is extremely time consuming, not to mention its accuracy limitations due to the unavoidable changes in the deposition conditions.

A special system was designed to overcome the problem. The new design ensured a uniform and homogeneous film growth and a calibrated method for Mn doping.

As seen from fig 4.3, the assembly consists of a solid Cu block (175 mm x 90 mm x 12 mm) welded to a hollow 304 stainless steel cylinder with a wall thickness of 1.6 mm. A solid Cu cylinder was brazed to the flat copper block. Two holes were bored through this cylinder to house the cartridge heater (Chromalax CIR 2020) and a thermocouple (marked 'A' in fig 4.3). Thermocouple B was connected to an Omega temperature controller in conjunction with the heater,

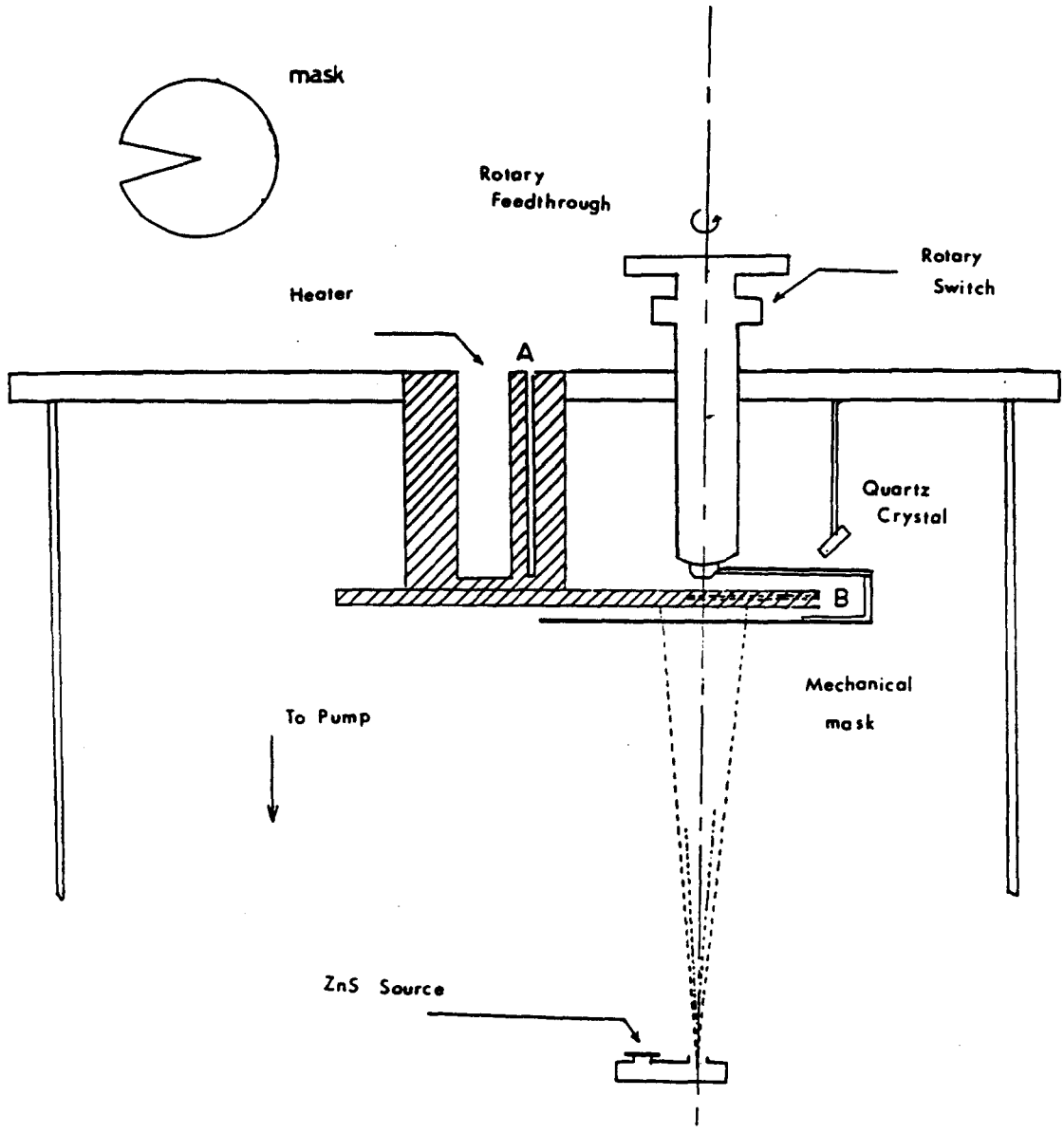

Fig 4.3 Side view after taking a vertical section of the top plate; in the inset is the mask.

to monitor the substrate temperature. The air gap between the Cu and SS cylinders acts as an insulator and prevents any possible overheating of the SS top plate.

This assembly was welded to the top plate such that the substrate, rotary feedthrough, rotary switch and the evaporation source would be coaxial. An arrangement of this type leads to a uniform thickness of ZnS (or Mn, as the case may be), concentrically. A 16 position, manually operated rotary switch was coupled to the rotary feedthrough, at the end of which was attached the mechanical mask. The top view of this 304 SS, 1.6mm thick mask is shown in the inset of fig.4.3.

In situ monitoring of the film thickness was done by the Sloan quartz crystal thickness monitor (model 200) using 5 MHz crystals. A high vacuum water - BNC feedthrough made possible the flow of cold water and electrical connections to the crystal oscillator inside the chamber. The crystal was placed as close to the substrate as possible.

The CTM unit utilizes piezoelectric properties of quartz. Contact is made on the two sides of a thin quartz wafer. Shear oscillations are induced by the ac field which cause it to resonate at a frequency f, dependent on the propagation velocity of the elastic wave (v_o) (in the direction of the thickness) and d the thickness of the wafer, as

$$f = v_o/2.d \qquad .....(v.1)$$

Addition of a small mass on the crystal will change its resonance frequency. Knowing the density of the material being deposited, film thickness may be calculated.

4.1.3 Choice of the substrate :

The ZnS films were grown on single crystal, n-type (111) Si wafers (Monsanto Co., USA). The maximum resistivity of the 76 mm diameter wafers was 7 Ω-mm and the thickness 20 mils (1 mil = 1/1000 inch). For the study of its luminescent properties, ZnS is usually deposited on ITO (indium tin oxide) coated glass. Ceramic substrates have also been used, especially to fabricate ACTFEL devices [68].

Si was chosen keeping in mind its semiconducting properties. Any problems arising due to charging of the sample during CL and auger electron spectroscopy (AES), could then be avoided.

A clean substrate is necessary to ensure a uniform thin film growth [83]. Presence of dust particles or other foreign materials is detrimental to thin film quality.

The following procedure was adopted to clean the Si wafer: as received wafer was first immersed and then rinsed with acetone. Following this it was blow dried with dry air and cleaned with concentrated HCl. The residual acid on the surface was rinsed with deionised water. This step would be repeated 3-4 times to attain a dust free surface. Acetone

was then used to rinse the substrate, after which it was blow dried with dry air. Finally the Si wafer was rinsed in methanol and blow dried as before. If any foreign particles were detected visually, all the steps outlined above were repeated till a dust and grease free surface was obtained. No effort was made to remove the native oxide, estimated to be about 40 Å thick.

The clean wafer was then mounted on the substrate holder, polished side facing the evaporation source. Careful alignment of the top plate was done ; the Si wafer and the source were coaxial.

4.1.4 Procedure of deposition of ZnS thin film :

Prior checking of temperature controllers, thermocouple gauges, CTM etc was necessary, after which the Ta boat was filled (50 % - 80%, subject to the desired film thickness) with phosphor grade, ZnS powder (99.9%) obtained from Johnson Mathey, Canada. The clean wafer was then mounted on the sample holder, polished side facing down. The viton gaskets were cleaned and greased (apiezon vacuum grease) to get a good vacuum seal. The system was pumped on by the mechanical pump until the backing pressure reached ~100 microns when the gate valve was thrown open. Before opening the gate valve (which allows the diffusion pump to work on the system), the cold trap was filled with liquid nitrogen. Intermittent filling was required throughout the

deposition period.

The ZnS source was gradually heated, once the chamber pressure has reached ~10^{-5} T. Extreme care needs to be taken here because a higher rate of heating would shoot up the chamber pressure. The temperature of the boat could be read on the Omega controller and the current flowing through on the ammeter. Typically it took about 100 - 120 minutes to attain a boat temperature of 900 - 940 °C at an average pressure in the 10^{-6} T range. The current at this point would normally be about 260 - 300 amp, depending on the age of the boat (because the resistance of the boat changes with ageing due to sulphurization). Simultaneous heating of the substrate was accomplished by the controller - heater - thermocouple assembly. It is known that the crystallinity of the ZnS film is superior when the substrate is held at ~ 200°C [10]. Keeping this in mind the substrate temperature was maintained at ~ 200°C during the deposition. The shutter was not opened until after the start of ZnS evaporation, so as to allow a constant evaporation rate to be attained. It was closed when the desired film thickness was achieved. Premature opening of the shutter invariably spoils the quality of the film. The thickness of the film could be indirectly read from the CTM. Direct reading is not possible due to the difference in the:

i) temperature of the substrate and the quartz crystal, and hence the sticking coefficient and

ii) that in its position with respect to the ZnS source The calibration factor was determined the following way: thickness of the films grown under identical conditions, without disturbing the position of the quartz crystal was determined by the alphastep. The ratio of the exact thickness to that displayed by the CTM gives the calibration factor (0.33 in this case).

After achieving the desired thickness, the shutter was closed and the substrate heater turned off. The current through the boat was gradually decreased to zero using the transformer. The vacuum was not broken till the substrate cooled to ambient temperature. The reason is obvious : surface oxidation may take place if the heated substrate is exposed to atmosphere. Typical deposition conditions are outlined in table 4.1 .

table 4.1

Press.	Boat curr.	T_{sub}	time	thickness	rate
$2x10^{-6}$ T	270 amp	200°C	700 s	1500 Å	2.1Å/s

The Si wafer with a ZnS thin film on it, was then stored in a desiccator under vacuum, after determining the exact thickness of the thin film by the alpha step (tencor instruments, USA).

The instrument compares the vertical movements of the stylus travelling across the sample, with that on a 'flat'

reference surface. The signal is converted to an electrical pulse, is amplified and fed to the chart recorder. It is clear that the use of this method necessitates the presence of a 'step'(for the 'flat' reference surface) on the sample. Placing a broad clip to hold the wafer on the Cu block automatically created the required step. AES and RBS later confirmed the thickness measured by the alphastep.

4.1.5 Doping with Mn :

In spite of taking all the precautions, not all the films were of an acceptable quality. Only those, free from any type of visual defect were used as hosts for the Mn dopant. The doping procedure is outlined in the following paragraphs.

It was mentioned before that Mn was incorporated in ZnS by thermal diffusion of a known amount of Mn. The ZnS film was cleaned by dry nitrogen following the usual pre-deposition checking (section 4.1.4) of the vacuum system. The rotary feedthrough, rotary switch and the mask were installed in position. Boat #3 (fig 4.1), whose design was different than that of the ZnS source served as the Mn evaporation source. Four nines pure Mn powder (Metron) was the source material.

The pumping procedure followed was identical to that previously described (section 4.1.4). The amount of manganese to be deposited being very small, the distance

between Mn source and the substrate was much more than that for ZnS. Knowing the thickness of the parent ZnS thin film, that of Mn can be calculated by straightforward manipulation, to yield a specific doping level. As an example : for a 2000Å host film and 1 wt % Mn doping, a Mn film thickness of 1 Å is required. If the calibration factor of the CTM is 0.66 (determined in a fashion similar to that for ZnS) the corresponding CTM reading should be 2 Å. Remember that Mn is deposited only on that part of the ZnS film not covered by the mask. By changing the position of the mask (using the rotary switch), a different portion of the film could be exposed to Mn vapour every time. Hence it was possible to prepare as many as 16 samples, with a different level of Mn doping in each, from a single ZnS film. As the samples were prepared from the same ZnS parent film, the thickness and the surface morphology was identical. In other words, in one set of samples virtually everything but the manganese concentration was identical. This allowed a better comparison for the electro-optic properties; the difference in them attributed solely to the change in Mn concentration. All the samples, of a set, were prepared in a single vacuum pumpdown, eliminating contamination due to air pressure.

It may be pointed out that Mn deposited this way stays on the surface, while we are interested in a homogeneous and random distribution of Mn in the parent ZnS.

The next step is to carry out thermal diffusion of Mn. Hurd and King [6] have reported that a fairly homogeneous distribution of Mn in ZnS can be accomplished by annealing the 300 nm film at 400°C for four hours. The extent of Mn diffusion is further discussed in the next chapter. For the present study, annealing was carried out in two stages. First the film was vacuum annealed in the deposition chamber at 345 ± 2°C for four hours. After cooling the film to room temperature, the sample was removed. The individual samples were then cut using a diamond scribe and clean glass slides. The second anneal was carried out in a nitrogen tube furnace for two hours. The flow of N_2 was maintained at 5 cc/sec and was started 15 min before inserting the samples to drive the residual oxygen. The samples (now individually cut) were mounted on a quartz boat and heated to 400 ± 2°C for two hours. They were allowed to cool to the ambient temperature, still in a nitrogen atmosphere. It is necessary to take these precautions as Mn is known to be extremely reactive with oxygen. Despite the extensive precautions RBS and AES showed the presence of oxygen in those samples with a higher Mn content. The films with a lower Mn content were, however, almost entirely free of oxygen. Sands et al [82] have also reported detecting O_2 in their ZnS films.

The samples, now ready for further analysis, were stored in a desiccator under vacuum. To avoid any possible errors, the area close to the edges was neglected during CL,

AES, RBS etc.

It must be stressed that the method adopted here,has a tremendous advantage of having the same conditions throughout sample preparation. Exact concentration of Mn was latter confirmed by RBS, AES and NAA.

It is essential to appreciate the advantages of the indigenously designed assembly described above:

i) A uniform film can be grown on a substrate as large as 70 cm^2.

ii) the rotary switch along with the CTM gives a relatively easy and reliable method of doping various materials

iii) the number of samples doped in one run is limited only by size of the substrate and mask (as many as 16 samples could be doped simultaneously during the experiments)

iv) a post deposition vacuum anneal (up to 345 °C) to favour Mn diffusion was possible.

4.2 Cathodoluminescence measurements :

4.2.1 Experimental set-up :

Shown in figure 4.4 is a schematic of the experimental set up used for studying the cathodoluminescent properties of the ZnS:Mn films. The assembly consists of a SS main chamber (vacuum generators' 6-way high vacuum connector XXF38) meant to house the samples. The chamber is

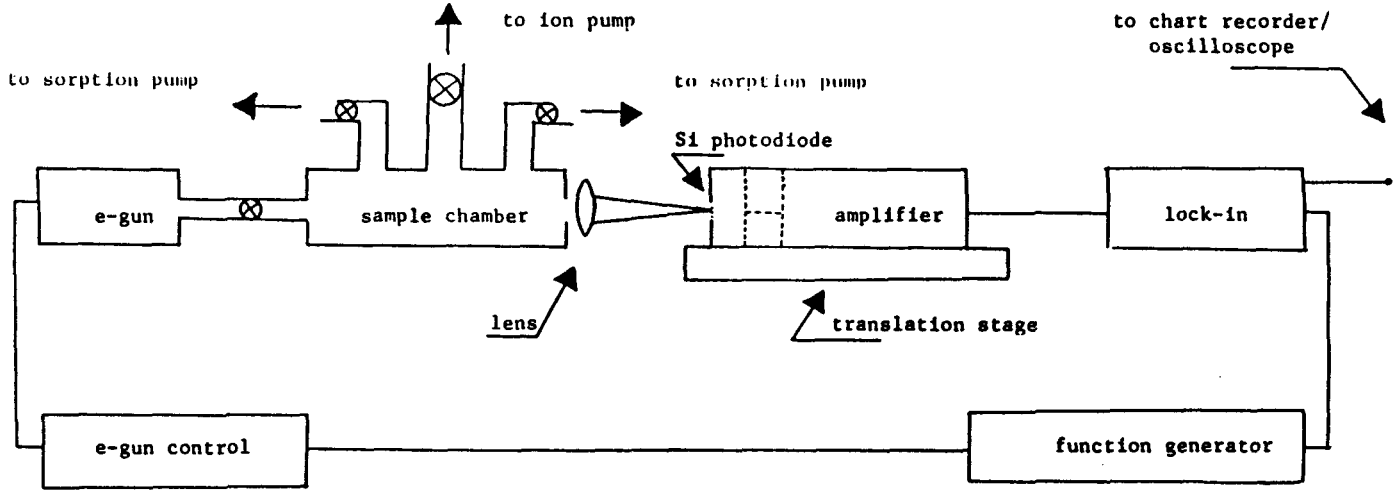

Fig 4.4 Schematic of the experimental set-up for cathodoluminescence

connected to two liquid nitrogen cooled sorption pumps (Varian, 941-6501) used to attain mechanical vacuum and an 110 l sec^{-1} varian ion pump to obtain and later maintain a high vacuum. A Perkin-Elmer grazing incidence (model 04-015) electron gun is attached to the chamber via a straight SS nipple. The electron gun is surrounded by μ-metal to reduce the effect of the surrounding magnetic field. The chamber is also equipped with an air release valve and a transparent window, that serves as a viewing port. The electron gun is isolated from the rest of the system by a gate valve and so is the ion pump. The samples could be mounted on a specially fabricated brass sample holder attached to a high vacuum linear feedthrough. This allowed the simultaneous analysis of more than one sample, without breaking the vacuum because movement of the feedthrough would bring the desired sample in line with the electron beam.

The electron gun used was controlled by a PHI 11-110 gun control unit. Beam voltages from 0 - 5 kV in calibrated steps of 500 volts were available. Fine control could yield intermediate values, if desired. The unit was capable of controlling the deflection (x-y plane), current and focus of the beam. The control unit had a inherent chopper circuit, which is necessary to get noise free and accurate measurements.

A lock-in amplifier (Stanford Research Systems, model

SR 510) was used in conjunction with the gun control module to measure the CL signal intensity. A modulating signal to the lock-in was applied through the gun control unit; a Philips function generator provided reference signal. A toggle switch controls the operation of the gun: one position (d(N(E))/dE) turns it rapidly ON and OFF at a predetermined rate, while the other [N(E)] allows it to stay continually ON. We know that measurement of low-level signals immersed in noise is extremely difficult by conventional techniques. Use of a lock-in amplifier can overcome the problem and allow accurate and reliable measurements even if the S/N (signal to noise) ratio is very low. The instrument consists primarily of a phase sensitive detector, a low-noise amplifier and a phase shifter. More elaborate explanation may be found in Appendix A.

The reference signal applied was a 1.5 V, 1 kHz square wave. Output of the detector unit, a voltage signal which is a direct measure of the CL intensity, was fed to the lock-in. To reduce the noise level, all possible instruments creating an ac - noise were kept at a distance. Saturation of the Si detector would occur in ambient light, hence all the experiments were performed in dark. The noise level was further reduced by using the line frequency notch filter and an auto tracking bandpass filter in the lock-in. The notch filters have a Q of 10 and a rejection rate of at least 50 dB. The obvious consequence is an increase in the

dynamic reserve. The bandpass filters, having a roll off of ± 6 dB and a Q of 5, can add upto 20 dB of dynamic reserve for noise signals outside the pass band. There are two post demodulator low pass filters, called pre- and post filters, each providing a 6 dB/oct attenuation. The control panel allows a manual adjustment of the time constant of these filters. Typical values were 3 sec for the pre- and none for the post filter. The phase shift between the reference oscillator and the detector signal should be adjusted. From appendix A it is clear that a maximum (and accurate) signal is obtained at an unique optimum phase shift.

It was stated before that the main chamber was equipped with a transparent window, to make the measurement of light intensity possible. To improve the results, a collimating lens (f = 25 mm) was placed next to the window, with the intention of collecting a maximum amount of light. The intensity of the light was detected using a Si photodiode and a lock-in amplifier.

The circuit diagram of the detector assembly is shown in the inset of fig.4.5 a. Operation of the circuit is easy to understand. Light energy incident on the active area of the diode, induces a photocurrent and hence a potential is developed across the cathode and the anode of the diode. This signal is amplified using a 741 type op-amplifier and a load resistor (470 kΩ). Capacitors in the circuit help to damp the oscillations created.

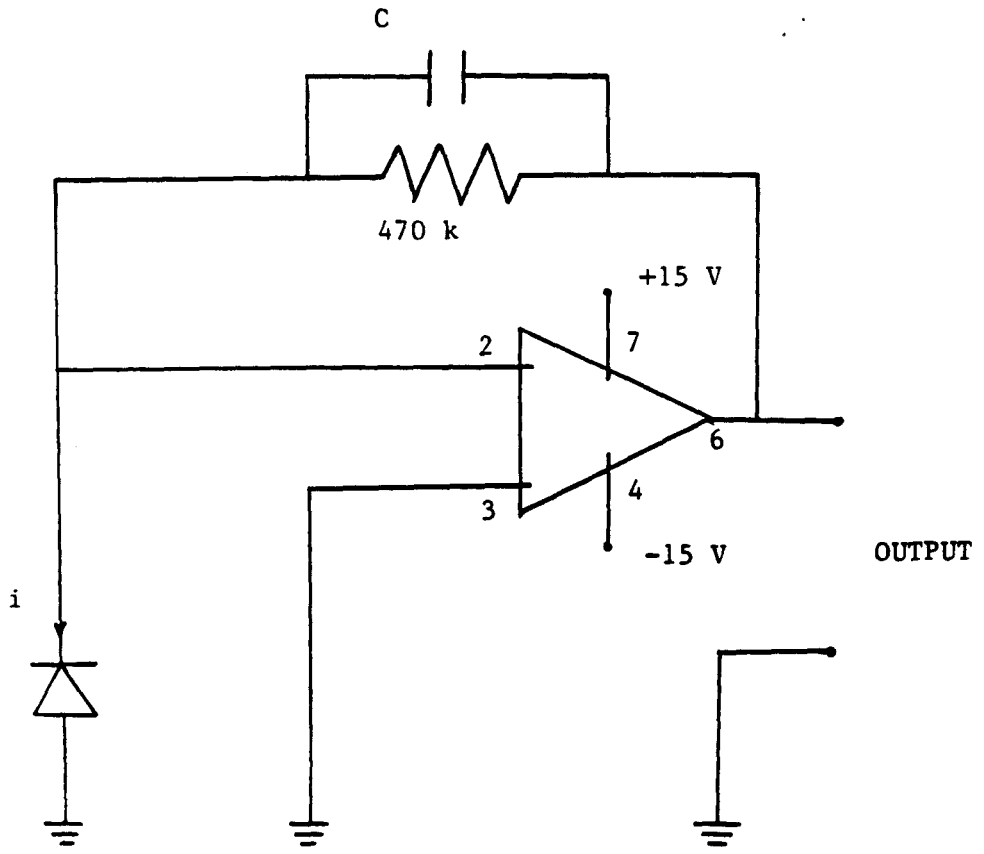

Fig 4.5 a Circuit diagram of the detector unit.

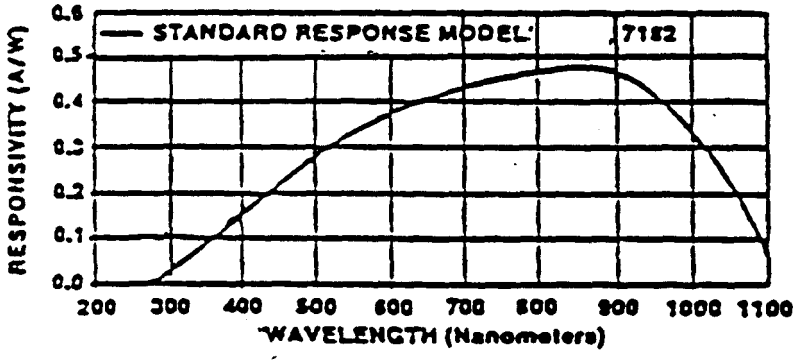

Fig 4.5 b Response curve of the photodiode used in the detector unit.

The diode (Oriel, Si 7182) has an active area of 100 mm^2. The choice of the diode reflected the need for a wide band spectral response, good sensitivity and an area sufficient to capture all the light. The response curve for the same is reproduced in fig 4.5 b. The whole unit was mounted on a x-y-z translation stage capable of a maximum of 2.5 cm displacement in any direction. The experimental apparatus was not disturbed throughout all the experiments because change of experimantal conditions might have lead to erroneous results.

One of the samples in every set (two individual sets of samples were analyzed) was taken as an internal standard. Observations were recorded for the standard and the sample(s), simultaneously. A comparison of the normalised (intensity of sample/intensity of the std.) CL intensity was done, rather than that of the absolute intensities. Elimination of an error due to the slight changes in the experimental conditions e.g. a change in the beam current or energy etc. was thus possible.

4.2.2 Measurement of the CL intensity :

Let us now discuss, in brief, the procedure of recording the intensity of cathodoluminescence of ZnS:Mn thin films. The samples shaped like a sector of a circle (due to the shape of the mask), were cut in two. Before analysis, the film would be cleaned by dry nitrogen. As

mentioned in the last section, an internal standard was used in every set of experiments. A maximum of four samples: one standard and three samples could be mounted on the brass sample holder at one time. The holder was connected to a 2-3/4 inch flanged high vacuum linear feedthrough. The whole assembly was then mounted on the main chamber such that the electron beam would impinge on the samples at ~ 45°. A viton gasket was used to achieve a leak proof seal between the feedthrough and the 6-way connector.

Making sure that the air inlet valve was closed, the liquid nitrogen cooled sorption pump was connected to the system by opening the connecting valve. Action of the pump was stopped after the chamber pressure had reached ~ 20 microns, indicated by a Granville-Philips 275 convectron gauge. Ensuring that the voltage of the ion pump does not drop below 2 kV, the gate valve connecting the ion pump was thrown open. After about 15-20 hours of pumping, the pressure would normally be below 4-5 x 10^{-7} T. All the measurements were made at a pressure lower than 1 x 10^{-6} T.

When the pressure in the chamber was below 1 x 10^{-6} T, the electron gun was turned ON and a circular beam of about 4-5 mm diameter focussed on the sample. Changing the filament and emission currents, the current density of the beam could be adjusted. Typical settings throughout the entire set were 2 mA for the emission while a maximum possible current flowed through the filament. The beam was allowed to

stabilize for about 3-4 min, before attempting to record any observations. The emitted yellow-orange light was collimated by the lens and detected by the Si-photodetector unit. The translation stage allowed the movement of the detector to a desirable position, so that all the light could be collected. Typical distance of the detector from the window was ~ 25 cm. Confirming that the entire light fell on the active area of the diode, the power supply to the detector unit was turned ON. The signal level was then measured using the lock-in amplifier (see section 4.2.1), after adjusting the phase shift. For a 3 sec time constant of the pre filter, the signal would typically take about 6 - 7 sec to stabilize. The signal,usually, was of the order of a few tens of microvolts. A representative set of conditions is given in table 4.2 below.

Table 4.2

Press.	beam volt.	emission curr.	intensity signal
5×10^{-7} T	5.0 kV	2 mA	84 μV

By changing the position of the linear feedthrough, another sample could be brought in line of sight of the electron beam. No change would be made, nor was any desired, in the rest of the conditions, except a possible movement of the detector unit to ensure the detection of all the emitted light. Signal would once again be recorded off the

lock-in, as in the previous case. A similar procedure was followed to measure the intensity of the remaining samples on the sample holder.

CL signal intensities were taken at spatially different points, on the same sample. Although in some cases, a large discrepancy was observed, the majority of the samples showed less than 10 % deviation in the intensity. Measurements were taken as a function of the beam voltage keeping the current density constant. It was observed that the intensity at a given potential increased with current density, but no systematic observations were recorded.

To confirm the accuracy of the internal standard, its CL intensity was examined intermittently, under identical set of conditions. As expected there was no appreciable difference in these readings. It is interesting to note that no significant damage to the standard due to electron bombardment was observed even after an (cumulative) exposure for ~ 3 hours.

For the analysis of another set of samples, the system is opened to atmosphere and the above procedure is repeated, the internal standard remaining in place.

CHAPTER 5

RESULTS AND DISCUSSION

5.1 Compositional analysis of the thin films :

Several techniques were used to analyze the deposited thin films. Discussed in the following paragraphs are results based on the analyses.

5.1.1 X-ray diffraction :

The as deposited films were characterized using a Nicolet x-ray diffractometer. In section 1.2. mention was made of the two stable crystal structures of ZnS, namely wurtzite (cubic) and sphalerite (hexagonal). Several authors have reported detecting both the structures in vacuum deposited zinc sulphide. Roth [83] has suggested a possible existence of some intermediate polytypes.

Shown in fig 5.1a is the diffraction pattern obtained from a film ~ 120 nm thick (on Si). For the sake of comparison, a standard pattern for cubic zinc sulphide is given in fig 5.1b. A similar pattern was obtained from a film grown on 7059 glass proving beyond doubt that the peak is due to ZnS and not Si. It should be realized that some of the reflections are lost due to the film being too thin to provide reflections of detectable intensity. The lone peak,

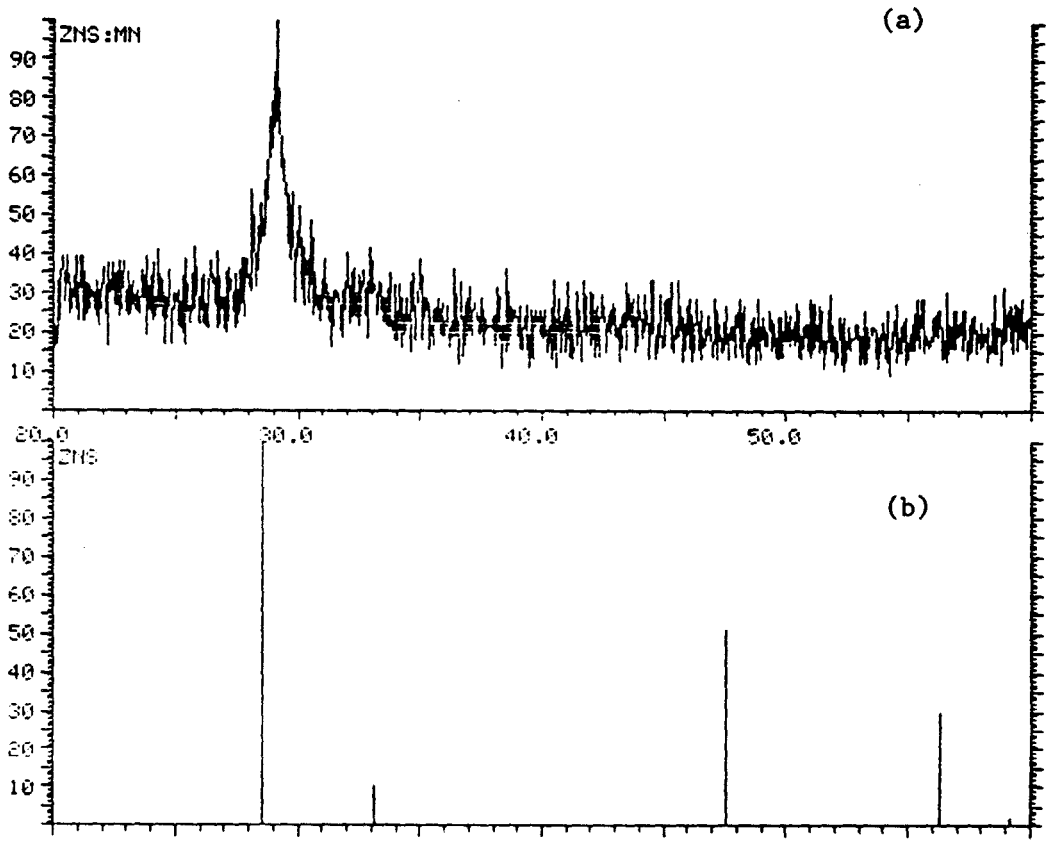

Fig 5.1 a. X-ray diffraction pattern of a ZnS thin film grown (120 nm)

b. Standard pattern of ZnS (cubic) crystal.

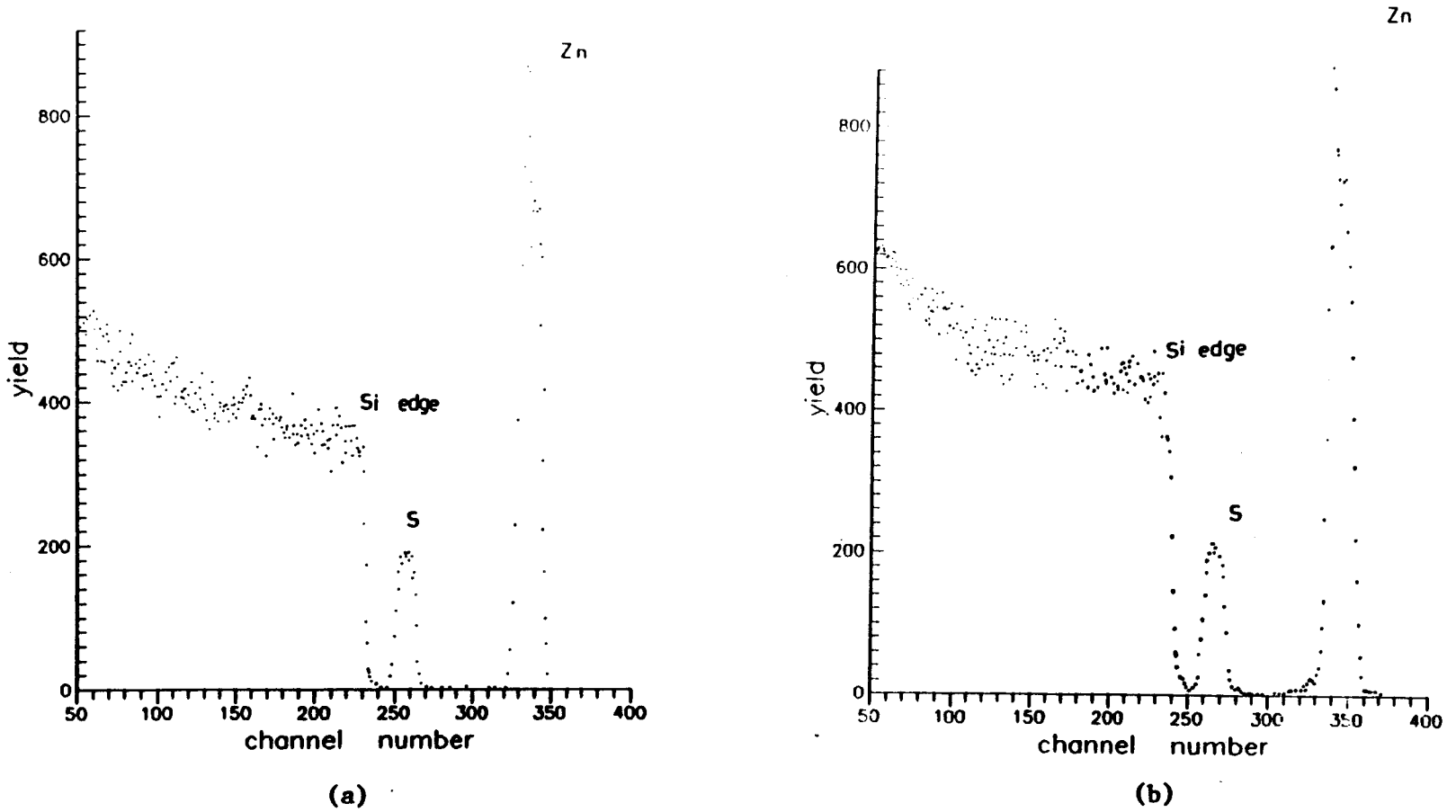

Fig 5.2 Backscattering spectra of a ZnS:Mn thin film (sample 14) containing 0.91% Mn, a) centre spot and b) upper spot.

table 5.1

Results of the RBS analyses

sample	portion	Zn:S
14	upper	1.18:1
	central	1.15:1
	lower	1.21:1
27	upper	1.18:1
	central	1.21:1
	lower	1.22:1

at 2θ = 28.47°, represents the (111) plane of cubic zinc sulphide [83]. This might be an indication of a preferred orientation of the film, but should be confirmed by electron microscopy. It was not possible to detect the peaks characteristic of hexagonal zinc sulphide. The results should be interpreted with caution, for the reasons outlined above. Though no additional peaks could be detected, it is expected that the film is a blend of the hexagonal and the cubic structures. Reflections corresponding to the Mn compounds (oxide and sulphide) could not be detected, because their quantity in the thin film is not enough to generate detectable diffraction peaks.

5.1.2 Rutherford back scattering :

Rutherford back scattering of thin films is a versatile method to determine the chemical composition, thickness and depth distribution of the impurity. Back scattering spectra of sample 14 are shown in fig 5.2 a,b. These spectra are typical of the ZnS:Mn thin films with a low Mn content. Fig 5.2a is obtained from the upper region of the sample, while that from a lower region is depicted in part b of the figure. Spectra obtained from another portion of the same sample were almost identical to those of fig 5.2. One can calculate the number of atoms of the individual elements, per unit volume of the film [84] (see Appendix B for a detailed description). Results thus

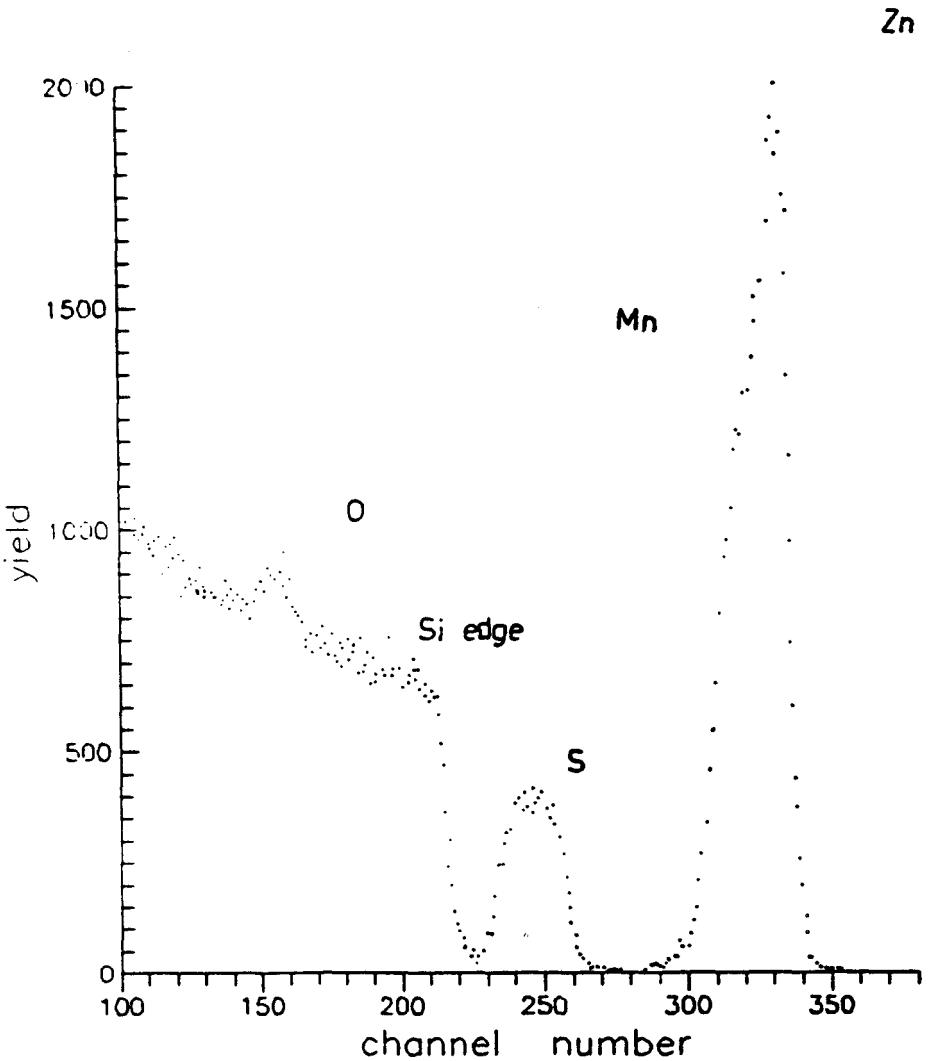

Fig 5.3 **Backscattering spectrum of a ZnS:Mn thin film (sample 27) with a higher Mn content, 9.2 wt%. Note the presence of Oxygen.**

obtained are tabulated in table 5.1. They point to an almost stoichiometric zinc sulphide film, slightly rich in zinc. Zn rich films are a routine product, when ZnS is grown by vacuum deposition [90]. The table also confirms the uniformity of the film composition throughout the sample.

It is interesting to note that RBS analysis of the film with a higher Mn content, shows the presence of oxygen (fig 5.3). In this case too, three different portions of the film were analyzed independently. The results are included in table 5.1. A possible reason for the presence of oxygen is the high reactivity of Mn with O_2. Incorporation of oxygen could have been either during the deposition or annealing; the substrate was at an elevated temperature in both the cases. We believe that the oxygen is present as a surface layer of manganese oxide. The resolution of the experimental system does not allow detection of an element $< 1\%$ of the bulk.

Chu et al [84] (Appendix C) describe a method of deducing the thickness of the thin film from its back scattering spectra. Based on this method, the thickness of sample 14 (set 1) was estimated to be ~ 200 nm. This is the same as that estimated by the alpha step and Auger depth profile, see table 5.2.

table 5.2

Thickness of the films indicated by various methods

sample	set	thickness as indicated by AES	RBS	alphastep
14	I	~ 200 nm	~ 192 nm	200 nm
12	I	~ 200 nm	---	200 nm
25	II	~ 200 nm	---	190 nm
31	II	~ 200 nm	~ 180 nm	190 nm

5.1.3 Auger electron spectroscopy :

AES is a powerful technique used in the surface analysis of thin films. When used with an internal standard quantitative chemical analysis is also possible.

Figure 5.4 shows a typical AES profile of the manganese doped zinc sulphide film. A scan of the entire film surface failed to detect any other impurities. The results confirm those indicated by RBS of the thin films. Both these techniques along with neutron activation analysis, show beyond doubt the absence of any metallic impurities. The importance of the result is obvious; traces of metallic impurities can act as luminescence activator in ZnS.

It is possible to predict the diffusion profile of Mn in the ZnS film. An extensive model will not be presented here, although approximate calculations shall be shown.

Considering diffusion of Mn deposited on the surface of the ZnS film, the concentration of Mn at a depth x and time t is given by,

$$C(x,t) = \frac{\alpha}{2\sqrt{\pi Dt}} \exp(-x^2/4Dt) \qquad \ldots(v.1)$$

where α is the number of Mn atoms, on the surface, per unit area, initially. Assuming a constant diffusivity of Mn, 6.8×10^{-15} cm^2/sec at 400°C [81], the calculated profile is shown in figure 5.5a. The apparent discrepancy between the calculated and observed profile (fig 5.5b) is a result of the approximations made above. The diffusivity of Mn near the ZnS/Si interface will not be the same as in pure ZnS and will change with time and distance. It is estimated that the diffusivity of Mn in Si, at 400°C is of the order of 10^{-20} cm^2/sec, based on the D value of Zn in Ge [92]. So 'reflection' at that interface should be considered for a detailed model. Existence of a SiO_2 layer at the interface adds to the complexity of the problem. These considerations lead to a prediction of Mn build up near the interface. This is indeed observed in practice (see fig 5.5b).

As the predicted diffusivity of Zn in Si is of the order of 10^{-20} cm^2/sec, the diffusion of Zn in Si should not be significant. It is expected that Si diffuses into the ZnS. Here too, the presence of the oxide layer at the interface makes the problem difficult to model.

The diffusion conditions were chosen as a compromise for conflicting needs, namely the achievement of uniform Mn

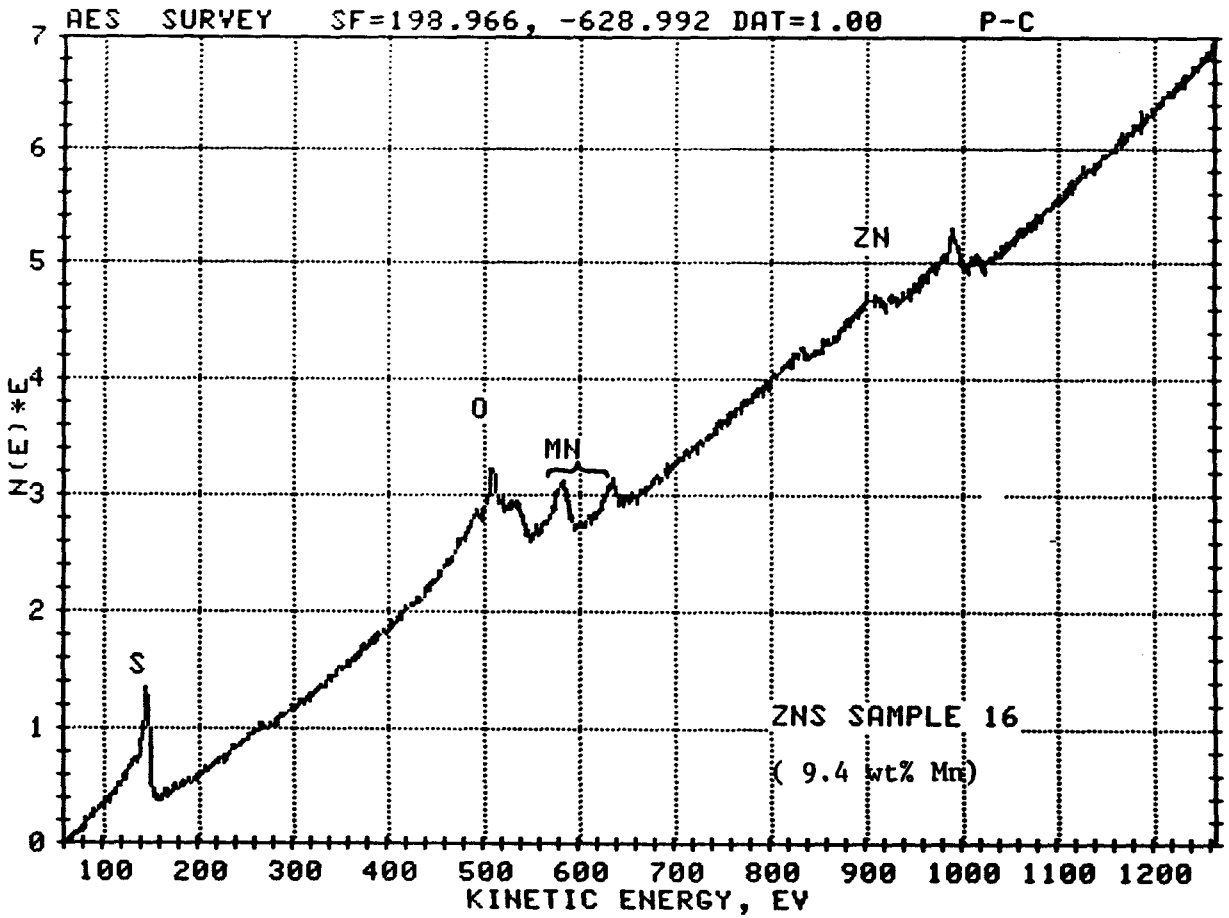

Fig 5.4. Typical Auger profile of the surface of a sample with a high Mn content.

doping while limiting Si diffusion in ZnS. A Mn concentration nonuniformity well within a factor of two is achieved under these conditions.

Depth profile of sample 25 (set II) is shown in figure 5.5b. 4 kV Ar^+ ions were used to sputter the surface at an approximate rate of 200 Å/min. Formation of manganese oxide on the surface is clearly seen. Some diffusion of Si in the ZnS film was evident. It was for this reason that the films were not annealed at a higher temperature and a longer time. The profile confirms an almost uniform concentration of Mn throughout the depth dimension of the film, except a thin surface later, which is Mn rich. The results are not corrected to the individual sputtering yields of the elemental species, so quantitative comparisons will not be accurate.

5.2 Determination of Mn concentration :

The level of the dopant species, Mn, was determined by three independent techniques - AES, RBS and the calibrated mask system. NAA (Neutron Activation Analysis) is potentially capable of quantitative chemical analysis, provided an internal standard is used. However, for the analysis of thin films, the method poses several hurdles. It is extremely sensitive to the geometry and density of the sample [86]. Hence the standard should necessarily be a thin film of a similar quality and dimensions. For this

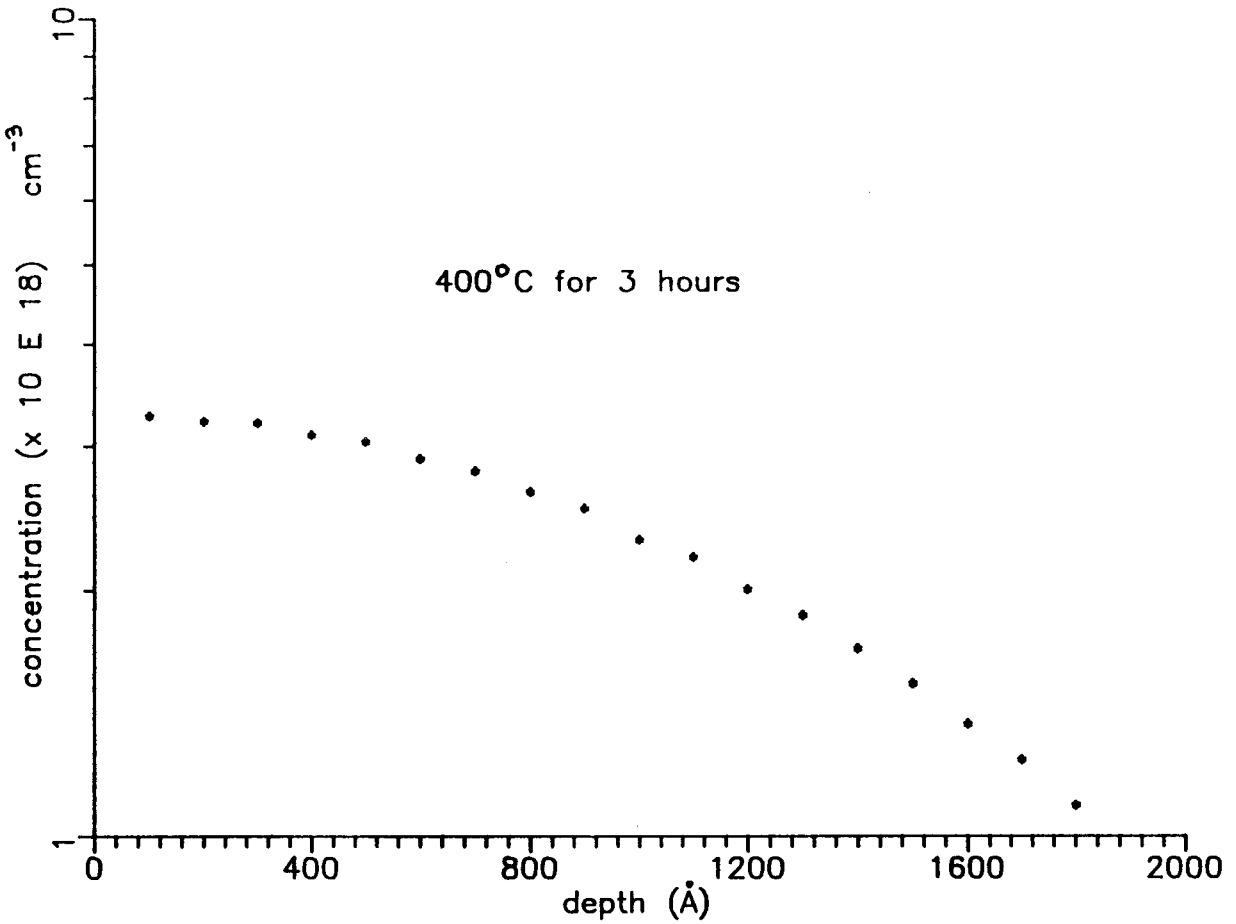

Fig 5.5 a Calculated diffusion profile of Mn in the ZnS film

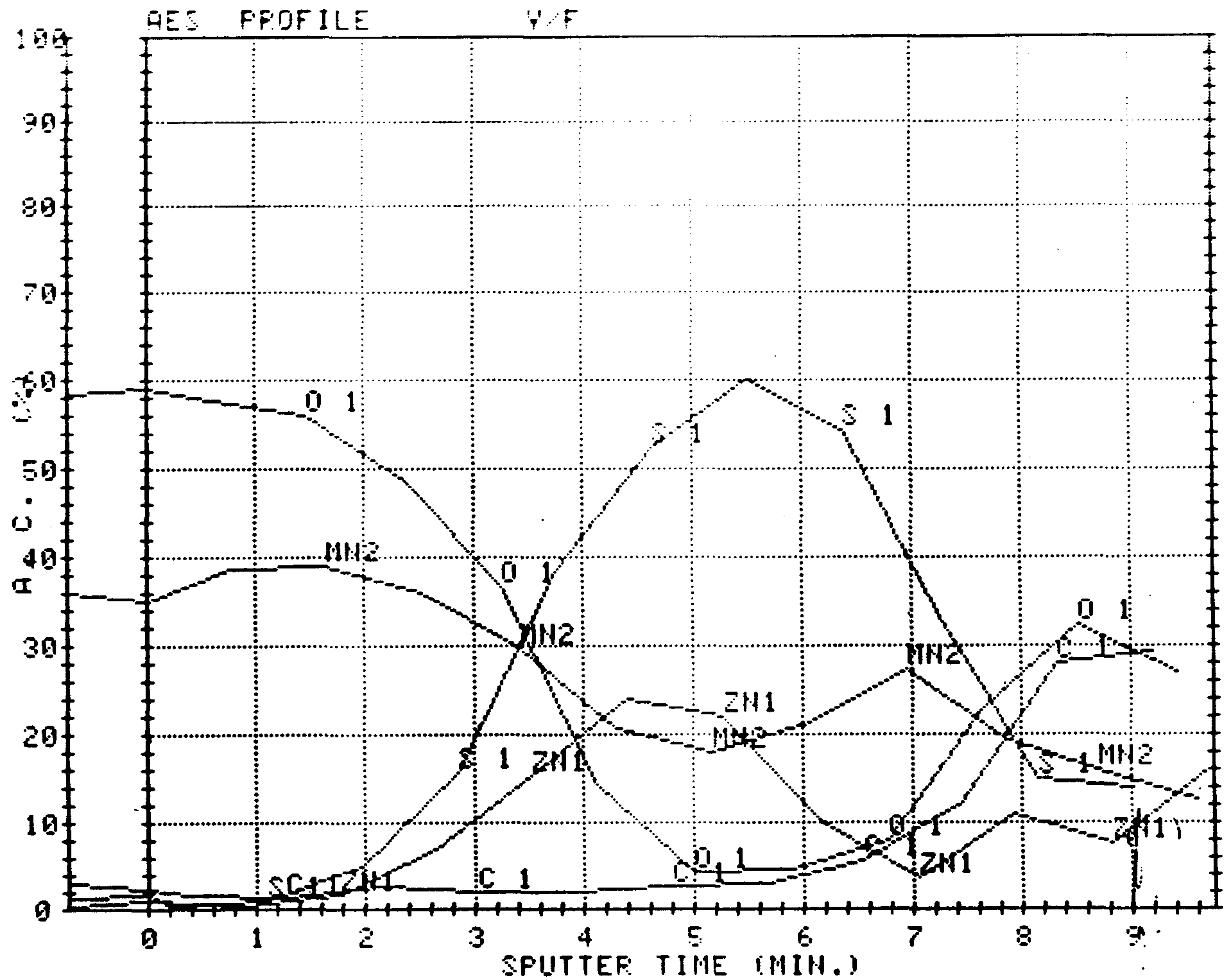

Fig 5.5 b Auger depth profile of sample 25. Plot not corrected to individual yields of the elements. Note that negligible O_2 is present beyond a thin surface layer of ~ 400 Å. O_2 after 8 minutes of sputtering is due to the Si interface. Right hand edge of the profile approximately corresponds to the Si/ZnS interface. also note that the Mn distribution is fairly uniform.

reason NAA was done only to detect the trace impurities and to confirm the composition of the bulk internal standard to be latter used during AES.

Comparing the yield from the sample to that of the standard, one can quantitatively determine the concentration of the chemical constituents of the sample. Unfortunately, for reasons unknown, quantitative Mn determination was not possible on the AES facility at McMaster.

It was mentioned in the previous section that RBS analysis can indicate the amount of the elements present. Mn and Zn, being very close in atomic mass, have closely spaced high energy edges, when analyzed by a 2 MeV $^4He^+$ beam. As a result, the back scattering spectrum of a thin film with these two elements, will not show two near-gaussian peaks due to Mn and Zn, but an overlap of the two. However, deconvolution of this peak into the two individual ones is possible, provided the high energy edges of Mn and Zn are known. A spectrum of sample 27 (set 2) is reproduced in fig 5.6. Deconvolution of the individual peaks is also shown in the figure. Area under the individual peak would then lead to their respective amount of the corresponding element. Table 5.3 gives the value of Mn concentration calculated by various methods.

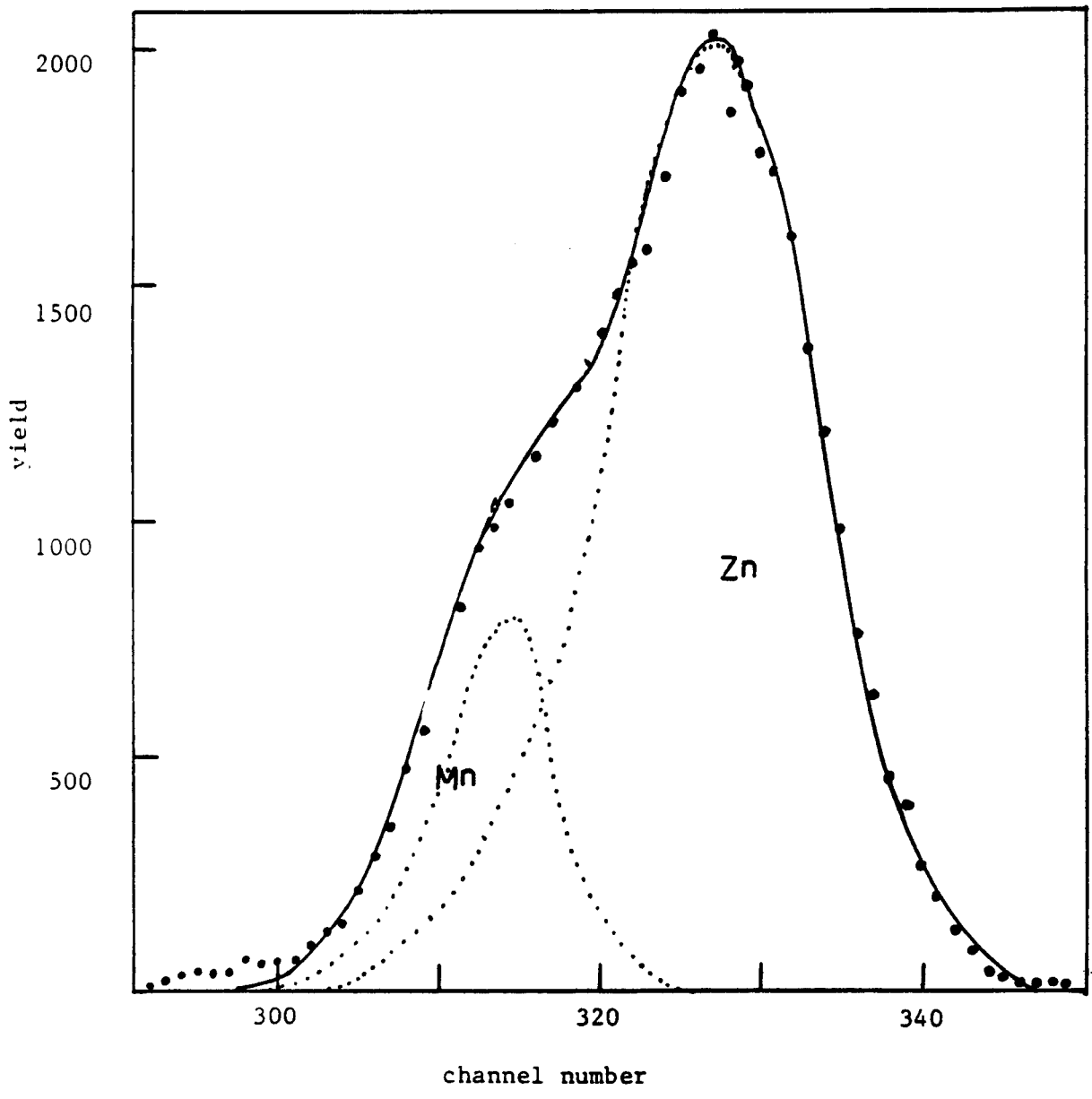

Fig 5.6 Part of the backscattering spectrum of sample 27. The individual peaks due to Zn and Mn, where they are thought to exist, are shown.

table 5.3

Determination of Mn content by different methods

sample	technique	Mn content	est. error
14	RBS	1.2 wt%	±10 %
	mask	0.91 wt%	±5 %
27	RBS	10.2 wt%	±10 %
	mask	9.4 wt%	±5 %

One of the distinct advantages of the mask system used during the current experiments, was its ability to incorporate a known amount of Mn. The procedure to do so was explained at length in section 4.1.5. From table 5.3, the accuracy of the mask system is evident.

5.3 CL Intensity vs. Mn concentration :

It was mentioned in section 1.2.7 that no systematic measurement of the change in the cathodoluminescent intensity with Mn concentration in ZnS:Mn has been reported to our knowledge. The present study reports the results of such an investigation.

Shown in fig 5.7a is the relationship between c_{Mn} and the intensity of the CL emission for ZnS:Mn thin films. The experimental points correspond to the intensity of individual samples. The samples were obtained from the same

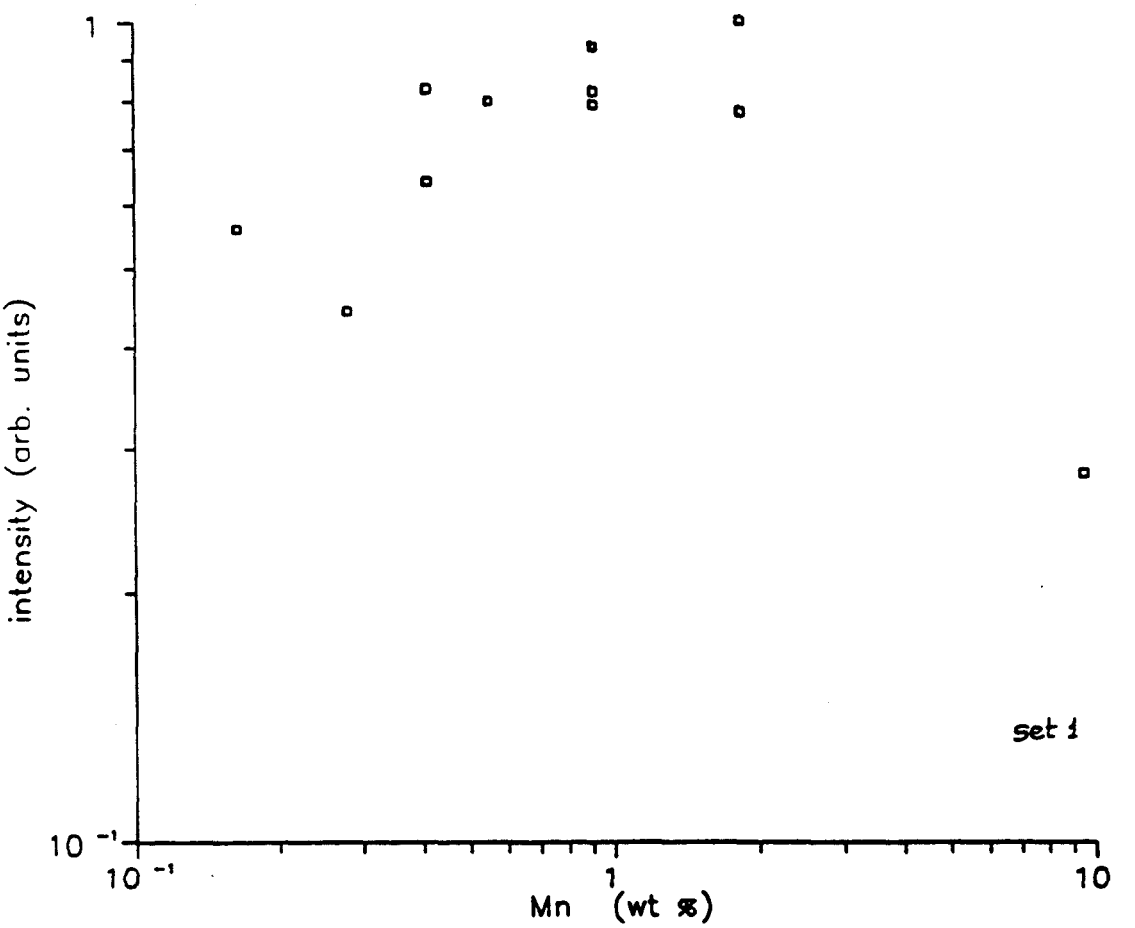

Fig 5.7 a Variation of relative CL intensity with Mn concentration, set I

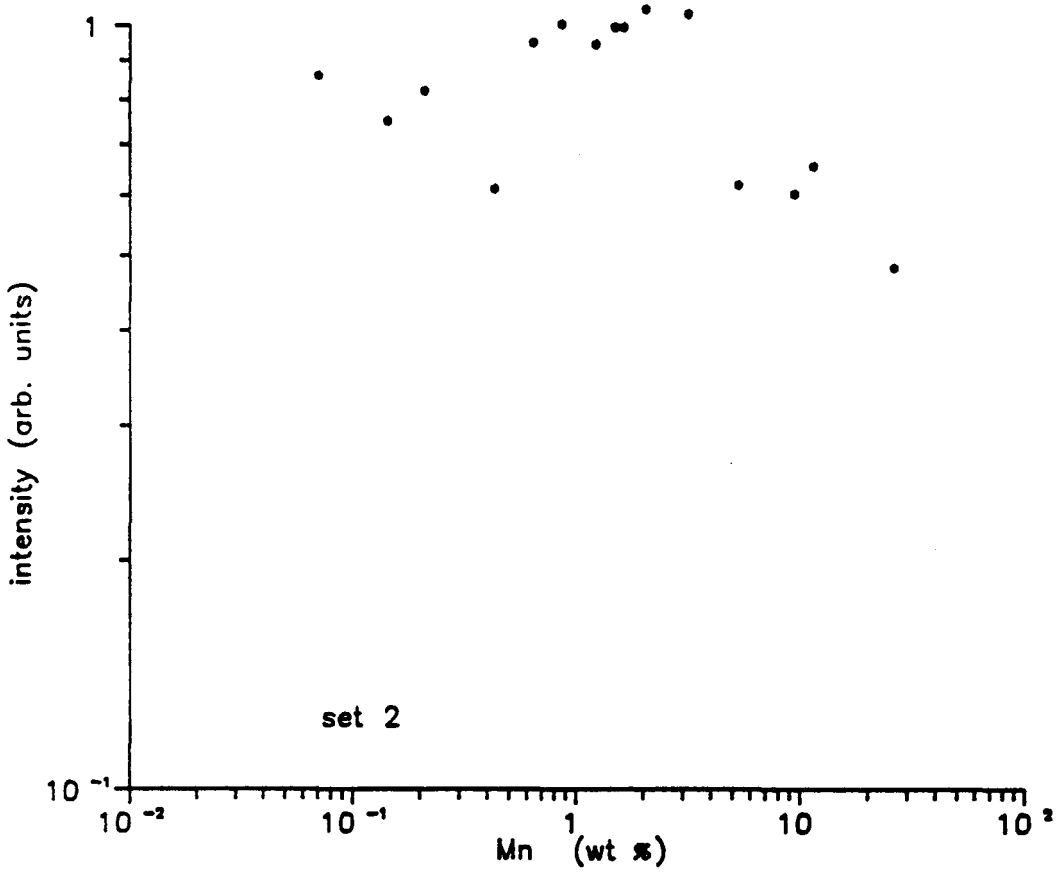

Fig 5.7 b Variation of relative CL intensity with Mn concentration, set II.

parent film of ZnS (~200 nm), as explained previously (sec 4.1). The Y-axis of the figure denotes the relative intensity of the samples with respect to the internal standard. For a discussion on the use of an internal standard, refer to section 4.2. Results of another independent set of samples are plotted in fig 5.7b. Intensity of CL emission rises, initially, with c_{Mn}. After reaching a maximum, the intensity drops rapidly. The maximum in both the sets occurred at c_{Mn} ~2 wt %. Similar observations have been reported in the case of EL [3,6,7] and PL [3,4,55] of ZnS:Mn. The possible reasons for quenching are discussed in the next section. In the literature, several models have been proposed [3,4,53,57] to explain this unusual phenomenon, none of which is thouroughly convincing.

Both the plots are for an accelerating potential of 5 kV. The results of two independent sets of samples are plotted on one scale in fig 5.8.

The relative CL intensity for various beam voltages is tabulated in table 5.4. A plot of the emission intensity as a function of the accelerating potential (fig 5.9) is a straight line parallel to the X-axis. In other words, the accelerating potential of the exciting electrons did not influence the CL intensity, in the given range. This is thought to be an evidence of complete penetration of the ZnS thin film by the primary electrons. Depth of penetration of

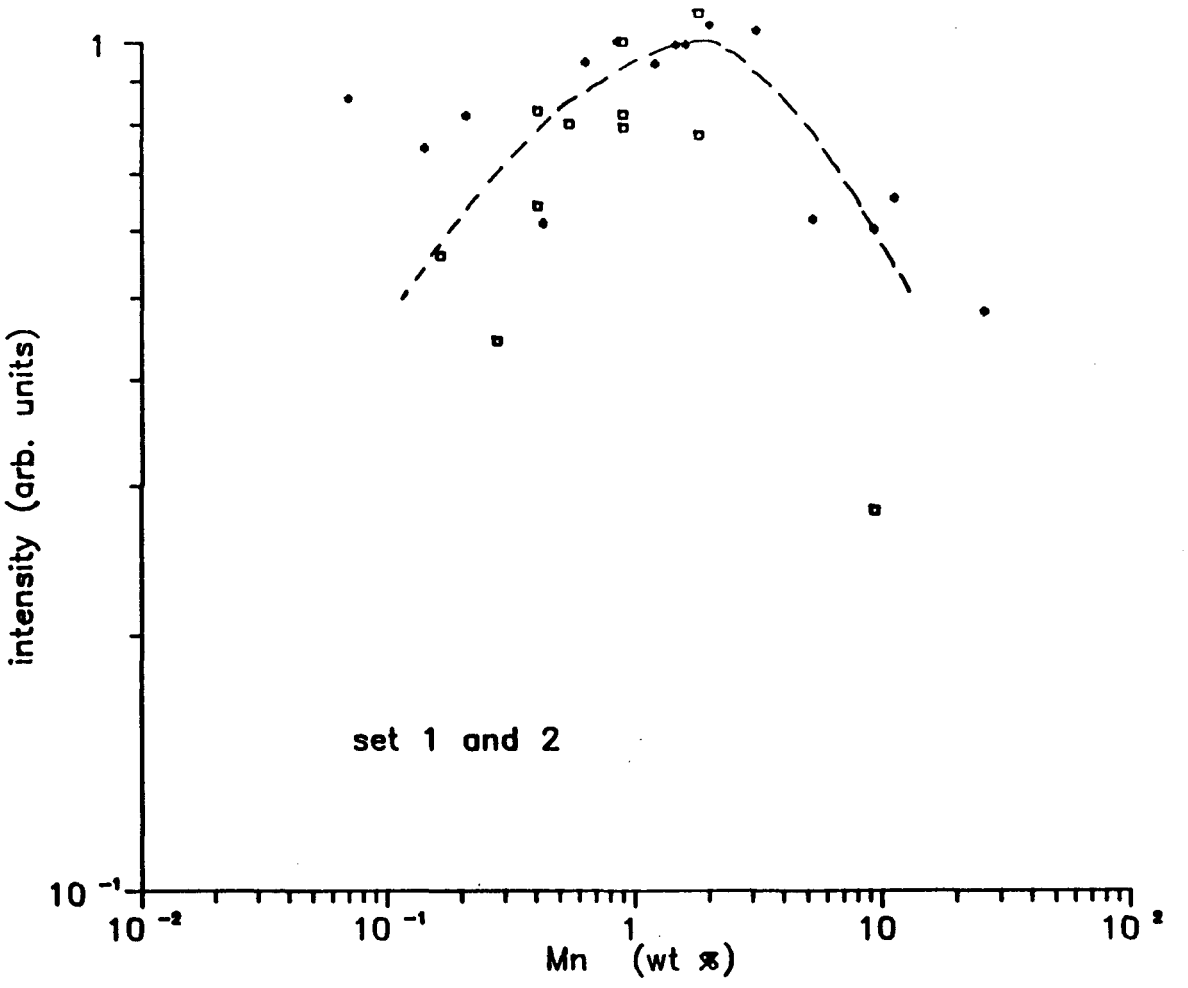

Fig 5.8 Variation of relative CL intensity with Mn concentration, □: set I and *: set II.

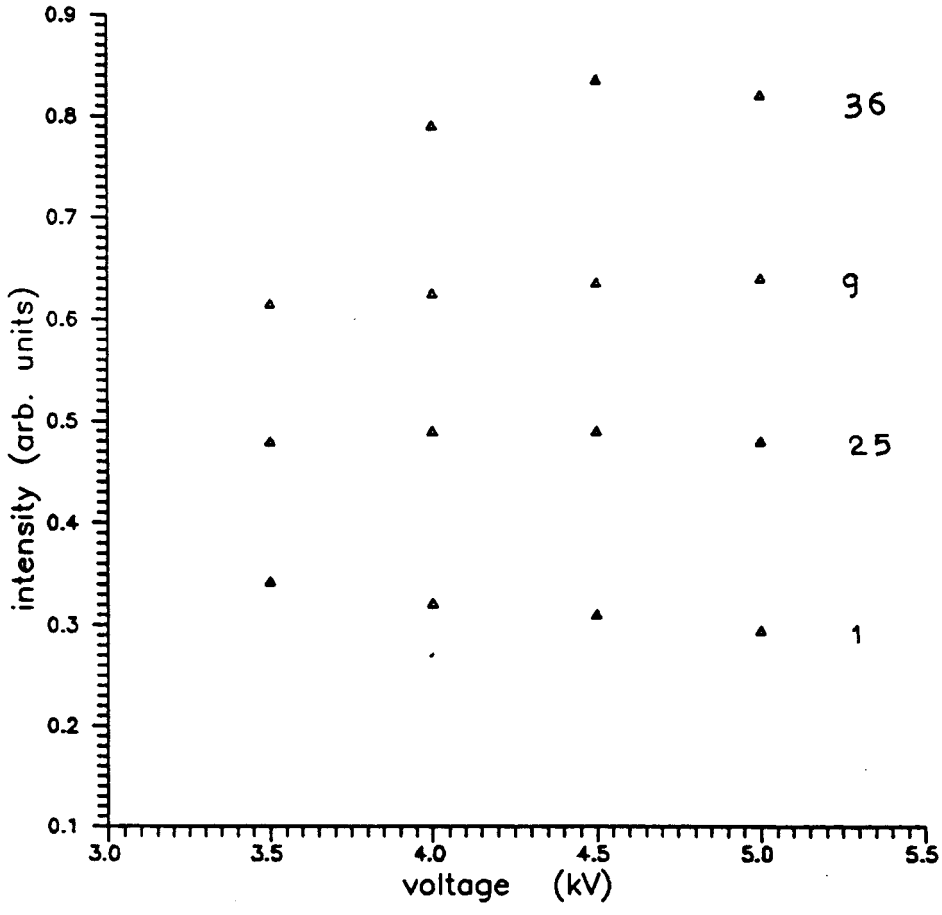

Fig 5.9 Relative CL intensity of ZnS:Mn thin films (~200 nm) as a function of applied beam voltage, present study.

table 5.4

Relative CL intensity of ZnS:Mn thin films at different beam voltages

sample	Mn wt%	Relative intensity at 3.5 kV	4.0 kV	4.5 kV	5.0 kV
01	1.1	.35	.33	.31	.30
02	0.41	.82	.81	.82	.83
03	0.28	.44	.44	.48	.44
06	0.165	.73	.56	.55	.55
08	0.55	.79	.77	.70	.80
09	0.41	.61	.63	.63	.64
11	0.91	.85	.82	.85	.82
12	0.91	.75	.68	.83	.79
13	1.84	1.08	1.10	1.10	1.08
14	0.91	1.	1.	1.	1.
15	1.84	.89	.70	.89	.79
16	9.48	.25	.25	.24	.28

table 5.4 (contd)

sample	Mn wt%	Relative intensity at 4.0 kV	4.5 kV	5.0 kV
25	26.1	.49	.49	.48
26	11.4	.59	.62	.65
27	9.4	.60	.59	.58
28	5.3	.63	.64	.65
29	3.16	1.01	1.02	1.03
30	2.04	1.03	1.02	1.05
31	1.63	.95	.95	.99
32	1.22	.80	.78	.78
33	0.86	1.0	1.0	1.0
34	0.64	.90	.98	.95
35	0.43	.62	.60	.61
36	0.21	.79	.83	.81
37	0.14	.57	.73	.74
38	0.07	.51	.73	.74
39	1.49	.96	1.0	.99

electrons in ZnS was discussed in section 1.2.7; accordingly equation (i.2) did predict a complete penetration of a ~ 190 nm film of ZnS by 3.0 kV electrons.

Typical emission spectra of ZnS:Mn (with a lower Mn content), showing the characteristics due to $Mn^{2+}(3d^5)$ viz. a broad band emission centred at 580 nm, is depicted in fig 5.10. An immediate question that arises is, how does the CL emission spectrum vary with Mn concentration, if it does at all?

To investigate this, CL emission spectra of ZnS:Mn films with a different amount of the dopant were recorded. The results show a peculiar behaviour. In addition to the yellow peak associated with the lowest energy transition $^4T_1$-$^6A_1$ of the excited Mn ion, a red peak appears in samples with a higher concentration of the dopant. Figure 5.11 shows the emission spectra of the four samples. The concentration of Mn increases as one goes from bottom to the top of the plot. It may be seen that although the position of the yellow peak is not altered with the level of Mn doping, the intensity of the same does drop with c_{Mn}. Similarly the relative intensity of the red peak increases with the Mn concentration. These results are in agreement with the photoluminescence results of ZnS:Mn, as reported by Goede [56..59] except for the threshold of the onset of the red peak. While [56..59] reported the appearance of this lower energy peak in samples having ~ 1 mol% Mn; it was not

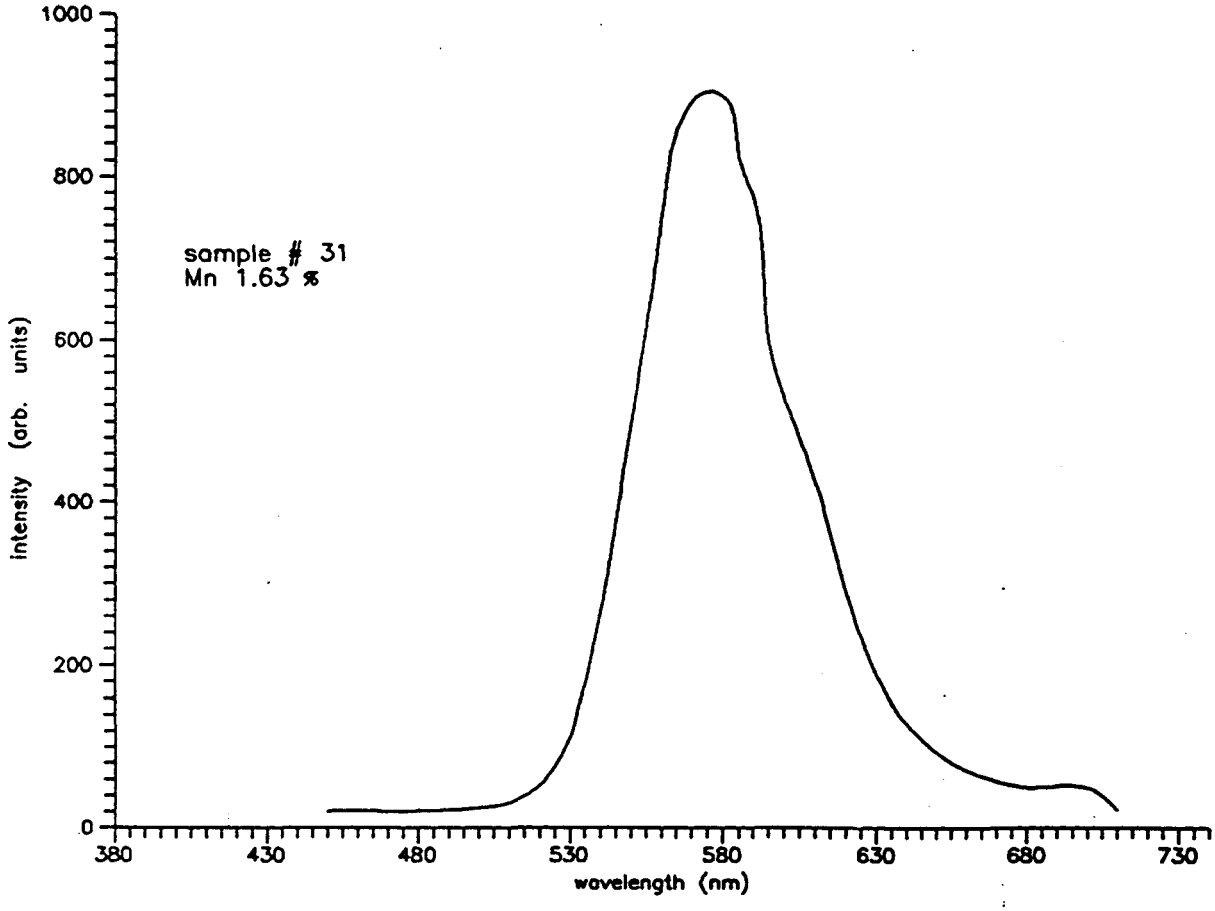

Fig 5.10 Typical CL emission spectra of a ZnS:Mn thin film.

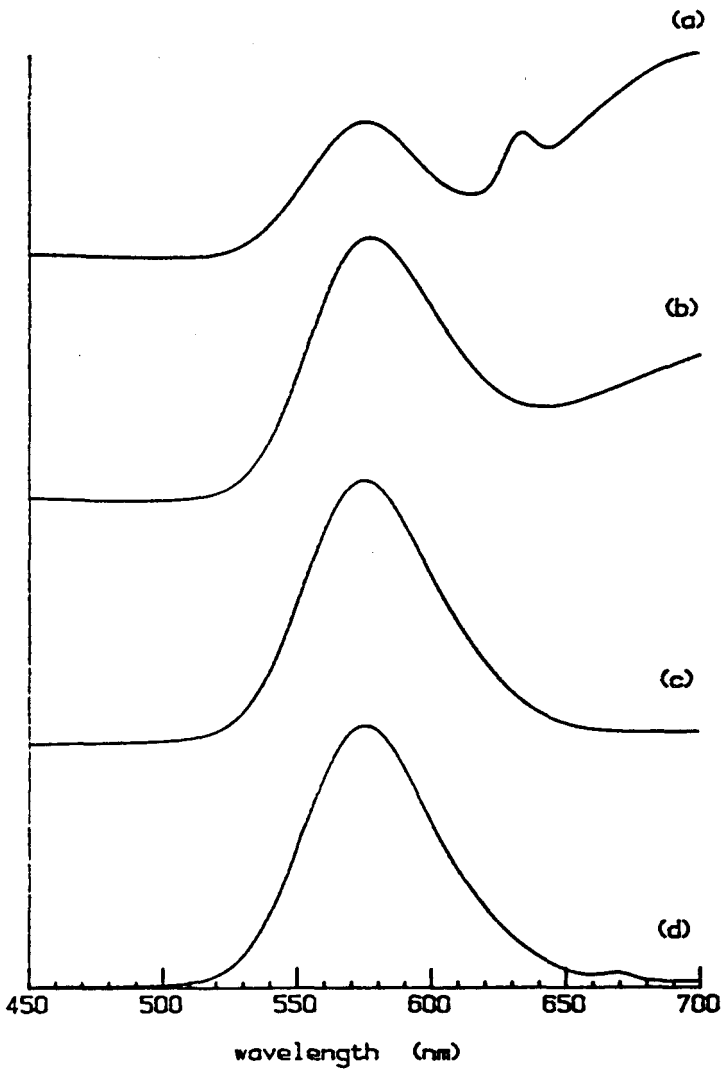

Fig 5.11 CL emission spectra of ZnS:Mn thin films: a) 26.4 wt% Mn, b) 11.4 wt% Mn, c) 1.64 wt% Mn and d) 0.43 wt% Mn. Spectra shifted for clarity; y-axis is not to an identical scale for each.

detected in the samples containing < 1.64 wt % Mn (< 2.3 mol %) during the present investigation. Emission spectra for samples with Mn concentration between 1.64 wt % and 11.4 wt % were not recorded, hence it is difficult to predict the exact threshold concentration of Mn in ZnS thin films for the occurrence of the red emission. The empirical relationship suggested in [58]

$$B_r\ (c_{Mn}) = c_{Mn}^{\ 1.5} \qquad .. \text{ (v.2)}$$

could neither be confirmed nor refuted, because the absolute intensity of the individual samples was not recorded. The ratio of the intensity of yellow peak (580 nm) to that of the red one (700 nm) changes with c_{Mn} as shown in figure 5.12. The results indicate a threshold for the appearance of the red peak, rather than an almost linear relationship

$$I_r/I_y = (c_{Mn})^{1.4} \qquad \ldots \text{ (v.3)}$$

as reported in [58] (see fig 1.13b). Let us now discuss the reasons for the observed 'concentration quenching' of the CL brightness. Comparison of fig 5.8 with fig 1.5,1.11 may seem to suggest that the quenching in case of CL is less pronounced than that in PL and EL of ZnS:Mn. The drop in the intensity of yellow emission (when excited by cathode rays) is, in fact, much more drastic than seen from fig 5.8. This is due to the appearance of the red peak at higher Mn concentrations. So the total light intensity indicated by the diode is the integrated intensity under the yellow and

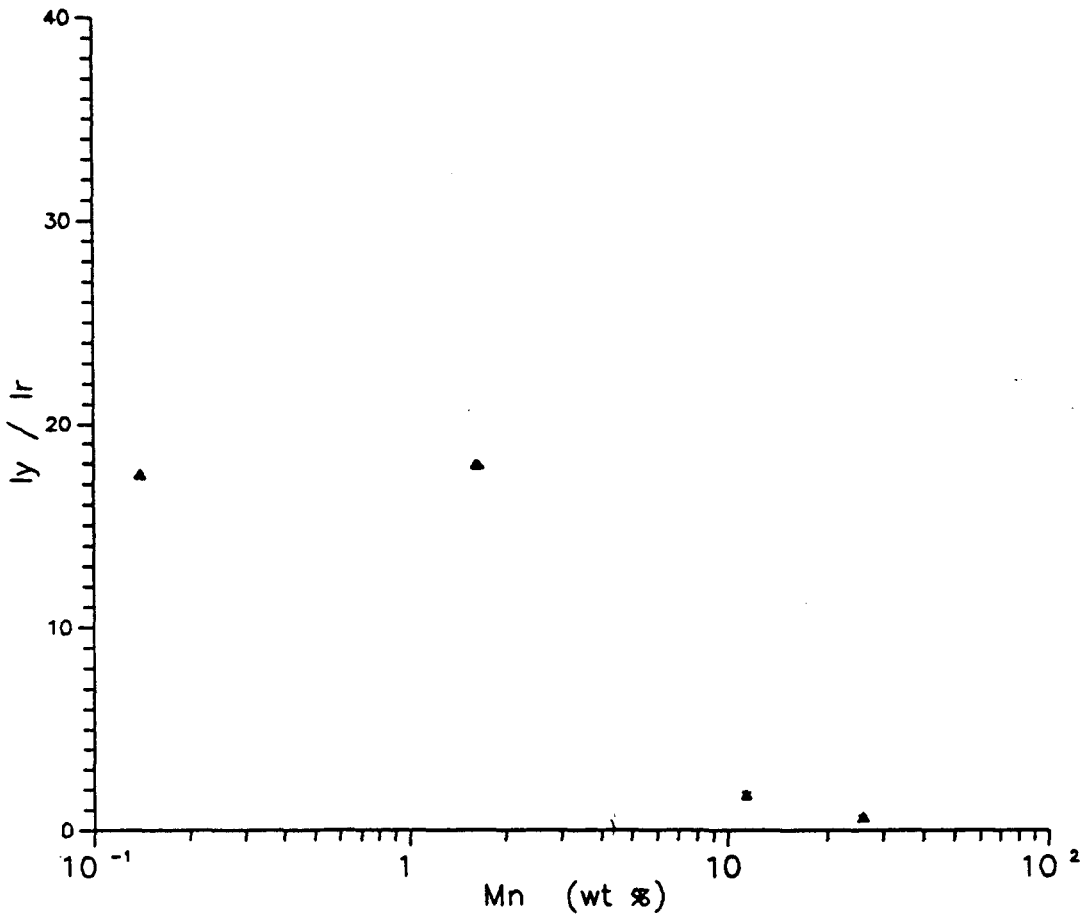

Fig 5.12 I_y/I_r versus Mn content for CL emission of ZnS:Mn. I_y is the peak yellow intensity, while I_r is the intensity at 700 nm.

red peak. Moreover, response of the Si photodiode used to detect the light, is stronger to the red light than to the yellow (see fig 4.5 b).

5.4 Physical basis of concentration quenching :

5.4.1 Formation of Mn pairs and complexes :

A possible reason for the observed quenching is the existence of Mn pairs, triplets and complexes, which have a different optical absorption cross section than an isolated Mn ion [38]. Recall that Mn substitutes Zn in the ZnS lattice. Assuming a random distribution of the Mn ions , the probability, P_i, that an available site is occupied by it, is given as

$$P = N_i / N_t \qquad \ldots(v.4)$$

$$= c_{Mn} \text{ (mol \%)} \qquad \ldots(v.5)$$

where N_i is the number of filled sites occupied by the impurity and N_t is the total number of available sites. Consider that one of the N_i sites is known to be occupied. Let $(N_1 - 1)$ be the number of impurity atoms surrounding the one under consideration. Further, consider the m^{th} possible configuration, which may be produced in m equivalent ways, each of which provides N_m available sites, adjacent to at least one of the Nl filled sites. If $N_i << N_t$ then, the probability of finding a N_1 group around the site is

$$P_{Nl} = m\, P^{(N_1 - 1)}\, (1 - P)^{N_m} \qquad \ldots(v.6)$$

It follows that the probability that a given Mn atom is

isolated is given by setting m = 1 and N_1 = 1; i.e.

$$P_1 = (1 - c)^{12} \qquad \ldots(v.7)$$

as there are 12 nearest neighbour cation sites in the ZnS lattice. Similarly the probability that a given Mn atom has a nearest neighbour Mn is

$$P_2 = 12c(1 - c)^{18} \qquad \ldots(v.8)$$

Similarly, the probability of finding higher order Mn complexes may be calculated. Fig 5.13 shows the proportions of Mn 'lones', pairs, triplets etc. The dotted line in the figure corresponds to the optimum Mn concentration for CL intensity of ZnS:Mn. It is clear from the graph that, the probable concentration of pairs is close to its maximum, while that of the isolated ions is about half of its initial value. Beyond this value of c_{Mn}, the concentration of higher order complexes of Mn increaeses dramatically. As the concentration of the isolated Mn decreases, the yellow luminescence is quencehed. The Mn complexes may well be the red emitting centres, but no experimental proof has yet been obtained. Goede found that the excitation spectra of the red and yellow centres is similar in nature and corresponds to that of the isolated $Mn^{2+}(3d^5)$.

The relative concentration of the isolated Mn ions, equal to $c_{Mn}\ (1 - c_{Mn})^{12}$, peaks at c_{Mn} ~ 8%; whereas the brightness peaks at ~2 wt%. Kitai [87] pointed out that consideration of next- and next-next nearest neighbour Mn also fails to explain the observed quenching behaviour, in

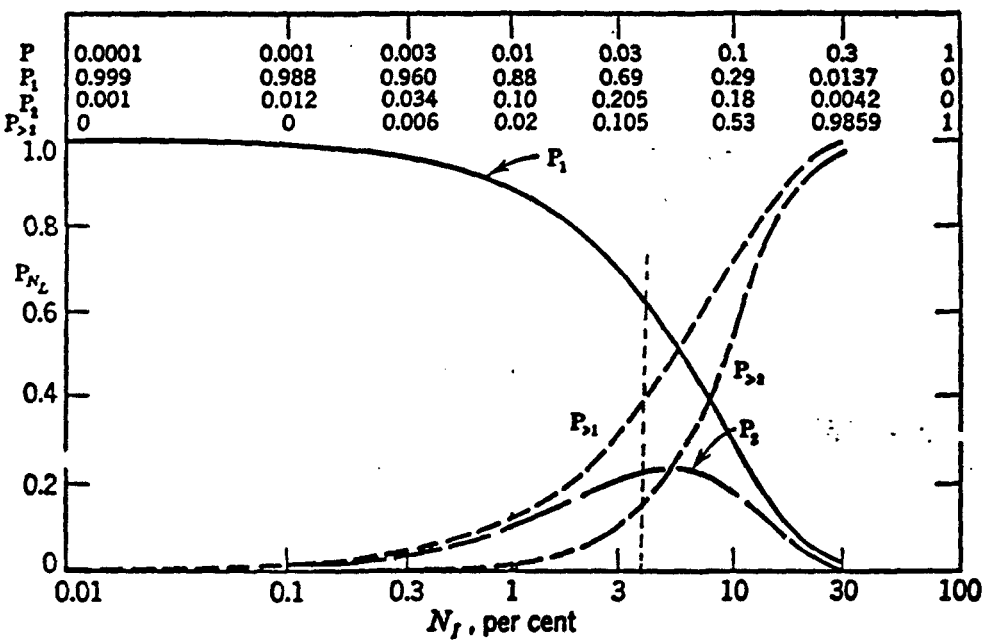

Fig 5.13 Proportions of Mn in ZnS: —— isolated, — — pairs, and - - - - higher order complexes. Dotted line denotes the optimum concentration for CL emission.

quantitative terms. Nevertheless, it seems that formation of Mn pairs and complexes might be one of the many reasons for luminescence quenching. Mn pairs and/or complexes may well be the energy sinks, as described in the next section.

5.4.2 Radiationless energy transfer :

Energy transfer processes, other than the standard excitation - decay of the luminescent centre, are possible in the semiconductor phosphor. These may be either radiative or non-radiative. Before excitation of the Mn centre under consideration, energy may be lost to the following radiationless processes :

i) Stoke's shift

ii) phonon generation during impact

iii) band-band transition

iv) ionization of defects due to electron collision

Non-radiative processes involving the excited Mn ion include:

i) resonance energy transfer from an excited Mn ion to an energy sink via other unexcited Mn ions.

ii) resonance energy transfer from an excited Mn ion to 'poison' centres in the host lattice.

Yang et al [88] suggest that the predominant non-radiative decay process in ZnS:Mn is the last one. Inherent lattice defects or other impurity atoms e.g. Fe, Co, and Ni are the likely 'poison' centres. Energy can migrate from an excited Mn^{2+} to a nearest neighbour energy 'sink'(fig

5.14a). If this is the case then decay should follow an exponential law. The mechanism is physically similar to the random walk diffusion problem, with the nearest neighbour poison centres acting as sinks. If this were entirely true, the quenching would be dependent on temperature and the site location at which initial excitation occurs. Site selective spectroscopy is an extremely sophisticated technique and to date only [89] has reported the results on ZnS:Mn. Increase in the concentration of the poison centres should then induce more quenching.

Site-to-site resonant energy transfer among the Mn ions, until a sink, is another possibility. In fact, this process is by far the most likely to occur. A schematic of the process is shown in figure 5.14b. The sink can be a red-infra-red or a non-radiative centre. At larger Mn concentrations, this type of energy transfer can become (undesirably) efficient because of the decreased distance between nearest neighbour Mn. This process can also be pictured as a random walk problem, with a different activation energy for each step.

To calculate the number of excited Mn ions we take the following approach:

At 580 nm (characteristic Mn emission), for a 1 cm^2 area:

$$1 \text{ watt} = 580 \text{ lumen}$$

$$= 5.39 \times 10^5 \text{ fL}$$

Taking the experimental values for sample 31 (1.63 wt% Mn),

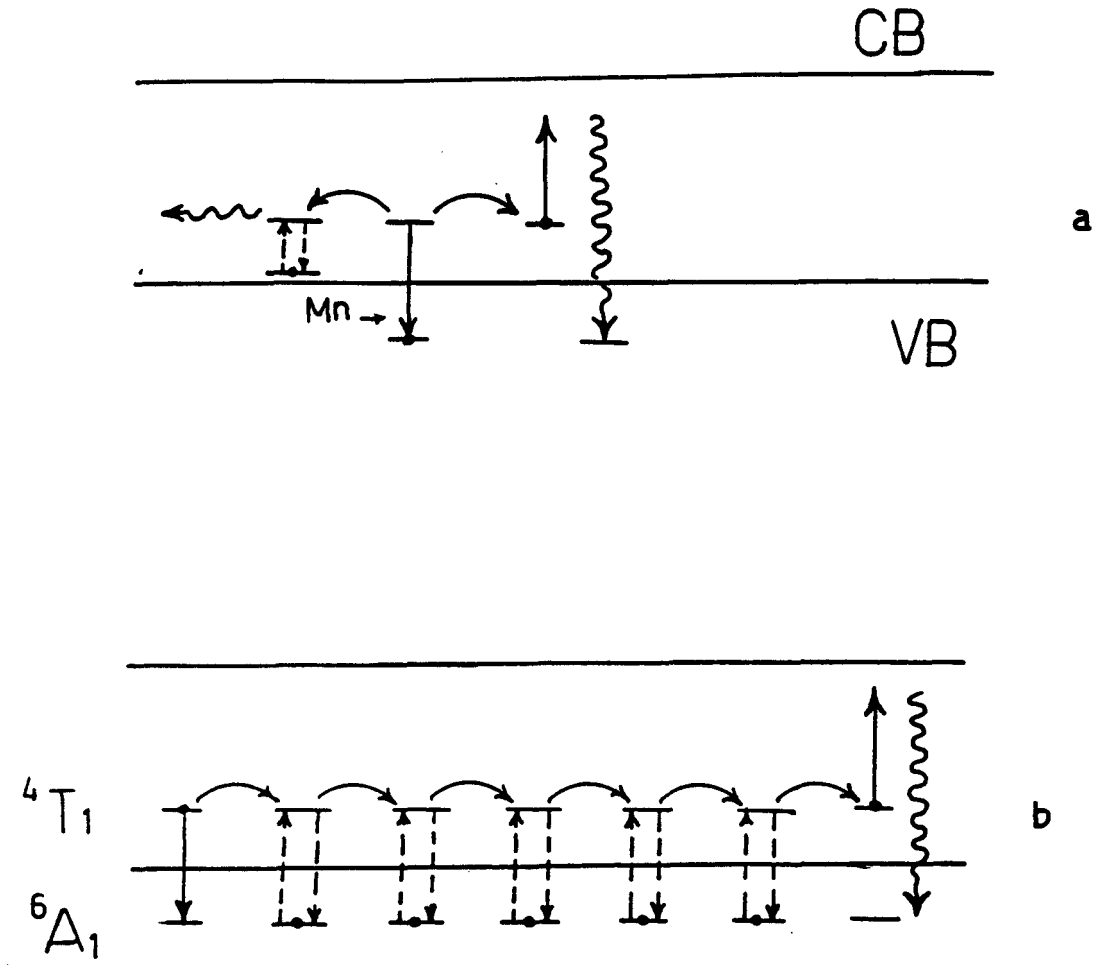

Fig 5.14 Schematic of energy transfer processes in ZnS:Mn: a) resonance transfer directly to adjacent 'poison' centres and b) resonance transfer to a sink via other Mn ions.

i.e. 2.8 fL at 3 mA filament current emitted by a 190 nm ZnS:Mn film:

$= 5.20 \times 10^{-6}$ watts of optical power from a 1 cm^2 surface.

One Mn atom may be excited every 2 msec (~ 2 msec), so in 1 sec it is excited ~500 times. The power output by one Mn ion in one second is then:

$= 500 \times 2.2$ eV $\times (1.6 \times 10^{-19}$ J/eV)

$= 1.76 \times 10^{-16}$ J

Assuming that 85% of the emitted light is lost to scattering, total internal reflection etc., the corresponding value is

$= 2.64 \times 10^{-17}$ J

The number of excited Mn ions is then

$$= \frac{5.20 \times 10^{-16}}{2.64 \times 10^{-17}}$$

$= 1.97 \times 10^{11}$ per cm^2

But the number of Zn sites per cm^2 in the thickness is,

$= 4 \times 190 \times 10^{-7}/(5.41 \times 10^{-8})^3$

$= 4.80 \times 10^{17}$

Knowing the concentration of Mn (~2.4 mol%) the number of Mn atoms may be estimated as

$= 0.024 \times 4.80 \times 10^{17}$

$= 1.15 \times 10^{16}$ per cm^2 in the film.

Therefore, the fraction of excited Mn atoms is 1.71×10^{-5}, which means that the distance between nearest neighbour

excited Mn is of the order of tens of nanometers. This immediately rejects any possibility of interaction among the excited Mn ions. Similar calculations based on the values of Theis and Wengert [65] tell us that the fraction of excited Mn (0.7 mol%, 630 nm thick film) is 2.5×10^{-4}. The apparent descripency in the two values is probably due to the different film thickness and a larger beam current density used in their investigations.

Sensitized luminescence is a process in which an impurity atom (activator) is made to emit visible or near-visible radiation upon excitation as a result of absorption by and transfer from another atom (sensitizer). If the sensitizer is an impurity atom, the process is termed as impurity-sensitized luminescence; if the host lattice absorbs and then transfers the energy, it is known as host-sensitized luminescence [91]. The energy transfer from the sensitizer to the acceptor is radiationless. It is obvious that, in certain cases, the activator is capable of luminescing at a wavelength at which it has no substantial absorption e.g. $Mn^{2+}(3d^5)$ emitting at 1.8 eV. Another impurity or the host lattice itself can act as a sensitizer, as mentioned previously. Resonance energy transfer is possible between an allowed transition in the sensitizer and a forbidden one in the activator. The mathematical formulation of such an energy transfer is somewhat complicated and will not be dealt with here in detail,

although a brief mention will be made. It should be mentioned that the transfer probability is determined by the overlap of the wavefunctions of the sensitizer and the activator and according to Kröger [91], occurs only if they occupy adjacent sites. Since the actual distribution of the sensitizer and the acceptor is most likely close to random, the probability of the occurrance of this process increases non-linearly with Mn concentration.

5.4.3 Mathematical model :

Based on the non-radiative energy transfer from an excited Mn ion directly to the red or a non-radiative emission centre(fig 5.10), the following model may be presented.

$$\frac{dN_y}{dt} = A - \frac{N_y^*}{\tau_y} - \frac{N_y^*}{\tau_{yr}} - \frac{N_y^*}{\tau_{yn}} \qquad ..(v.9)$$

$$\frac{dN_r}{dt} = \frac{N_y^*}{\tau_{yr}} - \frac{N_r^*}{\tau_r} \qquad ..(v.10)$$

where A is the excitation rate, N_y^* and N_r^* the concentration of the excited yellow and red centres respectively; their radiative transitions occur in τ_y and τ_r sec. $1/\tau_{yr}$ and $1/\tau_{yn}$ are the mean energy transfer probabilities to the red emission and non-radiative centres. Assume a no saturation case and neglecting the effect of temperature and Mn concentration on τ_y and τ_r (not true in practice). Then, at steady state

$$I_y = \frac{N_y^*}{\tau_y} = \frac{A}{\tau_y}\left(\frac{1}{\tau_{yr}} + \frac{1}{\tau_r} + \frac{1}{\tau_{yn}}\right)^{-1} \qquad ..(v.11)$$

$$I_r = \frac{N_r^*}{\tau_y} = \frac{\tau_y}{\tau_{yr}} I_y \qquad ..(v.12)$$

$$I_y/I_r = \tau_{yr}/\tau_y \qquad ..(v.13)$$

Simultaneous solution of equations v.9 and v.10 will give the time dependence of the emissions. It will not be presented here due to its limited applicability to the present work.

The mean energy-transfer probability to the red centres, $1/\tau_{yr}$ is proportional to the probability of resonance transfer from one Mn to another unexcited Mn (P_{11}) and the fraction of Mn ions being able to transfer their energy to the red centres (c_r^y)

$$1/\tau_{yr} \alpha c_r^y$$
$$\alpha P_{11}$$

5.5 Nature of the red Centres :

The chemical nature of the red centres is discussed in this section. Due to the limited extent of the available information, a firm decision about the chemical identity of the red centres is not established. Nevertheless, the various possibilities viz. impurities, lattice defects, Mn ion in a locally changed environment, will be discussed.

The red centres cannot be impurities because only iron as Fe^{3+} and Cu at a higher concentration [58], is known to produce a red emission in zinc sulphide. NAA, AES (fig 5.4) or RBS (fig 5.2,5.3) could not detect any of these impurities in the luminescent thin film.

If the Mn ion is in a strong crystal field, the splitting (section 3.2.1) of its energy levels will be

different. It is possible that the energy difference between the $^6A_1(^6S)$ - $^4T_1(^4G)$ would reduce. For an observed red emission of ~1.72 eV, the decrease should be about ~250 meV. Anti-ferromagnetic attraction of Mn ion pairs leads to an estimated reduction of ~10 meV. Another reason for the change in the crystal field splitting of the Mn ion is the substitution of an anion for S in the ZnS lattice. Our results show the presence of oxygen in the samples with high Mn concentration, but most of it is expected to be associated with Mn, to form its oxide(s) on the surface. This is obvious from fig 5.5b. Also, [58,59] report seeing the red emission at ~1 mol %, at which there was little or no oxygen in the samples.

Octahedrally coordinated Mn^{2+} i.e. when MnS (rocksalt structure) separates out from ZnS:Mn, may cause the lower energy emission. Thong and Goede [58,59] found that the corresponding $Mn^{2+}(3d^5)$ absorption peaks are shifted to lower energies. They measured the position of the lower energy absorption peak to be ~2 eV. Hence an emission at ~1.8 eV cannot be ruled out; although additional data confirming this is necessary.

In [58], it is stated that the excitation spectra of the yellow and the red centre is similar to and corresponds to the well known optical transitions of $Mn^{2+}(3d^5)$ in ZnS. This strengthens the idea of radiationless energy transfer among Mn ions, but once again fails to give a convincing

evidence for establishing the chemical identity of the red centre.

It is hoped that the above discussion will help to clarify the phenomenon of concentration quenching in ZnS:Mn. The author is aware of the slightly predictive argument, with reference to the red centres, but limited data and theoretical complexity of the problem puts a unavoidable constraint.

5.6 Suggestions for further research :

A possible way to obtain additional information, is the measurement of the radiative lifetimes of the red and yellow centres. These quantities will be influenced by the dopant concentration. Assuming a radiationless energy transfer model suggested above, it should be possible to compare the theoretical prediction of such a behaviour with the observed one.

Time resolved spectroscopy will be useful to explore the exact occurrance of the red emission. Validity of the energy transfer model will be endorsed by a time lag between the red and the yellow emission. As pointed out in a previous section, SSS (site selective spectroscopy) of the phosphor is a definite way to yield useful information about the identity of the luminescent centres.

TEM of the thin film specimen might identify the spatial positions of isolated Mn and Mn clusters.

The best investigative method, for yielding

information regarding the red centres and possible reasons for quenching is, perhaps, EXAFS - extended X-ray absorption fine structure spectroscopy. EXAFS analysis can give information like Mn-Mn distance, the identity of chemical species surrounding Mn etc. Preliminary work in this direction was carried out during the present research project [93]. The results suggested that in a sample with ~2 wt% Mn, most of the Mn was bonded to oxygen. The probable reason was its heat treatment in air (30 min). Further investigation is necessary on vacuum annealed samples to yield convincing results.

CHAPTER 6

SUMMARY

An experimental system to incorporate dopants in a thin film, has been designed, fabricated and successfully used. This technique of doping thin films is unique in many ways. Not only does it reduce the time to prepare the samples drastically but also eliminates the possible errors due to its capability of producing all the samples (with a different dopant concentration) in a single vacuum pumpdown. An added advantage is that the samples so produced originate from the same parent (ZnS) film and can be annealed under identical conditions. This makes the comparison of the properties of the films (ZnS:Mn) accurate because a change in properties is due, solely, to a change in concentration of Mn.

The analysis of the thin films showed an almost stoichiometric ZnS uniformly grown on the Si substrate. The films were thought to be highly oriented in the (111) direction. Amount of Mn in the samples was determined by RBS, AES and the mask assembly. A very close agreement was observed in the values indicated by these different methods.

Effect of Mn content on the cathodoluminescent emission of ZnS:Mn was studied. Observations for two

independent sets of samples were recorded, each originating from a ZnS host film. The amount of Mn in the samples varied from 0.07 wt% to 26.4 wt%. It was found that, at a constant beam current and voltage, the relative CL intensity of ZnS:Mn thin films increased non-linearly with the amount of Mn present. Maximum intensity was observed for a Mn content of ~ 2 wt %; a further increase in c_{Mn} decreases the CL intensity. The optimum Mn concentration (~2 wt%) is not the same as that for PL (~ 1.6 wt%) or EL (0.7 wt%) of ZnS:Mn.

This phenomenon of concentration quenching was explained on the basis of radiationless energy transfer from an excited Mn^{2+}, either directly or via other Mn^{2+} ions, to an energy sink. This sink may then decay non-radiatively or may emit at different energy. It was proposed that the existence of Mn pairs and/or higher order complexes may be partially responsible for the quenching of luminescence in ZnS:Mn.

In addition to the characteristic 580 nm emission of $Mn^{2+}(3d^5)$, an additional red emission was detected in those samples with a higher Mn content. This lower energy emission was not observed for $c_{Mn} \lesssim 1.64$ wt%. This phenomenon and concentration quenching are probably interrelated; the energy sinks in the energy transfer model may be red emitting centres. No metallic impurities could be detected, so the red centres cannot be metallic impurities known to emit at that wavelength. A possibility is the Mn^{2+} ion in a

different local environment leading to a different crystal field splitting of its energy levels. Possibilities for further investigation were proposed.

A study of the coverage of rough substrates by ZnS thin films was made. Thin films deposited by vacuum evaporation (resistance and e-beam heated) on ceramic substrates exhibited a non-uniform coverage of the substrate and an effect of shadowing. Such was not the case with the films deposited by ALE on similar substrates under identical conditions. This was attributed to the fundamental difference in the physics of film growth between different techniques.

APPENDIX A

LOCK-IN AMPLIFIERS

Detection of a signal buried in noise is, nowadays, an almost routine requirement in semiconductor and optical engineering research. A lock-in amplifier is an extremely sensitive and a versatile instrument that allows the user to accomplish this.

The instrument consists of a phase shifter, a phase sensitive detector and a low noise amplifier. The 'heart' of the lock-in is a mixer which may be thought as a double throw reversing switch; its position determined by the polarity of the reference signal.

Consider fig A.1; part (a) shows an idealized, noise-free input signal in phase with the reference. The output will then be as shown in part (b) of the figure. It is proportional to the rms value of the input, when passed through the low pass filter. On the contrary, the filtered output will be zero if the input signal and the reference signal are out of phase by 90°.

The total transfer function of a lock-in is:

$$E_{out} = (E_{in}) \cos\theta \qquad \ldots(a.1)$$

where θ is the phase angle between the input signal and the reference.

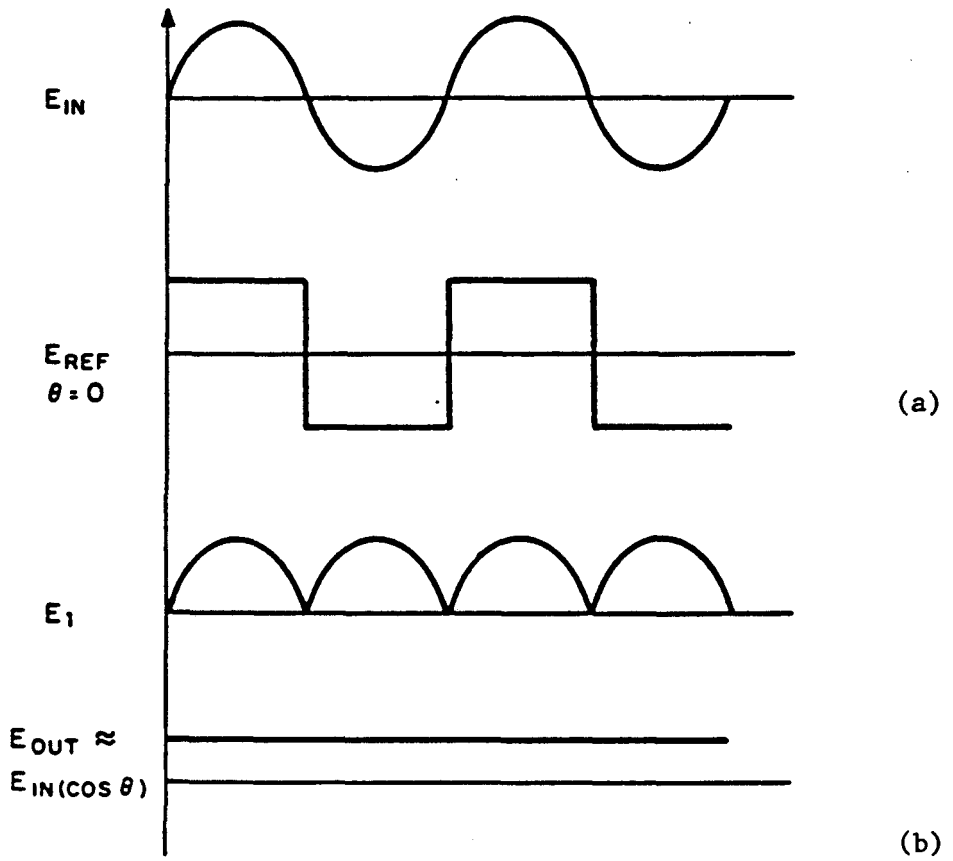

Fig A.1 Diagram explaining the operation of the lock-in amplifier.

Considerable elimination of low frequency, dc and 1/f noise is accomplished by the instrument. Moreover, the time constant of the filter helps in reducing the non-synchronous noise frequencies out of the pass band.

Sometimes noise frequencies may be prefiltered before the mixer, to avoid overload. In these cases signals as low as a few picovolts buried in tens of microvolt can be detected.

APPENDIX B

DETERMINATION OF FILM THICKNESS FROM RBS

The thickness of a thin film can be easily calculated from its backscattering spectra. It is directly proportional to the energy loss of the beam particals on inward and outward passage through the film.

As an example consider an idealized spectrum of a ZnS film on Si shown in fig b.1. The left edge of the peak due to an individual element corresponds to the deeper part of the film. For a thickness, t, not too large (< 500 nm), ΔE is proportional to t as

$$\Delta E = [S]\, t \qquad \ldots(b.1)$$

where ΔE is the total width of the signal and [S] the energy loss factor. [S] is a function of the energy loss per unit length dE/dx. For our analysis the above equation can be written as

$$\Delta E_{Zn} = [S]_{Zn}^{ZnS}\, t_{ZnS} \qquad \ldots(b.2)$$

$$\Delta E_{S} = [S]_{S}^{Zn}\, t_{ZnS} \qquad \ldots(b.3)$$

where $[S]_{Zn}^{ZnS}$ is the energy loss factor of ZnS for scattering from Zn. There is only about 5% deviation in the value of [S] with depth for a 500 nm film of most materials. Hence as a first approximation [S] may be considered independent of film

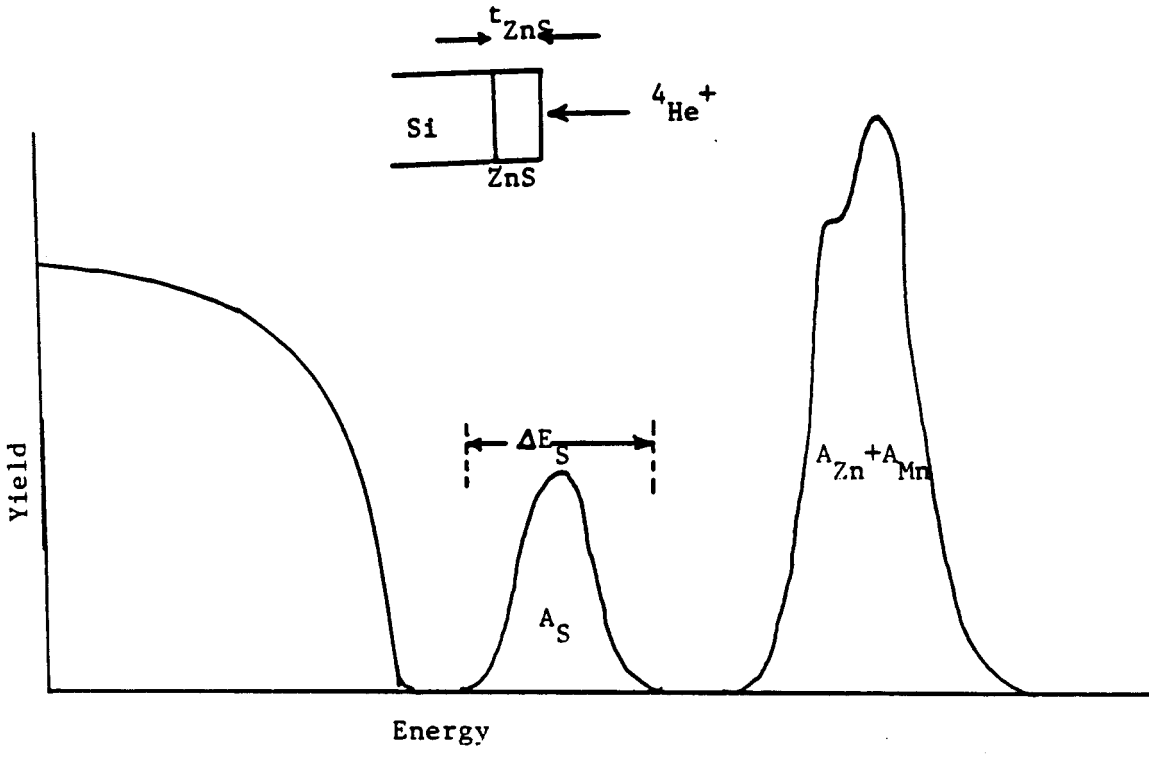

Fig B.1 Idealized backscattering spectra of a ZnS:Mn film on Si

thickness, provided t<500 nm.

Substituting the appropriate values in equation (b.2) and (b.3), the thickness of the ZnS film (sample 14, set I) is 198 nm and 187 nm. A mean value of 193 nm is reported as the thickness of the film.

See table 5.2 for the thickness of other set.

APPENDIX C

ANALYSIS OF COMPOUND THIN FILMS BY RBS

One of the advantages of backscattering analyses is that the composition ratios of the individual species can be determined (in most of the cases) directly from the spectrum. The analysis is almost accurate except when the elements are either too light or too heavy.

The area under each peak of fig b.1 is proportional to the total number of atoms per unit area (Nt) of the corresponding element and to the differential scattering cross section of each atom, σ. Here, N is the number of atoms per unit volume and t the thickness. So

$$A_i \alpha \sigma_i (Nt)_i \qquad \ldots(c.1)$$

For ZnS this transforms to

$$\frac{N_{Zn}}{N_S} = \frac{A_{Zn}/\sigma_{Zn}}{A_S/\sigma_S} \qquad \ldots(c.2)$$

The values of σ for all the elements are tabulated in standard texts (see e.g.[89]) and the area under the peak can be directly obtained from the spectrum. Substituting the appropriate values based on the spectrum of sample 14 (fig 5.3) the above equation leads to

$$N_{Zn}/N_S = 1.19$$

Similarly the composition ratios of other samples

were calculated. The results are tabulated in table 5.1.

The absolute value of (Nt) from the integrated number of counts requires a careful calibration of the scattering geometry, current integration and measurement of the active area of the detector. For an integrated charge Q of $^4He^+$ and a detector solid angle Ω, the total area A (for the film) in counts under the peak is given by:

$$A = Q\ \sigma\ \Omega\ (Nt) \qquad \ldots(c.3)$$

For the analyses during the current investigations the integrated charge was 2 μC and the detector angle 2.61 mstr. Knowing A from the spectrum, (Nt) may be calculated for the individual species.

Value of N_{Zn}/N_S reported in table is the mean of those obtained from equations (c.2) and (c.3).

BIBLIOGRAPHY :

1. Nakamura T., IEE (Jan 1980) 67.
2. Shionoya S. in "Luminescence of Inorganic Solids", Paul Goldberg ed., Academic (1966).
3. Warren A.J., Thomas C.B., Reehal H.S. and Stevens P.R.C., Jl. of Lumi., 28(1983) 147.
4. Warren A.J., Thomas C.B., and Stevens P.R.C., Jl. Phys. D, 16(1983) 225.
5. Inoguchi T., Takeda M., Kahihara Y., Nakata Y. and Yoshida M.,in Dig. Tech. Papers, Soc. Int'l Display, Int'l Symposium, Los Angeles (1974) pp 84.
6. Hurd J.M. and King C.N., Jl. of Elect. Matl., 8(6)(1979) 879.
7. Sasakura H., Kobayashi H., Tanaka S., Mita J., Tanaka T. and Nakayama H., Jl. App. Phys., 52(11)(1981) 6901.
8. Glang R., in "Handbook of Thin Film Technology" Maissel L.I. and Glang R. eds., McGraw Hill(1970) chapter 1.
9. Eckertava L., "Physics of Thin Films", Plenum (1977).
10. Nakanishi Y. and Shimaoka G., Jl. Vac. Sci. and Tech. A, 5(4)(1987) 2092.
11. Cusano D.A. in "Physics and Chemistry of II-VI compounds" Aven M. and Prener J. eds., North-Holland (1967) ch 14.

12. Stutis W., Jl. Cryst. Growth, 59(1982) 1.

13. Wright P.J. and Cockayne B., Jl. Cryst. Growth, 59(1982) 148.

14. Hirabayashi K. and Kozawaguchi H., Jpn. Jl. App. Phys., 25(1986) 711.

15. ----------, Jpn. Jl. App. Phys., 25(1986) L379.

16. Yoshikawa A., Yamaga S. and Tanaka K., Jpn. Jl. App. Phys., 23(6)(1984) L388.

17. Shibata T., Hirabayashi K., Kozawaguchi H. and Tsujiyama B., Jpn. Jl. App. Phys., 26(10)(1987) L1664.

18. Suntola T., Antson J., Pakkala A. and Lindfors S., Dig. Tech. Papers, Soc. Int'l Display, Int'l Symposium (1980) pp 108.

19. Goodman C.H.L. and Pessa M.V., Jl. App. Phys., 60(3)(1986) R65 and refernces therein.

20. Hunter A. and Kitai A.H., Jl. Cryst. Growth, 91/92 (1988) 111.

21. Theis D., Phys. Stat. Sol.(a), 81(1984) 647.

22. Bhise M.D., Sanders B.W., Dalacu N. and Kitai A.H., accepted for publication, Jl. Matl. Sci.

23. Kitai A.H., Wolga G.J. and Skvarala M.J., Matl. Sci. Lett., 4(1)(1985) 30.

24. Takagi T., Yamada I., Sasaka A., and Ishibashi T., Record of IEEE Conf. on Display Devices, New York (Oct 1972) pp 51.

25. Jones A.P.C., Brinkman A.W., Russell G.J., Woods J, Wright P.J. and Cockayne B.,

26. Ogawa M., Nakada S., Sakurai M. and Yoshioka T., Jl. Lumi., 29(1984) 11.

27. Bhise M.D., Katiyar M. and Kitai A.H., submitted to Jl. Lumi.

28. Mita J., Koizumi M., Kanno H., Sekido Y., Abiko I. and Nihei K., Jpn. Jl. App. Phys., 26(5)(1987) L541.

29. Feldman L.C. and Mayer J.W., "Fundamentals of Surface and Thin Film Analysis" North-Holland (1986).

30. Leverenz H., "An Introduction to Luminescence of Solids", J. Wiley and Sons (1950) chapter 6.

31. Destriau G., Jl.de Chimie Physique, 33(1936) 587.

32. Gumlich H.E., Jl. Lumi., 23(1981) 73.

33. Tannas L.E., in "Flat Panel Displays and CRTs", Tannas L.E. ed., van Nostrand Reinhold (1985) ch 8.

34. Singh V., Morton D. and Miller M.R., IEEE ED-35, (1)(1988) 38.

35. "Current topics in Materials Science", vol 9, Kaldis E. ed. North-Holland (1982).

36. Mach R. and Müller G.O., Phys. Stat. Sol. (a), 69 (1982) 11.

37. Bernard J., Martens M., and Williams., Jl. Lumi.24/25 (1981) 893.

38. McClure D.S., Jl. Chem. Phys., 39(11)(1963) 2850.

39. Jaffe P.M. and Banks E., Jl. Electrochem. Soc. 111

(1952) 52.

40. Garlick G.F.J. and Dumbleton M.J., Proc. Phys. Soc. (London) B67(1954) 442.
41. Garlick G.F.J., Phys. Chem. Sol., 8 (1959) 449.
42. Avinor M. and Meijer G., Phys.Chem. Sol., 12 (1960) 211.
43. Ibuki S., Jl. Chem. Phys., 40 (1964) 796.
44. Ibuki S. and Langer D., App. Phys. Lett., 2 (1963) 95.
45. Anderson W.W., Phys. Rev. A, 136 (1964) 556.
46. Kittel C., "Introduction to Solid State Physics", 5^{e}, J.Wiley and Sons (1976) pp 100.
47. Schneider J., Dischler B. and Rauber A., Jl Phys. Chem. of Solids, 29(1968) 451.
48. Nitsche R., Jl. Cryst. Growth, 9(1971) 238.
49. Chen Y.S. and Krupka D.C., Jl. Appl. Phys., 43 (1972) 4089.
50. Cattel A.F., Cockayne B., Dexter K.F., Kirton J. and Wright P.J., Proc. Soc. Int'l Display meeting, Cherry Hill (1982).
51. Marello V. and Onton A., App. Phys. Lett., 34(8), (1979) 525.
52. Marello V. and Onton A., IEEE, ED-27(1980) 1767.
53. Benoit J., Benalloul P., Geoffroy A., Balbo N., Barthou C., Denis J.P. and Blanzat B., Phys. Stat. Sol. (a), 81(1984) 709.
54. Mach R. and Müller G.O., Phys. Stat. Sol. (a), 81 (1984) 609.

55. Katiyar M., private communication.

56. Thong D.D. and Goede O., Phys. Stat.Sol. (b), 120 (1983) K145.

57. Thong D.D., Heimbrodt W., Hommel D. and Goede O., Phys. Stat. Sol. (a), 81(1984) 694.

58. Goede O. and Thong D.D., Phys. Stat. Sol. (b), 124 (1984) 343.

59. Benecke C., Busse W., Gumlich H.-E. and Moros H.-J., Phys. Stat. Sol. (b), 142(1987) 199.

60. Leverenz H., "An Introduction to Luminescence of Solids", J.Wiley and Sons (1950) pp 205.

61. Garlick G.F.J., "Luminescent Materials", Oxford (1949) chapter 7.

62. Studer F.J., Cusano D.A. and Young A.H., Jl. Opt. Soc. Am., 41 (1951) 559.

63. Garlick G.F.J. and Sayer M., Jl. Electrochem. Soc. 109 (1962) 678.

64. Strange J.W.and Henderson S.T., Proc. Phys. Soc. (London) 58 (1946) 368.

65. Theis D. and Wengert R., Jl. Elec. Chem. Soc., 132(10) (1985) 2507.

66. Espe W., "Materials of High Vacuum Technology", vol.3, Pergamon Press (1968) pp 113.

67. Feldman C., Phys. Rev. 117(2)(1959)

68. Sano Y., Nunomura K., Koyama N., Sakuma H. and Utsumi K., Proc. Soc. Int'l Display, 27(3)(1986) 169.

69. Matsuoka T., Kuwata J., Nishikawa M., Fujita Y., Tohda T. and Abe A., Jp. Jl. App. Phys., 27(4) (1988) 592.

70. Tannien V.P., Oikonnen M. and Tuomi T.O., Phys. Stat. Sol. (a), 67(1981) 573.

71. Everhart T.E., Jl. Chem. Phys., 31 (1960) 1483.

72. Tomlin S.G., Proc. Phys. Soc. (London), 82 (1963) 465.

73. Garlick G.F.J. in "Luminescence of Inorganic Solids" Paul Goldberg ed., Academic (1966) chapter 12.

74. Leverenz H., "An Introduction to Luminescence of Solids" J.Wiley and Sons (1950) chapter 7.

75. Parrot R. and Blanchard C., Phys. Rev. B, 6(10) (1972) 3992.

76. Gumlich H.-E., Pfrogner R.L., Shaffer J.C. and Williams F.E., Jl. Chem. Phys., 44 (1966) 3929.

77. Skolnick M.S., Jl. Phys. D: App. Phys., 14 (1981) 301.

78. Brill A. and Klasens H.A., Philips. Res. Rep., 7 (1952) 401.

79. Brunner W.F. Jr. and Batzer T.H., "practical Vacuum Techniques", R.E.Krieger Publishing Co. (1974) pp 59.

80. Brown R., in "Handbook of Thin Film Technology", Maissel H. and Glang R. eds, McGraw Hill (1970) chapter 6.

81. Hunter A. and Kitai A.H., Jl. App. Phys., 62(10) (1987) 4244.

82. Sands D., Brunson K.M., Cheung C.C., and Thomas C.B., Semicond. Sci. Tech., 3(1988) 816.

83. Roth W.L. in, "Physics and Chemistry of II-VI

Compounds", Aven M. and Prener J.S. eds., J.Wiley and Sons (1967) chapter 3.

84. Chu W.K., Mayer J.W. and Nicolet M.-A., "Back-scttering Spectrometry", Academic Press (1978) chapter 4.

85. Theis D., Oppolzer H., Ebbinghaus G. and Schild S., Jl. Cryst. Growth, 63 (1983) 47.

86. McKlveen J.W., "Fast Neutron Activation Analysis - Elemental Data Base", Ann Arbor Science Publ.

87. Kitai A.H., Jl. Lumi., 39(4) (1988) 227.

88. Yang K.W., Owen S.J.T. and Smith D.H., IEEE, ED-28 (6) (1981) 703.

89. Busse W., Gumlich H.-E, Meissner B. and Theis D., Jl. Lumi., 12/13 (1976) 693.

90. Dexter D.L., Jl. Chem. Phys., 21(5)(1953) 836.

91. Kröger F.A., Physica XV (1949) 801.

92. Boltaks I, "Diffusion in Semiconductors", Academic (1967).

93. Tyliszczak T., Hitchcock A.P. and Kitai A.H.at, Symp. Synchrotron Radiation in Chem., Brookhaven (Nov. 1987).

In science, all facts, no matter how trivial or banal, enjoy democratic equality.

Mary McCarthy